

ABSTRACT

MULTI-SCALE MECHANICS OF COMPOSITE SANDWICH STRUCTURES WITH BIOLOGICALLY INSPIRED FIBER REINFORCED FOAM CORES: A POTENTIAL TEMPLATE FOR DEVELOPING MULTIFUNCTIONAL STRUCTURES

Title of Dissertation:

Sandip Halder, Doctor of Philosophy, 2013

Directed By: Professor Hugh A Bruck
Department of Mechanical Engineering

This dissertation describes a novel multi-scale characterization and modeling approach for developing bio-inspired composite sandwich structures. The source of bio-inspiration was chosen to be Palmetto wood, a naturally occurring porous composite material with macrofiber reinforcement. Characterization of Palmetto Wood at multiple length scales revealed that the mechanical behavior is dominated by the stronger and stiffer macrofibers, while the porous cellulose matrix controls load transfer and failure between macrofibers. Shear dominated debonding and pore collapse mechanisms have been identified as the leading modes of failure mechanism. The role of macrofiber volume fraction and strain rate on macroscale response and damage evolution has been evaluated through experiments. It is seen that increase in macrofiber concentration increases the stiffness of the Palmetto wood, leading to a higher concentration of macrofiber in the outer region of the wood by evolution. A damage model has been developed to decouple the effect of the plastic strain and pore collapse on damage evolution.

Using Palmetto wood as a template, prototype bioinspired sandwich composite structures have been fabricated using carbon fiber reinforcement in the foam core to translate the mechanics principles of Palmetto wood. The sandwich composite structures with bioinspired foam core and standard foam core have been characterized under quasi-static and dynamic three-point bending load. The model developed to study damage evolution in Palmetto wood has been applied to the behavior of bioinspired sandwich to quantify the parameters. The enhancement in mechanical behavior has been achieved by reinforcement of the carbon rods in the core like the macrofibers in the Palmetto wood. An increase in macroscale reinforcement in the core led to the behavior that tunes the material response to a better combination the flexural stiffness, energy absorbance and damage evolution characteristics.

A Finite Element Analysis (FEA) model has been developed to numerically study the effects of reinforcement in the foam core on its flexural behavior as observed in the experimental characterization. The simulations performed using homogenized, isotropic properties from simulations of the bioinspired core affirm the experimental observations.

The viability of developing multifunctional sandwich structures from the multiscale characterization and modeling of the bioinspired foam cores has also been investigated. Prototype sandwich battery structures were fabricated using copper coated fiberglass and Zn plate facesheet, a carbon foam core, and an adhesive of NH_4Cl and ZnCl_2 bound by HTPB and epoxy polymers. Very low power generation was demonstrated using the prototype batteries, however it was determined that the mechanical strength and energy absorbing capability were compromised, as expected from the model, indicating that the use of macrofiber reinforcement could potentially enhance multifunctional behavior.

**MULTI-SCALE MECHANICS OF COMPOSITE SANDWICH
STRUCTURES WITH FIBER REINFORCED FOAM CORES
INSPIRED BY PALMETTO WOOD: A POTENTIAL TEMPLATE
FOR DEVELOPING MULTIFUNCTIONAL STRUCTURES**

By

Sandip Haldar

Dissertation submitted to the Faculty of the Graduate School of the
University of Maryland, College Park, in partial fulfillment
of the requirements for the degree of
Doctor of Philosophy
2013

Advisory Committee:

Professor Hugh A. Bruck, Chair/Advisor
Professor Abhijit Dasgupta
Professor Satyandra K. Gupta
Assistant Professor Sarah Bergbreiter
Professor Sung W. Lee (Dean's representative)

© Copyright by
Sandip Haldar
2013

Acknowledgements

I hereby acknowledge everyone who directly or indirectly influenced me to live the present, dream the future and to learn from the past.

I express my deep gratitude to Professor Hugh Bruck for shaping my academic as well as personal potential and I am indebted to him for instilling confidence in me right from my first day at UMD with his guidance, encouragement and support and a wonderful mentoring.

I acknowledge my dissertation committee for their suggestions, encouragement and motivation.

I acknowledge the support and encouragement of Prof Balachandran. I am grateful to the Department of Mechanical Engineering, especially Amarildo, Melvin and Business staffs for making our activities much simpler. I acknowledge my lab-mates, graduate and undergraduate students who worked in our lab including Jach, Manuel, Florian who worked partly towards my dissertation research.

I must acknowledge Brad, Joe and Ananth for their academic as well as personal attachment with me. In particular, Brad has been a great friend in helping me with several issues of dealing with a new culture in a new country.

SusantaDa, TrishaDi, Suman, Nili-madam deserve a special mention as precious gifts in my life.

Table of Contents

Acknowledgements	ii
Table of Contents	iii
List of Tables	vi
List of Figures	vii
Chapter 1 Introduction.....	1
1.1 Background	1
1.2 Motivation.....	6
1.3 Dissertation Goals and Scope	8
Chapter 2 Literature Review.....	11
2.1 Sandwich Structures.....	12
2.2 Bioinspired and Biomimetic Design	19
2.3 Multifunctional Structures	22
2.4 Summary	27
Chapter 3 Multiscale Mechanical Characterization of Palmetto Wood, a Hierarchically Structured Natural Composite as Template for Bioinspiration	28
3.1 Motivation and Challenges	29
3.2 Experimental Technique for Mechanical Characterization	29
3.2.1 Experiment - Deformation of Specimen	30
3.2.2 Deformation Measurement	33
3.3 Experimental Results	35
3.3.1 Characterization under Quasi-static Load.....	36
3.3.2 Characterization under Low Velocity Impact.....	50
3.3.3 Damage Evolution under Quasi-static and Dynamic Loading	59
3.4 Discussion of Results	66
3.4.1 Characterization under Quasi-static Bending	66
3.4.2 Characterization under Low Velocity Impact.....	68
3.5 Summary	69
Chapter 4 Fabrication and Characterization of Bioinspired Sandwich Structures through Reinforcement in Core.....	73
4.1 Motivation.....	73
4.2 Materials, Fabrication and Characterization Technique	75
4.3 Experimental Results	76
4.3.1 Characterization under Quasi-static Bending	77
4.3.2 Characterization under Low Velocity Impact.....	86
4.3.3 Damage Modeling of the Sandwich with Bioinspired Core	88
4.4 Discussion of Results	96
4.5 Summary	98

Chapter 5	Finite Element Modeling of Sandwich Structures	99
5.1	Motivation.....	99
5.2	Finite Element Analysis (FEA).....	100
5.3	Material Properties, Mesh and Model validation.....	101
5.3.1	Material Properties.....	101
5.3.2	Mesh Convergence.....	103
5.3.3	Model Validation	105
5.4	Global Flexural Response from FEA: Effect of Reinforcement.....	107
5.4.1	Effect of Reinforcement on Global Flexural Response	107
5.4.2	Variation of Flexural Modulus with Volume Fraction	109
5.5	Modeling of Foam Core with Reinforcement for Homogenization of Properties.....	111
5.6	Flexural Response of the Reinforced Sandwich from FEA and Experiment ..	113
5.7	Effect of Reinforcement on Local Strain Fields	115
5.8	Effect of Reinforcement on Damage Initiation.....	119
5.9	Discussion of Results.....	125
5.10	Summary	127
Chapter 6	Structural Battery: <i>Multifunctional Sandwich Structure</i>	128
6.1	Motivation.....	128
6.2	Materials, Fabrication and Characterization Technique	130
6.3	Experimental Results	131
6.3.1	Mechanical Characterization	131
6.3.2	Electrical Characterization.....	140
6.4	Discussion of Results.....	141
6.5	Summary	142
Chapter 7	Conclusions.....	143
7.1	Intellectual Contributions.....	143
7.1.1	Multi-scale Characterization and Modeling of a Hierarchically Structured Natural Composite: <i>Palmetto Wood</i>	144
7.1.2	Development, Characterization, and Modeling of a New Bioinspired Foam Core for Composite Sandwich Structures	144
7.1.3	Development of FEA Model for Bioinspired Foam Cores.....	145
7.1.4	Development of a Multifunctional Sandwich Composite Structure with Energy Storage Capability	146
7.2	Anticipated Benefits.....	147
Chapter 8	Future Work	148
8.1	Modeling of Porous Foam for Further Investigation of Failure Mechanisms ..	148
8.1.1	Motivation.....	148
8.1.2	Approach.....	149
8.1.3	Expected Outcomes	151
8.2	Incorporate the Bioinspired Core in Structural Battery and Integration of Conductive Nano-reinforcement in Foam	152
8.2.1	Motivation.....	152
8.2.2	Approach.....	153
8.2.3	Expected Outcomes	154

References.....	155
-----------------	-----

List of Tables

Table 3.1 The modulus, E , and Weibull parameters (ε_0, β) obtained by fitting the flexural stress-strain curves and the modulus, E , and damage initiation strain (ε_d) obtained from the new damage model for the Palmetto Wood specimens.	66
Table 4.1 The modulus, E , and Weibull parameters (ε_0, β) obtained by fitting the flexural stress-strain curves for the sandwich composite specimens under quasi-static and dynamic load.	85
Table 4.2 The modulus, E , and Weibull parameters (ε_0, β) obtained by fitting the flexural stress-strain curves and the modulus, E , and damage initiation strain (ε_d) obtained from the damage model for the sandwich composite specimens	93
Table 5.1 Material properties of foam core, facesheet and reinforcement used in the simulation.....	103
Table 5.2 Mesh details and flexural modulus determined from the simulation.....	105
Table 5.3 Properties of the foam core estimated from finite element simulation.....	115
Table 6.1 Ingredients and electrical properties of the structural batteries	141

List of Figures

Figure 1.1 Structure of a tree: a hierarchically-structured source of bioinspiration	1
Figure 1.2 Multifunctional structure: Active Aeroelastic Wing (AAW) [1]	3
Figure 1.3 Relative weight and stiffness of sandwich materials [2]	3
Figure 1.4 Schematic diagrams of two approaches to achieve multifunctional structure: (Top) constituents themselves performing multiple functionalities, (bottom) components of different functionalities are assembled in a single system	5
Figure 2.1 Different sandwich core types [23]	14
Figure 2.2 Facing wrinkling in sandwich structure under four-point bend test [25]	15
Figure 2.3 Critical load versus span length for failure initiation in sandwich beams under three-point bend [25].....	15
Figure 2.4 Interfacial failure in cleavage peel test of glass/epoxy facesheet and polyurethane foam core sandwich [13].....	17
Figure 2.5 Possible failure modes for layered materials based on material constitution [33].....	17
Figure 2.6 Dynamic failure modes and sequence in a layered specimen from a different field of view. Following interfacial delamination at the lower then the upper interfaces, cracks kink into the core layer to form intra-layer damage [33].....	18
Figure 2.7 (Left) Experimental and Numerical results under 3 J impact and (right) residual strength of truss core sandwich under different impact energy and stacking sequence [37]	19
Figure 2.8 (a) The morphology of dumbbell-like SiC whiskers [48] and (b) optical photographs of cross-sections of normal and reformed bamboo and the fiber volume fraction before and after processing [49]	21
Figure 2.9 Failure mechanism illustrating (a) plastic buckling for low-density balsa wood (b) kink band for high-density balsa wood and associated stress–strain curves [53]	22
Figure 2.10 Electrical conductivity of CNT/epoxy nanocomposites at various CNT	23
Figure 2.11 Cross-section of fully assembled flat heat pipe sandwich panel [59]	24
Figure 2.12 (Left) Temperature increase below cells due to heat production of cells and (right) voltage change during mechanical loading [63].....	25
Figure 2.13 (Left) Schematic lay-up of the sandwich structure with two solar cells as skin and (right) Curved prototype sandwich modules with 4 (top) and 8 (bottom) integrated m- Si S32 solar cells as a skin [65]	26
Figure 3.1 Three-point bend test set up to characterize the deformation of Palmetto wood, and Images of deformed Palmetto wood in three-point bending.....	32
Figure 3.2 Fields of view at several magnifications demonstrating the multiscale deformation measurement methodology where the interface is denoted by a dashed line and the matrix and macrofiber by M and F, respectively [69].....	32
Figure 3.3 (a) Low velocity impact test set-up in three-point bend configuration and (b) circuitry	35
Figure 3.4 Representative quasi-static macroscopic flexural stress strain response for Palmetto wood with a Weibull fit indicating that the failure response conforms to a Weibull distribution	37
Figure 3.5 Macroscopic (left) displacement (pixels) and (right) strain fields in Palmetto wood obtained under three-point bending before the onset of failure. The fields evidence	

macroscopically homogeneous behavior of the material. The load level corresponds to point A of Figure 3.4.....	38
Figure 3.6 (a) Vertical displacement field of the Palmetto wood specimen under quasi-static three-point bend test that resembles typical displacement field in three-point bending for homogeneous isotropic material, and (b) vertical displacement of the specimen along the line (shown in (a)) and quadratic fit used to calculate the strain from beam bending theory.....	39
Figure 3.7 Strain contours and strain distribution along depth in (left) compression side and, (right) tensile side of Palmetto wood during three-point bending at intermediate microscale magnification exhibiting more inhomogeneous shear strain distribution consistent with the porous microstructure of the matrix.....	41
Figure 3.8 (a) Local bending of macro-fiber (b) Strain fields in Palmetto wood at second intermediate microscale obtained near fiber-matrix interface	42
Figure 3.9 Strains measured 200 μm into matrix at microscale indicating concentration of shear strains very close ($\sim 0.25d_f$) to the fiber-matrix interface with associated pore collapse which may allow the shear strain to build up at the interface.....	43
Figure 3.10 (a) Strain fields in the Palmetto wood specimen under quasi-static three-point bend before failure initiation and (b) failure initiation in the by shear cracking in the cellulose matrix after a macro-scale flexural strain increment, $\Delta\epsilon$, of 0.001. The failure initiation corresponds to the high shear strain site.....	45
Figure 3.11 Evolution of shear cracking in cellulose material. The pores collapse (a) and coalesce together (b) and accumulate shear strain (c) leading to macro crack (d). The pore collapse mechanism helps for load absorption. The images correspond approximately to the points 0, A, B, C in Figure 3.12(c).....	48
Figure 3.12 Intermediate microscale shear strain field of interfiber matrix in (a) tensile and (b) compressive regions of the specimen, (c) macroscopic stress-strain response, and (d) the evolution of the microscale strains with macro-scale flexural strain (right side) in the tensile (solid line) and compressive (dashed line) regions. The strains were extracted at the encircled points in (a) and (b). The state of deformation corresponding to the points A, B, C and D are shown in the stress-strain response (d). 1:1 correspondence between the magnitudes of the microscale strains and macro-scale flexural strain is denoted by the dashed yellow lines.	49
Figure 3.13 Specimens prepared from several radial location of Palmetto wood stem. The specimen prepared from outer region had a higher macrofiber (MF) volume fraction of 20%, whereas that from the inner portion had a lower MF volume fraction of 12%.	50
Figure 3.14 Correlation of (Top) velocity and (bottom) displacement obtained from load cell response and optical measurement by high speed imaging	51
Figure 3.15 Flexural response of 12 and 20 vol. % macrofiber (MF) Palmetto wood specimens under low velocity (approximately 30 m/s) impact and quasi-static three-point bending with Weibull fits.....	53
Figure 3.16 Comparison of low velocity impact and quasi-static indentation response of Palmetto wood specimens with different macrofiber (MF) volume fraction.	53
Figure 3.17 (a) Transverse (vertical) displacement obtained from DIC of the Palmetto specimen under low velocity impact at a flexural strain level 0.027, and (b) displacements obtained along the dashed line and corresponding cubic fit. The strain determined using	

the curvature from the cubic fit also corresponds to a strain value of approximately 0.027.	55
Figure 3.18 Post-failure specimens after macrofiber-interface debonding leading to rupture (right side) and local indentation by projectile (left side) that absorbs all the kinetic energy of the projectile. The transformation of failure mode is attributed to macrofiber concentration in the Palmetto wood.	57
Figure 3.19 Images of deformed Palmetto wood under low velocity impact at a magnification of 10X. The local indentation failure consists of compressive axial strain associated with crushing of the porous cellulose matrix followed by higher levels of shear strain associated with shear cracking of the macrofibers and matrix.	59
Figure 3.20 (a) Damage evolution with total flexural strain, (b) evolution of plastic flexural strain with total flexural strain, (c) Flexural stress-strain curves with new model fit, (d) evolution of plastic flexural strain with damage, and (e) evolution of elastic flexural strain with total flexural strain for Palmetto wood of 12 and 20 vol. % macrofibers (MF) under quasi-static and low velocity impact three-point bending.	62
Figure 3.21 Impact-induced damage in Palmetto wood due to debonding at the macrofiber-porous cellulose matrix interface for (a) 12 vol. % and (b) 20 vol. % macrofiber concentrations. The specimen with 20 vol. % macrofibers absorbs the projectile and has lesser flexural deformation (3.8% flexural strain) compared to 12 vol. % macrofiber (11% flexural strain). Also, the specimen with a lower macrofiber concentration (a) has a significantly higher number of damage sites than the later (b) ...	65
Figure 4.1 (left) Sandwich structure with bioinspired core developed using Palmetto wood as a template and (right) post-mortem of the inside structure of sandwich	76
Figure 4.2 Flexural properties of (a) facesheet, (b) foam core and, (c) failure initiation in foam core	78
Figure 4.3 Global flexural response of sandwich composite structure under quasi-static load.	80
Figure 4.4 Weibull fit to the global flexural response of sandwich composite structures under quasi-static load. Since the Weibull model has been found to be useful for a bundle of fibers, the bilinear type response of the sandwich structures can not be captured well	81
Figure 4.5 Macroscale (a) flexural, (b) compressive and (c) shear strain fields in the sandwich core corresponding to around 130 N load (Point A in <i>Figure 2</i>) and (d) failure mode by pore collapse in foam core under indenter and shear dominated debonding at the facesheet-foam core interface	83
Figure 4.6 (a) Image of the core of the bioinspired sandwich composite structure at magnification of around 5X and (b) compressive and shear strain fields at the carbon rod – foam core interface and under flexure at high magnification. Dotted white line represents the reinforced pultruded carbon rod in foam core. Shear and compressive strains are dominant around the carbon rod.	84
Figure 4.7 Flexural response of sandwich composite with and without reinforcement to the in the core under low velocity impact and Weibull fit to the experimental data	87
Figure 4.8 (Left) Undeformed and (right) Deformed sandwich composite specimen under low velocity impact	88
Figure 4.9 Damage evolution with total flexural strain in the sandwich composite specimens under quasi-static bending	89
Figure 4.10 Damage evolution characteristics of sandwich composite specimens:	93

Figure 4.11 Dynamic damage behavior of the sandwich composite structures obtained from the damage model	95
Figure 5.1 Schematic of the FE simulation of flexure of sandwich composite structures	101
Figure 5.2 Experimentally determined properties of foam material under (a) flexure and (b) compression.....	102
Figure 5.3 Properties of facesheet material (a) experimental and (b) simulation input for plastic deformation.....	102
Figure 5.4 (a) Mesh density in the sandwich composite model and flexural modulus for different mesh density	104
Figure 5.5 Comparison of flexural response obtained from experiment and FEA of sandwich composite structure	106
Figure 5.6 Strain fields in the sandwich composite obtained from FEA and experiment	107
Figure 5.7 Flexural response of the reinforced sandwich composite structure with several vol % of reinforcement	108
Figure 5.8 Schematic of the cross-section of a reinforced sandwich composite	109
Figure 5.9 Effect of vol % of reinforcement on global flexural modulus.....	110
Figure 5.10 (a) Representative foam core with reinforcement and (b) flexural response of the reinforced core to determine the homogenized behavior.....	112
Figure 5.11 Model sandwich composite with reinforcement in the core and homogenized core.....	114
Figure 5.12 Flexural behavior of sandwich composite structure using homogenized properties of the reinforced core in simulation and experiment	115
Figure 5.13 (a) Global flexural response and (b) effect of reinforcement on the local deformation fields in sandwich composite under flexure. The strain fields correspond to a global flexural stress level of around 21 MPa (Point A) (c) experimental observations of strain concentrations at the reinforcement - foam core interface in sandwich composite structure.....	119
Figure 5.14 Damage initiation sites in the sandwich composite (a) with reinforcement and (b) without reinforcement. The value 1 corresponds to damage initiation, and 0 corresponds to no damage as discussed in Equation 5.1 and 5.2.....	122
Figure 5.15 Damage initiation sites (a) in the front face and (b) in the vertical plane of reinforcement in sandwich composite with reinforcement	124
Figure 6.1 Proposed model sandwich structure for a structural battery. The material system is designed to be a lightweight battery with enhanced structural support	130
Figure 6.2 Mapping of the multifunctional sandwich (structural battery) and a Zn-Carbon battery	130
Figure 6.3 (a) A structural battery, (b) three-point bend test on a multifunctional sandwich specimen, and (c) the flexural responses of the multifunctional specimens and the behavior of just the facesheets, unbonded and without core (both copper coated fiberglass and Zn facesheet specimens).....	133
Figure 6.4 (a) Flexural response of the sandwich structural battery and contribution of core and facesheet in bending behavior, (b) the deformed images corresponding to points A (before core failure) and B (after core failure), (c) strain fields obtained from DIC of the images	136

Figure 6.5 (a) Flexural response of the sandwich structural battery with fiberglass facesheet and contribution of carbon foam core and fiberglass facesheet in bending behavior, (b) the deformed images after core failure AB and CD, (c) strain fields obtained from DIC of the images	138
Figure 6.6 Battery specimens (a) HTPB polymer based interface, (b) epoxy based interface.....	139
Figure 6.7 Response of battery specimens (Figure 6.6) with HTPB and epoxy based interface.....	140
Figure 8.1 Detail modeling of the foam core for further investigation of failure mechanisms through foam cell response	150
Figure 8.2 Deformation modes of a hexagonal regular honeycomb (a) three distinct deformation shapes and deformation map for a regular honeycomb subjected to dynamic crushing and (bottom) deformation shapes of regular cellular structures with constant and functionally graded relative density at 50% crushing at low and high crushing rates [95]	151
Figure 8.3 Approaches to incorporate bioinspired core in multifunctional sandwich....	154

Chapter 1 Introduction

1.1 Background

Nature has evolved its systems over a long period of time such that its parts can perform their role in the most efficient manner. Most of the time, they serve multiple purposes, thereby, increasing the efficiency and requiring lesser amount of material for the task. For example, the root of a tree has branching inside the soil so that it can provide very strong support against wind load, seismic load as well as serves to draw minerals and water from soil for its livelihood. Thus, biological inspiration has been a huge resource to engineer materials and systems to develop to the best performance and efficiency. Recently, biologically inspired and biomimetic designs have drawn interests in all areas of engineering.

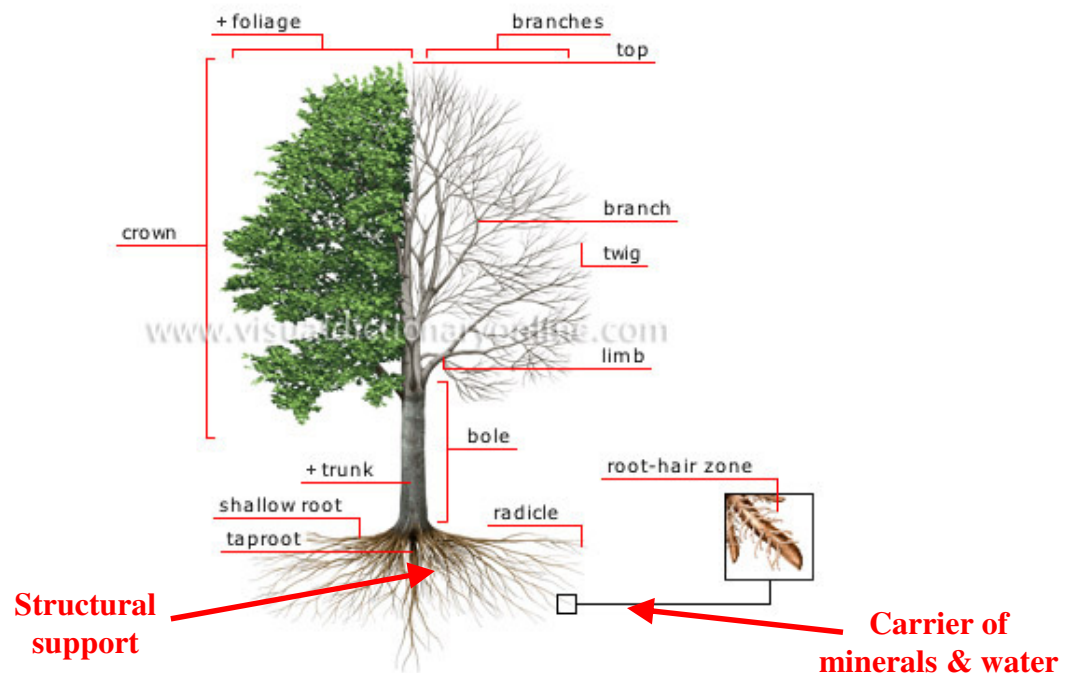


Figure 1.1 Structure of a tree: a hierarchically-structured source of bioinspiration

“Aerospace system designers are constantly trading-off between performance (maneuverability, observability, survivability) and efficiency (range, availability). Multifunctional “smart structures” have the potential to improve both sets of capabilities by performing multiple engineering functions using a single component or structure. An example is an active aeroelastic wing (AAW), which incorporates structure, controls, smart materials, and sensors capable of commanding shape changes based on real-time flight data” [1]. Employing multifunctionality in engineering systems enhances their system efficiency as well as makes the structure robust. For example, driving power from a structural member will help reduce the weight of batteries and hence increase efficiency, and thereby reduce the cost of several engineering applications, like aerospace, marine, ground transportation.

Structural batteries have been very promising and make significant impact in spacecrafts, air vehicles especially small scale vehicles, like Micro Air Vehicle (MAV), Flapping wing Vehicle, Unmanned Underwater Vehicle (UUV) etc. To achieve the best performance and functionality for these kinds of applications, light weight high stiffness material with multiple functionalities is of utmost importance.

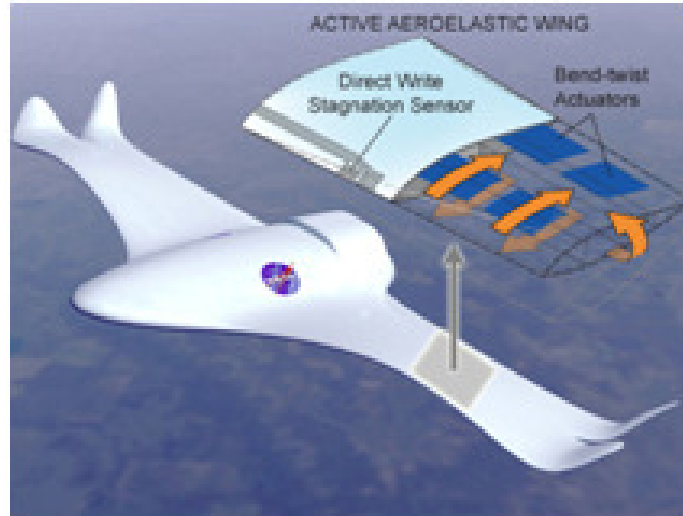


Figure 1.2 Multifunctional structure: Active Aeroelastic Wing (AAW) [1]

Over the development of several decades, the concept of sandwich materials has led to the structural strength with light weight replacing conventional material [2]. Considerable literature is available on the investigation of behavior of sandwich structures and their failure modes under compression tension [3], quasi-static load [4], blast and Impact [5, 33, 36], underwater impulse [6, 7], impact and air blast [8]. There are also literatures on modeling of sandwich structures [9, 10, 95], damage of smart composite and detection [11].




	Solid Material	Core Thickness t	Core Thickness $3t$
			
Stiffness	1.0	7.0	37.0
Flexural Strength	1.0	3.5	9.2
Weight	1.0	1.03	1.06

Figure 1.3 Relative weight and stiffness of sandwich materials [2]

Multifunctional material and structures have gained special attention in the last decade. This shows the increase in research articles in English related to multifunctional materials and structures [12]. The increased research effort has been guided by the need of developing multifunctional materials and structures simultaneously perform (a) multiple structural functions, (b) combined non-structural and structural functions, or (c) both. Examples of these types of multifunctional structure include (a) composite materials with high strength to weight ratio, high fracture toughness and damping, (b) load bearing structure with the capability of thermal insulation or efficient heat transfer or energy harvesting/storage, and (c) a structure that functions for both first and second types of purposes [2]. In his review article on the mechanics of multifunctional structure, Gibson [2] summarized several areas of structural and nonstructural multifunctionality.

There are two primary ways to realize multifunctionality in a material system: (i) the constituent materials themselves performing multiple functionality, and (ii) coupling/embedding components of different functionality in a single system. Schematic diagrams of the concepts of developing multifunctional composite sandwich material with structure-power capability are depicted in Figure 1.4.

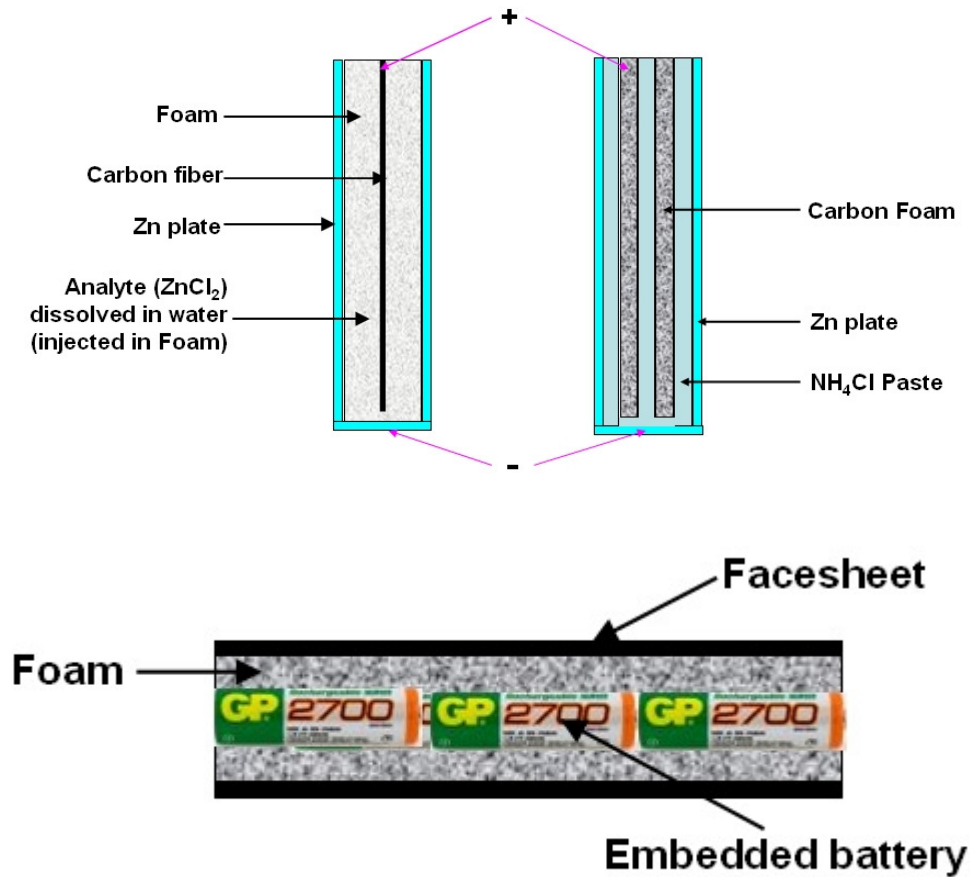


Figure 1.4 Schematic diagrams of two approaches to achieve multifunctional structure: (Top) constituents themselves performing multiple functionalities, (bottom) components of different functionalities are assembled in a single system

The first method involves selecting proper material for the required coupled performance while, the second one involves proper design of embedment leading to least sacrifice in their primary functionalities. Several research publications have explored the details of the second approach in realizing multifunctional structure [56, 59, 62, 65]. However, efforts have been made to develop several core materials to perform multifunctionality, structural and thermal, simultaneously [57].

1.2 Motivation

Palmetto wood, a naturally occurring hierarchically structured composite material has been found to exhibit enhanced mechanical behavior and damage resistance when used in the protective structures during the Civil and Revolutionary war. Thus, inspired by the enhanced mechanical properties and damage resistance, it has been a potential natural inspiration to developing engineering sandwich composite structures with enhanced mechanical behavior.

To utilize the full benefit of the behavior of the bioinspiration, Palmetto wood, the mechanical behavior of the Palmetto wood and the underlying mechanisms of its enhanced behavior and energy absorbance needs to be explored. The material being hierarchically structured at multiple length scale, ranging from the macrofibers to the bulk size, the deformation mechanism and the resulting global behavior must be elucidated to understand the effect of its hierarchical microstructure on its global behavior. Thus, experimental methodologies specially suited to characterize the deformation at multiple length scales have been developed to relate the behavior at lower length scale to the macroscale.

Using the mechanisms explored by the characterization of the mechanical behavior of Palmetto wood, it would be possible to translate the mechanisms that enhance the mechanical behavior and energy absorbance of engineering sandwich composite structures. To realize the benefits of the hierarchical structure of Palmetto wood, sandwich composite structures were developed with biologically inspired foam cores to translate the mechanisms into engineered sandwich composites. Effort has been made in this work to create biologically inspired foam cores by reinforcing the foam used in

composite sandwich structures with carbon fibers aligned in the longitudinal direction. Mechanical characterization under quasi-static and dynamic load was performed to verify the translation of the mechanics found in Palmetto wood through the benefits of using macrofiber reinforcement in the foam core.

Developing multifunctional structures with structure-power capabilities often involves multiple performance objectives. However, optimizing the overall system performance leads the development of new multifunctional materials, and this system level objective provides useful guidance in ranking the various design possibilities and parameters. Thus it is critical to select appropriate materials for a proper functionality so that the selected material can perform in the presence of other material. For example, a chemical naturally analyte for a battery should be able to sustain its performance when mixed with a binder to be used as interfacial adhesive of the sandwich.

Previous research reveals that carbon foam (CF17) does have the required electrical properties to be used as anode material; however, this being ceramic foam sustains negligible impact energy and thus trades off the mechanical performance of the composite sandwich structure. However, carbon foam core sandwich has been a potential structural material for armor applications for its high thermal and laser resistance. Typical metrics to indicate mechanical performance are Weight, Impact resistance, Static mechanical behavior, Energy density and that for electrical performance are discharge rate, AmpHr. However, as stated earlier, these metrics are often impeding and call for optimization based on application. Owing to some of these issues, developing an appropriate multifunctional structure is a challenging problem which can not be solved by the current state of the art.

This dissertation is therefore seen as the first attempt at characterizing the multi-scale mechanics of a novel hierarchically-structured natural composite, Palmetto wood, in order to develop prototype engineered sandwich composite structures with enhanced mechanical behavior for possible use as multifunctional structures in applications such as energy storage.

1.3 Dissertation Goals and Scope

The challenges outlined in the earlier elucidate that characterizing the mechanical behavior of hierarchical structured materials to fabricate sandwich composite structures with enhanced mechanical behavior is a non-trivial problem. As part of this dissertation, detailed understanding of the mechanical behavior of naturally occurring composite, namely, Palmetto wood a potential bioinspiration in developing sandwich composite materials with enhanced mechanical behavior and energy absorbing capability has been developed. The characterization and modeling is utilized to reveal the role of macroscale reinforcement in the mechanical behavior and damage evolution in the material.

Using the understanding of the mechanisms for load transfer and failure in Palmetto wood, sandwich composite structures using a bioinspired core can be developed to verify the enhancement in the mechanical behavior with respect to the conventional sandwich composite structure. The distinct aspects of developing sandwich structures namely, enhanced mechanical behavior and damage resistance have been explored. The role of macroscale reinforcement in the bioinspired foam core in damage evolution has been evaluated. A detailed model of the behavior of the sandwich material with bioinspired core will lay a path to help select the constituent material and their size and amount to achieve the best mechanical performance.

The experimental characterization of the bioinspired sandwich composite has been then verified using numerical simulation of flexural behavior of sandwich composite structure using Finite Element Analysis (FEA). Simulations have been performed to quantify the effect of the bioinspired core design on the global behavior of the sandwich composite using the experimentally determined material properties. To modeling approached, based on homogenization of properties of the reinforced core and detail model with discrete reinforcements have been developed to evaluate the global flexural response of the sandwich composite structure and the local deformation fields and damage initiation due to the reinforcement in the core of sandwich composite.

In developing a multifunctional sandwich composite structures (e.g., a structural battery), a bottom-up approach has been adopted using Zn-carbon battery as template and transforming to sandwich configuration. The potential and performance of the sandwich composite battery structures in terms of mechanical and electrical behavior has been characterized. This work will help in understanding how the multi-scale characterization and modeling of the bio-inspired foam cores will translate to multi-functional structures in order to enhance their multifunctional design for both mechanical behavior and energy storage.

The multi-scale mechanical characterization of Palmetto wood as a template for developing engineered material with enhanced mechanical properties has been presented in Chapter 3. Chapter 4 details fabrication and experimental characterization of sandwich structures with bioinspired core using the experimental methodology developed to characterize hierarchical structures and the model developed to quantify the damage parameters. Numerical analysis of the mechanical behavior of sandwich structures with

bioinspired core using Finite Element Method has been detailed in Chapter 5. The preliminary effort in developing multifunctional structures with structure and power capability has been discussed in Chapter 6. The conclusions and anticipated benefits of this dissertation research are reported in Chapter 7. The Chapter 8 lists the possible future direction for further understanding of the mechanics of the sandwich composite structures and developing multifunctional material systems.

Chapter 2 Literature Review

Multifunctional material systems have drawn attention of the researcher from the last decade and significant effort has been devoted in implementing, designing, developing concepts of multifunctionality. Multifunctional materials are those that serve multiple functionalities. While several components can be assembled together to utilize their respective functionality independently, systems are also developed such that a single component serve multiple purpose there by increasing the system efficiency by waiving off using multiple components. Thus, most of the implementations of multifunctional materials call for composite materials where different materials participate in the functionality with their own properties and leads to enhanced combined properties. The functionalities can be structural, electrical, thermal, magnetic, chemical etc. Thus the implementation of concepts of developing multifunctional systems is interdisciplinary. Most of the time, they are contradictory and requires trade-off in one for the other. Thus these kinds of designs often require optimization.

The present dissertation aims at developing and characterizing a multifunctional sandwich structure whose design is bioinspired and serves structural and electrical functionality that can be called structural battery. For this purpose it is important to develop an understanding and the survey of the research performed in the relevant areas. The following sections briefly describe the relevant areas pertaining to the present dissertation and the aspects that have been explored. Finally a summary of the literature review will be presented in Section 2.4.

2.1 Sandwich Structures

Sandwich composites are the advanced composites with high strength to weight ratio and that consist of a core material generally soft and two facesheets with higher strength attached to the soft core. The role of facesheets has been to provide stiffness, tensile as well as bending whereas the core enhances the energy absorbance, damage resistance and carries the shear load in thickness direction. Usually, high stiffness, high strength, and thin composite materials are used for faces to resist the in-plane and lateral loads, while, light but low stiffness and low strength materials such as foam, honeycomb, and balsa wood are used for cores [13]. Sandwich materials can be classified based on the type of facesheet or core. Typical facesheet materials include fiber-reinforced plastics laminates, e.g. glass fiber and epoxy resin or metal sheet.

The concept of developing composite sandwich structure dates back to 1849 [14]. In England, sandwich construction was first used in the Mosquito night bomber of World War II that employed plywood sandwich construction. During the World War II, the concept of sandwich structure in US originated with through the use of reinforced plastic as face and low density core [14]. The first research paper on sandwich structure was written by Marguerre in 1944 dealing with sandwich panels subjected to in-plane compressive load [14].

Several techniques have been developed to manufacture the foam cores like metallic foam core polymeric foam core of closed cell, open cell and stochastic type [15]. The foam manufacturing techniques may be categorized as investment casting, deformation forming and metal wire approaches [15]. Several techniques to manufacture foam include using open cell polymer templates for investment casting [16], chemical vapor deposition

[17], slurry coating [18], hollow spheres [19] or aggregates of soluble particles into which metals can be injected and solidified [20]. Truss core patterns with attached face sheets can be made from a volatile wax or polymer (eg polyurethane) by injection molding [21] or rapid prototyping methods [22].

Sandwich structures have been used for several applications like aerospace, automotive and several infrastructural applications as well. Since the engineering of transportation devices, materials with high strength and light weight have been of huge interest. The sandwich structures have been especially successful and leading material in aviation industry. The use of sandwich structure in the Apollo project that successfully landed on the moon in 1969 showed the high potential of sandwich structure in the field of aerospace [23]. The Beech Starship uses Nomex honeycomb with graphite and Kevlar faces for the entire structure - the first all sandwich aircraft. Also, a major portion of the space shuttle is a composite-faced honeycomb-core sandwich. Almost all satellite structures employ sandwich construction. The U. S. Navy uses honeycomb sandwich construction for bulkheads, deck houses, and helicopter hangars to reduce weight above the waterline [14]. Application of composites for large structures at AIRBUS started in 1983 when the A310 was the first aircraft in the AIRBUS fleet to be equipped with a composite honeycomb sandwich rudder. The composite Vertical Tail Plane for the A310 was soon to follow in 1985 [23]. Since 1980, composite front cabs of locomotives have been built for the XPT locomotives in Australia, the ETR 500 locomotives in Italy, the French TGV and the Swiss locomotive 2000. In Japan, the new Nozomi 500 bullet trains use honeycomb sandwich for the primary structure. Also in 1995, Starlinger and Reif reported that sandwich construction is now being used in double-decker buses [14]. In

Europe, COBRAE was founded (Composite Bridge Alliance Europe) which is leading the way in promoting composite bridges throughout the European Union. In wind energy systems, GE Energy states they have 6900 installations worldwide, and that their growth rate is 20% per annum. The Global Wind Energy Council ranks the leaders in wind energy installations as: Germany, Spain, U.S., and Denmark [14].

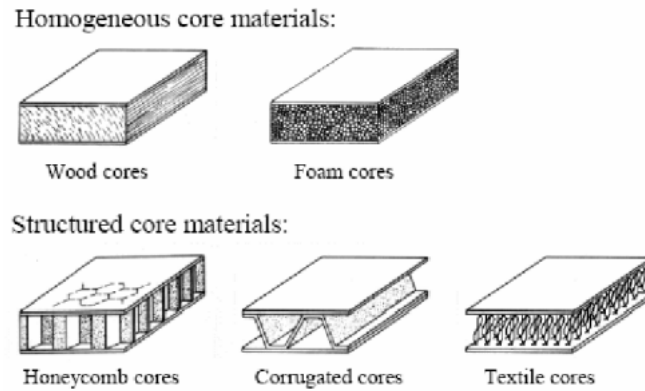


Figure 2.1 Different sandwich core types [23]

Several investigations have been performed to study the failure modes of sandwich composites. The failure modes of sandwich beams are typically face yielding and fracture, core shear and crimping, face wrinkling and dimpling, and overall buckling [13]. Haibin et al [] designed fabricated a thermoplastic sandwich structure for mass transit bus.

Gdoutos and Daniel [25] investigated several failure modes of sandwich beams of unidirectional carbon/epoxy facing and PVC closed-cell foam core under quasi-static three and four point bending. They observed compression facing wrinkling as evidenced by sharp change in strain (Figure 2.2). However, the core failure was observed under three-point bending and the failure occurred when the maximum shear stress reached shear strength of the core material. The failure envelope for a core material can be described by an appropriate failure criterion. The indentation failure has also been noted

under three-point bending. The indentation failure of the sandwich beam can be predicted by treating the loaded face as a beam resting on a foundation.

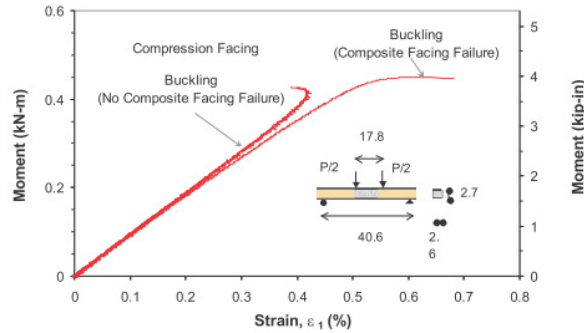


Figure 2.2 Facing wrinkling in sandwich structure under four-point bend test [25]

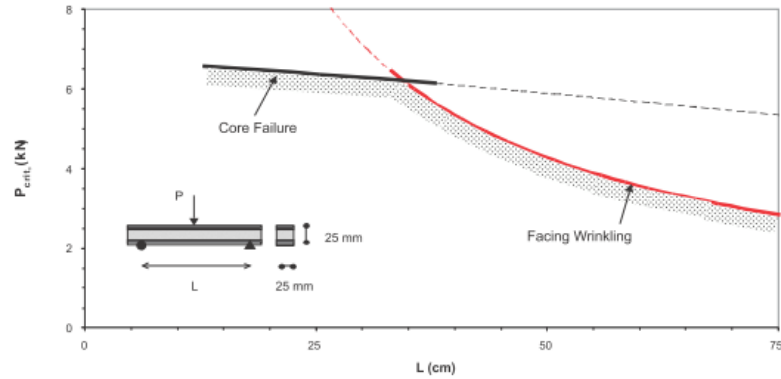


Figure 2.3 Critical load versus span length for failure initiation in sandwich beams under three-point bend [25]

Tension or compression facing failure in uniaxial stress by yielding or fracturing has been reported by Daniel and Abot [26]. The bending behavior of the beams, whether loaded under four-point or three-point bending, is governed by the face sheets. Hadi and Matthews [27] reported short-wavelength buckling or wrinkling of the compression facing of sandwich beams subjected to compression or bending. Indentation failure of sandwich construction results from application of highly localized external loads and is associated with local bending of the loaded facing into the core. The problem has been studied by Soden [28] using a rigid-perfectly plastic and an elastic-perfectly plastic type foundation model. Triantafillou and Gibson [29] developed a failure mode maps for

sandwich beams with aluminum facings and rigid polyurethane foam cores in three-point bending. Recently, Xiong et al [30] studied mechanical behavior and failure of pyramidal truss core sandwich with experiment and analysis considering core shear macro-buckling, face wrinkling, and face sheet crushing failure modes.

The interfacial delamination at the facesheet-core interface has been one of the leading failure modes in the sandwich due to the mismatch in mechanical properties. Debonding of the facing from the core may occur during fabrication or due to overloads. This failure mode was studied in terms of the critical strain energy release rate of the interface by Triantafillou and Gibson [31]. Efforts have been put to study the peel strength of the facesheet and core as the failure modes of the sandwich structures are closely related to this peel strength. Peel energy is commonly used to describe the adhesion characteristic of the facesheet and core material [13]. Thouless and Jensen [32] utilized the elastic fracture mechanics to the geometry of the peel test [9]. Cantwell et al. [33] have performed the three-point bending test for characterizing face-core adhesion in sandwich beams. Lee et al [13] performed cleavage peel test to characterize the interface and used surface resin impregnation of the foam to increase the peel strength of the facesheet and foam interface. Recently, Sun and Chen [34] studied the interfacial fracture behavior of foam core sandwich by viscoelastic cohesive model.

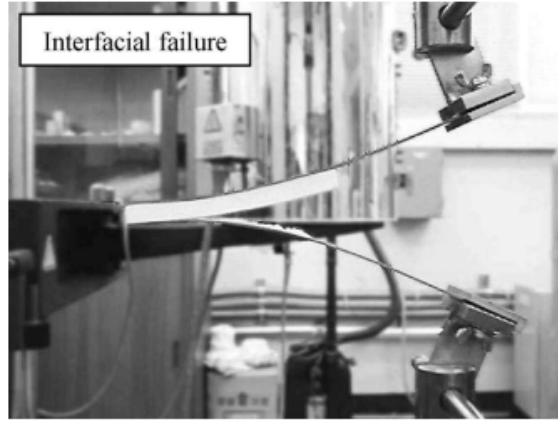


Figure 2.4 Interfacial failure in cleavage peel test of glass/epoxy facesheet and polyurethane foam core sandwich [13]

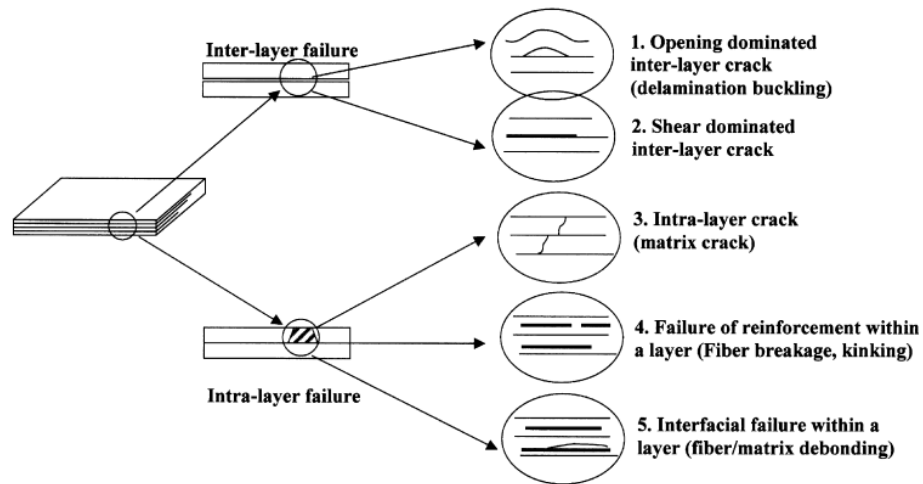


Figure 2.5 Possible failure modes for layered materials based on material constitution [33]

Several researchers have studied the failure modes of sandwich structure under dynamic load. Xu and Rosakis [33] investigated the failure modes in sandwich structure under low velocity impact. In this paper, all the possible inter-layer and intra-layer failure modes have been listed and discussed. Semenski and Rosakis [36] tested thin sections of soft PVC foam core and E-glass facesheet sandwich structures used in Naval application under impact load to visualize the failure modes.

Recently, Wang et al [37] investigated low velocity impact characteristics and residual tensile strength of carbon fiber composite lattice core sandwich experimentally and numerically validated the results.

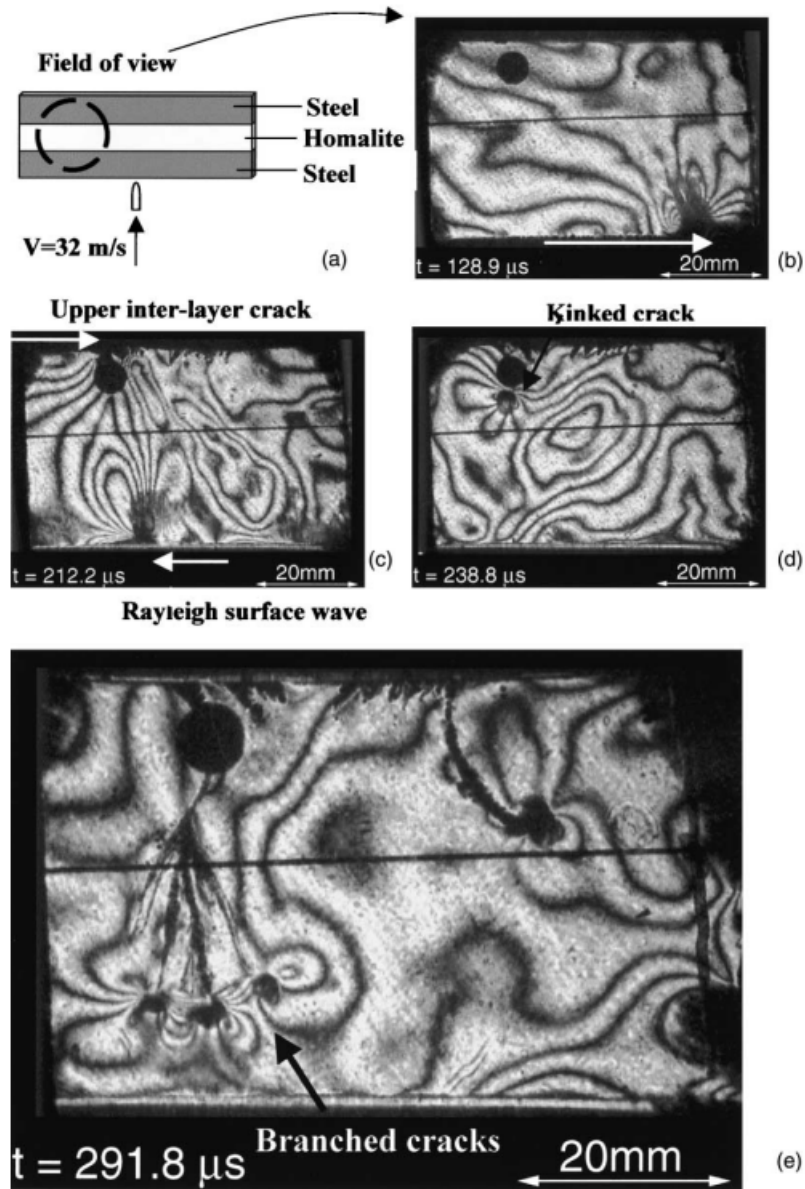


Figure 2.6 Dynamic failure modes and sequence in a layered specimen from a different field of view. Following interfacial delamination at the lower then the upper interfaces, cracks kink into the core layer to form intra-layer damage [33]

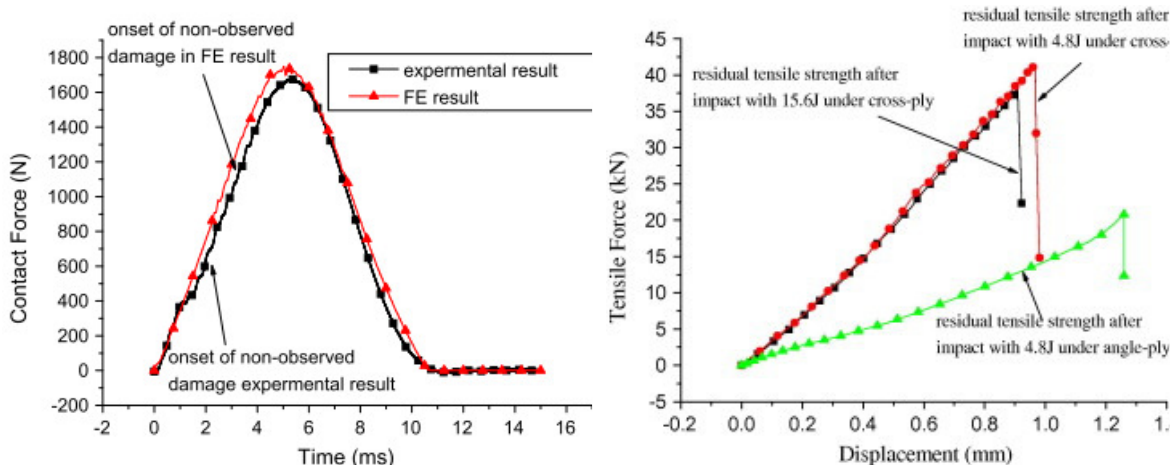


Figure 2.7 (Left) Experimental and Numerical results under 3 J impact and (right) residual strength of truss core sandwich under different impact energy and stacking sequence [37]

2.2 Bioinspired and Biomimetic Design

Natural processes have developed plenty of systems that perform multiple tasks within a variety of environment and constraints [38]. Similarly, to develop engineering systems with the ability of multitude performance nature has been the best resource for inspiration and sometime, mimicry. There have been several examples of natural resources being used as inspiration to leverage the scientific principle in developing engineering systems. Popular examples include bulletproof jackets by mimicking spider-webs; robots that mimic various forms of natural movement such as those by fishes, leeches, and earthworms; and materials that mimic various properties of natural materials [38]. Solution to several engineering problems has been inspired by biological phenomena [39]. Detailed understanding of the biological systems is required to utilize the full potential and to enable effective and efficient biologically inspired engineering. The term Bioinspiration or Biomimesis refers to elucidating natural models, systems, and processes to employ the principles to solve human problems in several areas of engineering [39]. Bioinspiration has been used in developing several engineered systems.

Most of the natural materials being hierarchically structured and composite in nature, the development of composite material as well has been significantly inspired by the biological resources. The mechanics principles in the load bearing and energy absorbing functionality can lead to a better design of materials with enhanced properties. Meyers et al [47] reviewed several classes of biological materials like ceramic (sponge spicules, shells, shrimp hammer, Marine worn teeth, Bone), Polymers (Ligament, silk, horn), elastomers (skin, muscle), cellular materials (wood, leather) etc.

Several structural materials have been developed and tailored through bioinspiration to suite the potential applications. The research group of Zhou works in bioinspired materials development and has reported several such advancements on structural materials [48]. It was found that the strength of composites with enlarged-end fibers is greater than that of the composites with plain fibers of the same properties and aspect ratio. To employ this principle, solid state reaction of SiO_2 with C has been used to fabricate dumbbell-shaped biomimetic whiskers to enhance the strength compared to the commercial plane fiber SiC whisker [48]. Motivated by strength of bamboo and its potential in engineering applications, Li et al [49] developed a technique to change the form of bamboo from its natural circular cross-section into a plate for convenient use. Craciunescu and Moldovan [50] detailed the design of bioinspired composite material for medical applications like bone. They covered the methodology to choose appropriate composition and structure to achieve unique morphology and properties of natural bone.

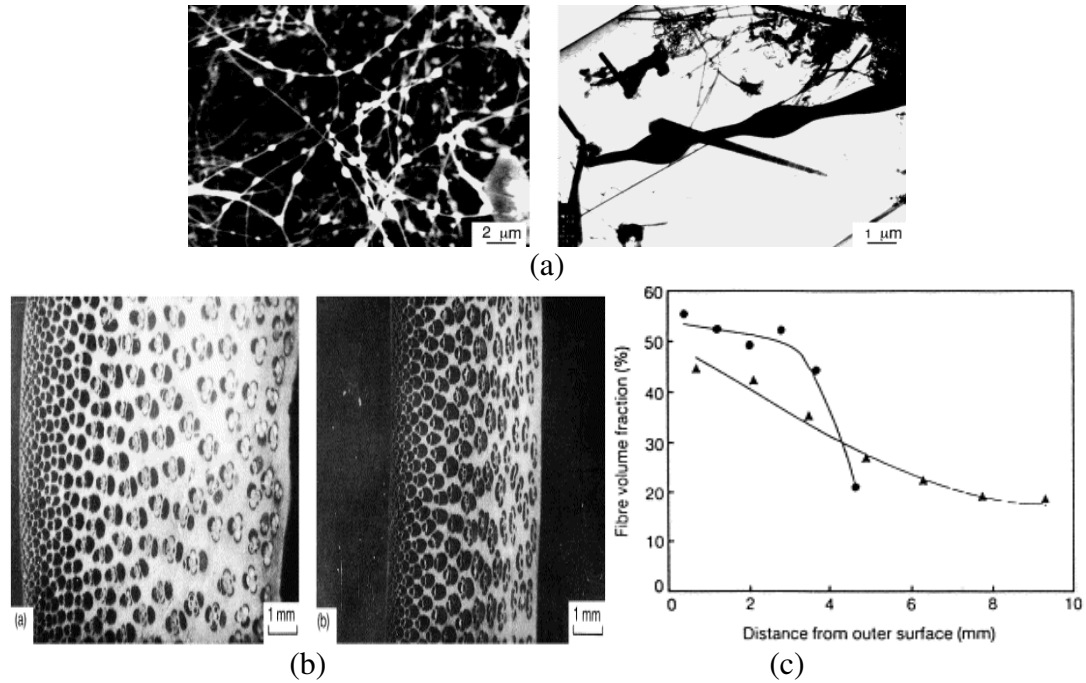


Figure 2.8 (a) The morphology of dumbbell-like SiC whiskers [48] and (b) optical photographs of cross-sections of normal and reformed bamboo and the fiber volume fraction before and after processing [49]

“Nature's pool of ideas is valuable only if it can be translated into concepts that engineers can incorporate in their designs” [51]. To mimic the mechanics principle in developing bioinspired materials with enhanced mechanical behavior, detail understanding of the mechanical behavior of biomaterials is necessary [52]. Several researchers have characterized natural composite, wood, probably the best bioinspiration to develop structural material. Balsa wood, a naturally occurring porous solid is one of the best core materials for high energy absorbing sandwich structure as it has high specific stiffness, strength, and energy absorbing capacity [53]. Vural and Ravichandran characterized the quasi-static and dynamic compressive response of balsa wood and identified the failure modes like buckling, end-cap collapse and kink band formation [53, 54]. Dynamic response and energy dissipation characteristic were reported and kinematics of deformation of the observed failure modes and associated micro-inertial

effects are modeled to explain the behavior. The transition in failure mode and its effect on energy absorption has been reported in [55].

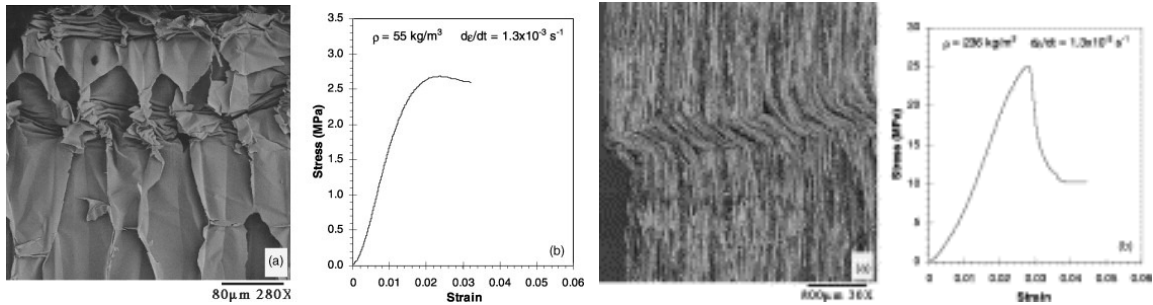


Figure 2.9 Failure mechanism illustrating (a) plastic buckling for low-density balsa wood (b) kink band for high-density balsa wood and associated stress–strain curves [53]

2.3 Multifunctional Structures

Multifunctional materials are materials capable of performing two or more functions, either simultaneously or sequentially in time. They are typically composite in nature, inhomogeneous at the meso- and/or micro-scale levels, and may best be described as a “material-system” or “system-material” [56]. These materials embody several attributes, including some or all of structural, thermal, electrical, and optical aspects, and are emerging as solutions providing decreased volume, mass, and power requirements [57] leading to improved system performance and system efficiency. The review article by Gubson [2] stands as a unique literature reviewing the recent advance in multifunctional composites. He reviewed several structural and non-structural advancements toward multifunctional structures.

Apart from the structural functionality, the most important functionality is probably electrical and thermal functionality. Very small concentrations of carbon Nanotubes or other conducting nanoreinforcements in polymers lead to disproportionately large

improvements in the electrical conductivity of the nanocomposite as shown in Figure 2.10 [58].

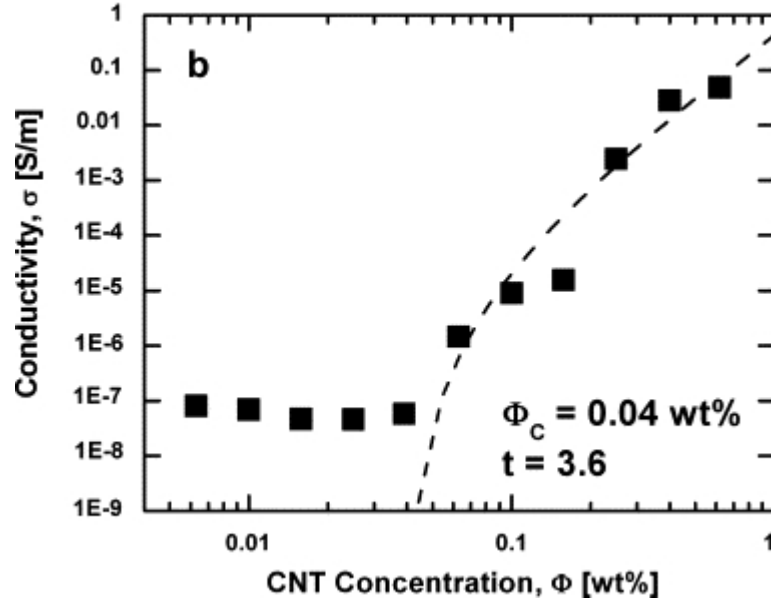


Figure 2.10 Electrical conductivity of CNT/epoxy nanocomposites at various CNT concentrations [58]

Queheillalt et al [59] developed and experimentally investigated the performance of multifunctional sandwich panel combining efficient structural load support and thermal management characteristics. They used truncated, square honeycomb sandwich structure. Effective heat transport is achieved by multifunctionally utilizing the core as a heat pipe sandwich panel and deionized water as working fluid. A thermodynamic model was used to guide the design of the heat pipe sandwich panel.

Vaidya et al [60] reported the dynamic behavior of a multifunctional sandwich composite where the core is designed to incorporate functions such as sound/vibration damping and ability to route wires or embed sensors. The multifunctional sandwich composite had number of curved core piles in the z -direction which are woven to the facesheets at top and bottom. They investigated low velocity impact response and failure

modes of 3-D sandwich composites with hollow core and polyurethane (PUR) foam filled core. The mode of failure for the unfoamed specimens was primarily the buckling of the core piles and the rupture of the facesheets, while for the foamed specimens, the foam core crushing along with the core piles failure were the primary modes of failure. Researchers also investigated the potential to realize multifunctionality in the cellular foam used in sandwich structures [57, 61].

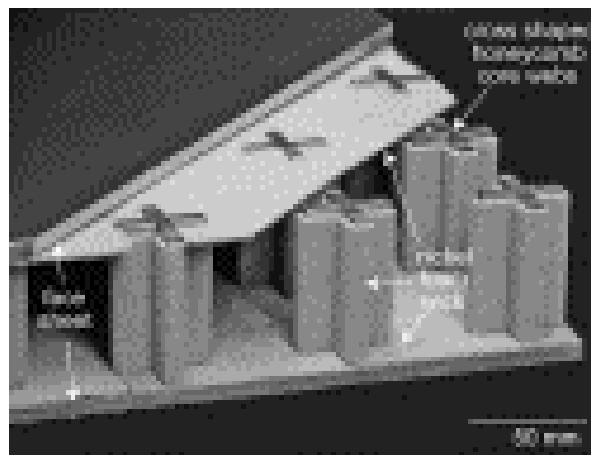


Figure 2.11 Cross-section of fully assembled flat heat pipe sandwich panel [59]

Roper [62] developed a model to study a micro-architected multifunctional sandwich structure as heat pipe with a micro-scale truss core and arterial wick. Optimization was performed on the objective function formulated for density, compressive modulus, compressive strength, and maximum heat flux. The trade-offs between density, compressive stiffness, compressive strength, and maximum heat flux in the design of multifunctional sandwich panel were investigated heat pipes with micro-scale truss cores. For optimal designs density is found to increase with increasing modulus, strength, and maximum heat flux. Optimal performance is found to vary widely with both working fluid and core material selection.

Keller et al [63] reported an exploratory study on the feasibility of encapsulating PV-cells into the transparent skins of multifunctional lightweight sandwich structures for application in building construction. The sandwiches were composed of glass FRP (GFRP) skins and polyurethane (PU) foam cores with two types of embedded PV-cell. They [63] assessed two issues: maintaining the structural integrity during heating of the structure caused by the PV-cells and ensuring the correct operation of the cells during loading of the structure.

Adames et al [64] proposed multi-functional sandwich composites to integrate separate objectives of radiation shielding, structural integrity, damage tolerance, thermal insulation, and debris/micrometeoroid shielding into a viable structural design for spacecraft applications. Hydrogen-rich polymeric materials were chosen for radiation shielding. Based on radiation shielding simulation prototype sandwich configurations were manufactured that featured transverse reinforcements for damage tolerance and an internal self-healing membrane was employed. Their results showed promise of using those sandwich structures to maximize the efficiency of advanced material usage in structural spacecraft applications.

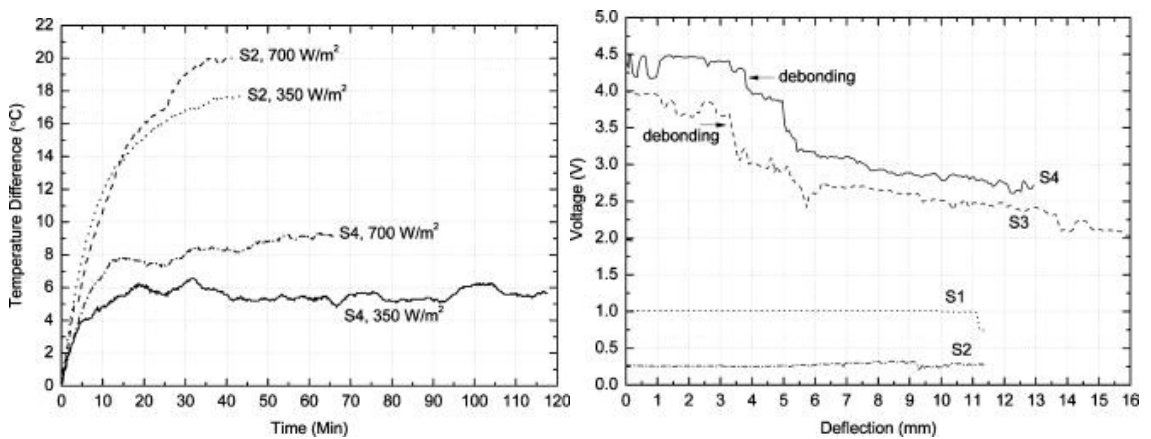


Figure 2.12 (Left) Temperature increase below cells due to heat production of cells and (right) voltage change during mechanical loading [63]

Furthermore, Rion et al [65] worked on the encapsulation of photovoltaic (PV)-cells into the skins of ultra-lightweight sandwiches for airplane structures. Ultra-light multifunctional structures can enable reducing weight and energy consumption in applications like solar cars, solar planes or satellites. They developed composite sandwich structures with a weight of $\approx 800 \text{ g/m}^2$ with facesheets being carbon fiber-reinforced plastic (CFRP) on one side and mono-crystalline silicon solar cells on the other aided with thin stress transfer ribbons between the cells and honeycomb core. They studied the strength of the solar cells under bending and tensile loads and the influence of sandwich processing on their failure statistics. The results of these asymmetric sandwich structures showed balanced mechanical strength confirming the potential of this concept for producing stiff and ultra-lightweight solar panels.

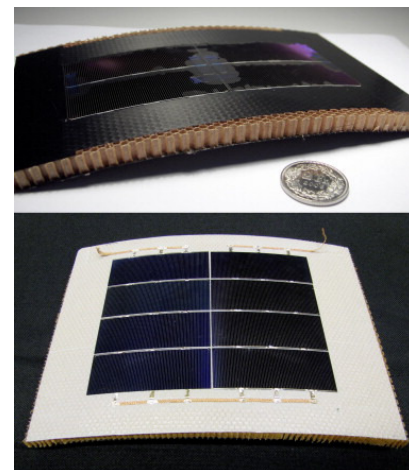
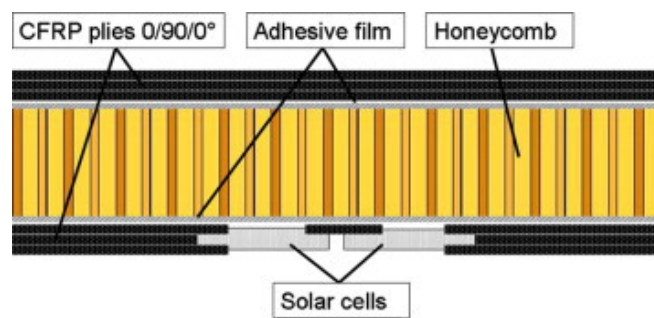


Figure 2.13 (Left) Schematic lay-up of the sandwich structure with two solar cells as skin and (right) Curved prototype sandwich modules with 4 (top) and 8 (bottom) integrated m-Si S32 solar cells as a skin [65]

According to The Alternative Energy eMagazine, the BAE Systems, claims to have developed “the most radical method of storing electricity since the invention of the battery!” The structural battery, BAE declares, represents a technological breakthrough that could lead to a redesign of all electrical technology, bringing with it major environmental benefits. In their technology, the carbon-fiber has been used in battery and the same material performs as structural material providing low weight and high strength.

Recently, the research group of Greenhalgh [66, 67] in collaboration with Volvo developed a structural component based on carbon fiber that has power storage capacity as well. Their material system is made of two layers of flexible woven carbon fiber (the electrodes) separating them with an insulating layer of glass fiber and infusing the whole sheet with a resin to give a hard structural material.

2.4 Summary

This chapter summarizes the several aspects of the research in the area of

- 1) Sandwich composite structures,
- 2) Bioinspired design, and
- 3) Multifunctional materials.

The present dissertation aims at developing bioinspired sandwich structure for marine applications with multiple functionality namely, mechanical and electrical and to establish the principles in developing such a material system. The understanding of mechanics principles of the behavior of palmetto wood have been used to develop bioinspired sandwich.

Chapter 3 Multiscale Mechanical Characterization of Palmetto Wood, a Hierarchically Structured Natural Composite as Template for Bioinspiration

Palmetto wood has been found useful in the Protective structures used in the Civil and Revolutionary war. Its damage resistance and sustainability to the impact of canon shots has demonstrated its potential as a bio-inspiration to develop engineered composites with enhanced mechanical properties. Following the multiscale structural characterization of the Palmetto wood, a multiscale experimental methodology has been developed to characterize its failure mechanisms and load transfer mechanics at multiple length scales. The Palmetto wood had been characterized under quasi-static and dynamic loads in three-point bend configuration to elucidate its mechanical behavior. The damage evolution associated with the loading rate has been characterized. Motivated by the graded distribution of macrofibers in the porous cellulose matrix, the role of macrofiber concentration in its mechanical behavior and damage evolution has been investigated. A damage model has been developed to decouple the plastic and elastic strain of the deformation under quasi-static and dynamic loading and quantify the damage parameters and damage evolution in the specimen.

This chapter reports the multiscale characterization technique and the failure mechanisms in Palmetto wood at multiple length scales. The following findings are detailed in this chapter. First, the load transfer mechanism and the role of macrofiber in load transfer at multiple length scales. The failure mechanisms of the Palmetto wood associated with three-point bend loading. The transition of macro-scale mechanical behavior associated with the microscale load transfer mechanism. Secondly, the role of macrofiber volume

fraction in the mechanical behavior of the Palmetto wood has been elucidated. Finally, a damage model has been developed to study the effect of loading rate and macrofiber volume fraction in the damage evolution in Palmetto wood under quasi-static and dynamic load.

3.1 Motivation and Challenges

The Palmetto wood had been successfully used in the protective structures in the Civil and Revolutionary war and sustained the impacts of the canon bullets [68]. Motivated by the historical benefit of using Palmetto wood, it has been assumed to be a potential biological inspiration to develop engineered materials with enhanced material properties. In nature the biological materials organize the simple building blocks in hierarchical order at various length scales to achieve enhanced properties. One such material, the Palmetto wood has the hierarchical structure and enhanced mechanical properties and has been considered for elucidation as a potential bio-inspiration.

While the multiscale structural characterization of Palmetto wood reveals its hierarchical structure across multiple length scale, a better understanding of its load transfer and failure mechanisms is required to utilize the principles of its behavior in developing engineered materials. The challenges in this goal are to characterize the microscale mechanical behavior and relate to the global behavior at macro-scale.

3.2 Experimental Technique for Mechanical Characterization

An experimental methodology has been developed to characterize the mechanical behavior of the Palmetto wood at multiple length scales based on optical characterization of the deformation. The Palmetto wood specimens under study have been deformed

under quasi-static and dynamic load in three-point bend configuration and the mechanical properties have been quantified.

3.2.1 Experiment - Deformation of Specimen

The motivation of choosing three-point bend test as a characterization technique lies in the versatility of the stress state in the specimen due to the presence of both compressive and tensile axial strains, as well as shear strain, in the specimen. Three-point bend specimens (10 cm x 9 mm x 9 mm) were prepared from a harvested palmetto tree for the present study with a volume fraction of macrofibers of 12%. Tests were performed in an Imada model MX 500 load frame with a Z2H-440 2 kN load cell that has a load resolution of 0.1 kg. The load on the specimen was obtained using the load cell attached to the base of the three-point bend test fixture, while vertical displacement of the load point was determined using a dial caliper attached to the load cell with a displacement resolution of 10 microns. Supports for the three-point bend test fixture were 62.5 mm apart, and the specimen was loaded in two different optical configurations: (1) around the center of the specimen for macro-scale tests, and (2) near the central loading point of the specimen for microscale tests. FL2-14S3C Point Grey high speed camera was used to capture the images of specimen under test. The specimen surface was illuminated by MI-150 high intensity fiber optic illuminator from Edmund Industrial Optics. The specimen under quasi-static bend and its failure under three-point bend test are shown in Figure 3.1. The specimen was loaded with the fibers oriented transverse to the loading direction. The specimens were prepared from the same trunk of the Palmetto tree and polished for imaging by fine sand paper. The quasi-static bending was performed under displacement control at a macro-scale flexural strain rate 1.6×10^{-4} /sec.

The methodology of multiscale characterization technique is demonstrated in Figure 3.2 [69]. Several experiments were performed sequentially and repeatedly on different samples at several magnifications in order to reliably measure deformations at multiple length scales. The fields of view at multiple length scales are shown in Figure 3.2. As depicted in the Figure, images were captured at several magnifications with the aid of optical lens to capture the deformation at the associated length scale. In the images, M and F indicate porous cellulose matrix and macrofiber, respectively, while the interface between the macrofiber and porous cellulose matrix is denoted by a dashed line. As mentioned earlier, the tests were performed on different specimens and the images only show the relative magnifications at which the deformation measurements were performed.

A 12.6 gm cylindrical projectile (velocity ~ 30 m/s) with 50.26 mm^2 circular impact area is shot to the specimen that is simply-supported (support-span 74 mm) at the ends. The specimen size is approximately 10 cm x 16 mm x 16 mm with fibers aligned perpendicular to the shooting direction. The projectile is ejected through a barrel by pressurized air and a laser-trigger mounted on the barrel projectile synchronizes oscilloscope and digital camera to capture output voltage from load-cell and images, respectively. A 1000 lb load cell (DLC 101-k, Omega) attached within a support of the specimen is used to capture the load applied on the specimen. The experimental set up for the low velocity impact test and circuitry are shown in Figure 3.3. High-speed digital camera (Phantom v12) has been used to capture instantaneous images of specimen (top view) during the dynamic deformation. The specimen is illuminated by two Vision Research Northstar lights (250W each). However, for the high speed camera, there is a

trade off between the magnification level/resolution and the frame per second (fps) to capture the images and this gives rise to a limitation to apply the multiscale measurement methodology established in the context of characterization under quasi-static deformation [69] on the dynamic deformation measurement. The specimens were prepared by cutting the wood from a harvested Palmetto tree stem and then were polished to achieve optical illumination.

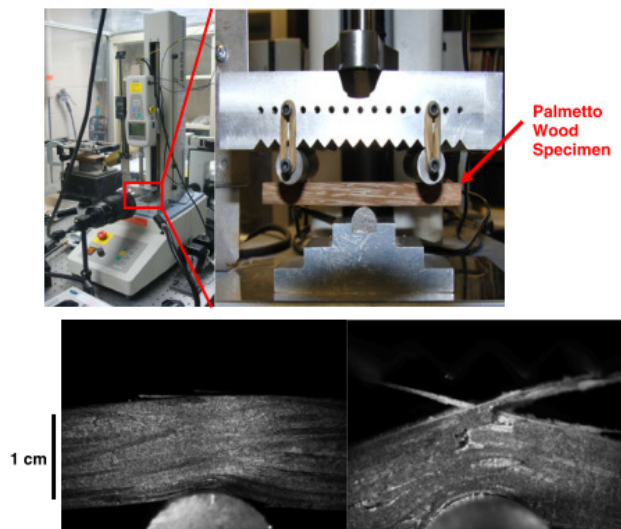


Figure 3.1 Three-point bend test set up to characterize the deformation of Palmetto wood, and Images of deformed Palmetto wood in three-point bending.

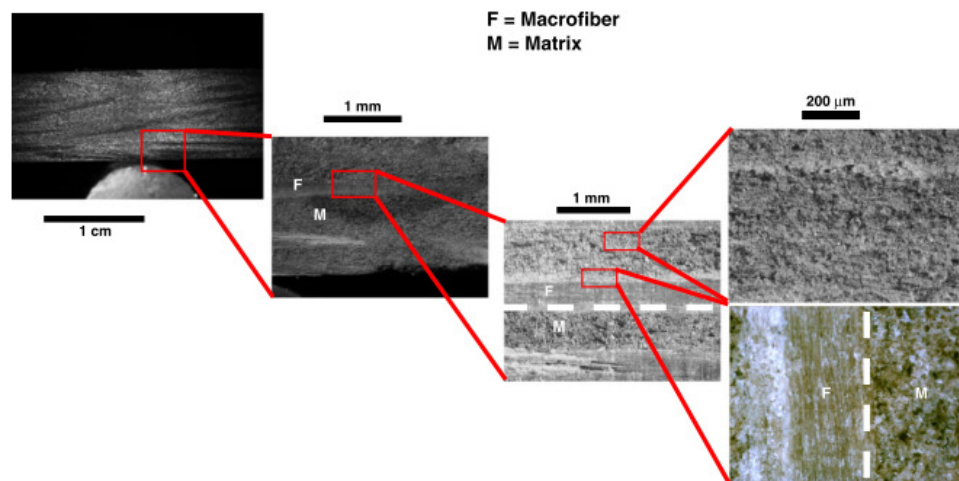


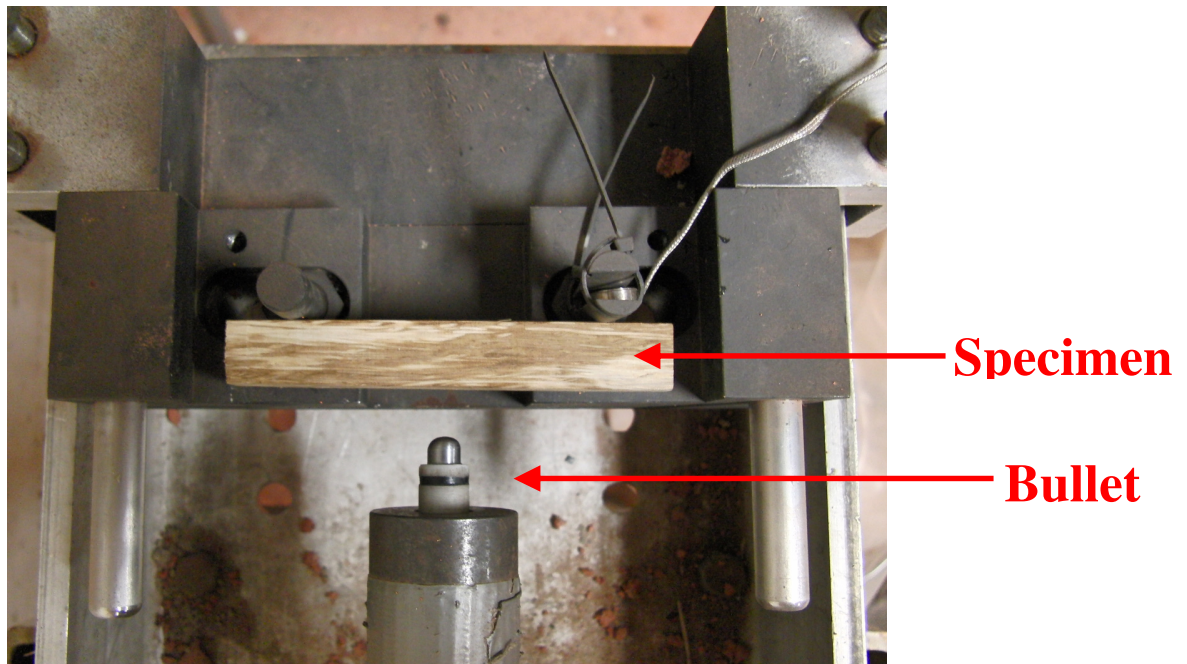
Figure 3.2 Fields of view at several magnifications demonstrating the multiscale deformation measurement methodology where the interface is denoted by a dashed line and the matrix and macrofiber by M and F, respectively [69].

3.2.2 Deformation Measurement

Due to its heterogeneous structure at multiple length scales, an advanced technique, namely, Digital Image Correlation (DIC) was chosen for full-field deformation measurements under mechanical loading [2]. The principle of DIC is to use undeformed and deformed images of a specimen to calculate the displacement and strain experienced by the specimen. The DIC method has been widely accepted and has grown its potential to be used in almost all the areas of engineering. Details of the DIC technique and its advancement and applications can be obtained from several review articles [71, 72]. DIC technique being length scale independent, has been successfully used at the macro to nano length scale and several time scale measurements with the use of appropriate camera and speckle pattern on the surface [73, 74, 75]. Lord et al [76] reviewed the experimental techniques for miniaturized testing for strength and strain measurement techniques and detailed the evolution and strengths of DIC method. DIC has been very successful to capture spatially inhomogeneous deformation fields. This potential has been applied in several material systems that include biological tissues [77, 78], particulate composite [79, 80], concrete [81], polymeric foam [82], binary aluminum alloy [83], closed-cell aluminum alloy foam [84], porous solid [85], glassy polymer [86] etc. Recently, Pan et al [87] used DIC for deformation measurement at high temperature. DIC has proved its potential as a rigorous optical measurement technique not only strain measurements multiple length scale, also other related properties like coefficient of thermal expansion [88], frictional properties [89], cohesive fracture properties [90], crack-resistance curve of polymer-matrix composite [91], constitutive model under

buckling [92] etc. Several dynamic characterizations have been performed using the DIC like dynamic buckling [93], high strain rate effects in unidirectional composites [94].

For the present application, the natural texture of wood being sufficient as speckle pattern for the image correlation waives off the need to apply any speckle pattern. However, for some specimens the texture was not sufficient so grid spots were applied to obtain a pattern for DIC. Commercially available software Vic-2D from Correlation Solutions Inc. (Columbia, SC) was used for DIC. Based on the surface texture and features, DIC parameters were optimally chosen to obtain accurate deformation fields. In all the correlations square subset has been used and correlation was possible on the images up to damage initiation. In addition to the DIC analysis performed on the images captured in real time, the projectile could be tracked through the Phantom software to determine the projectile displacement with time.



(a)

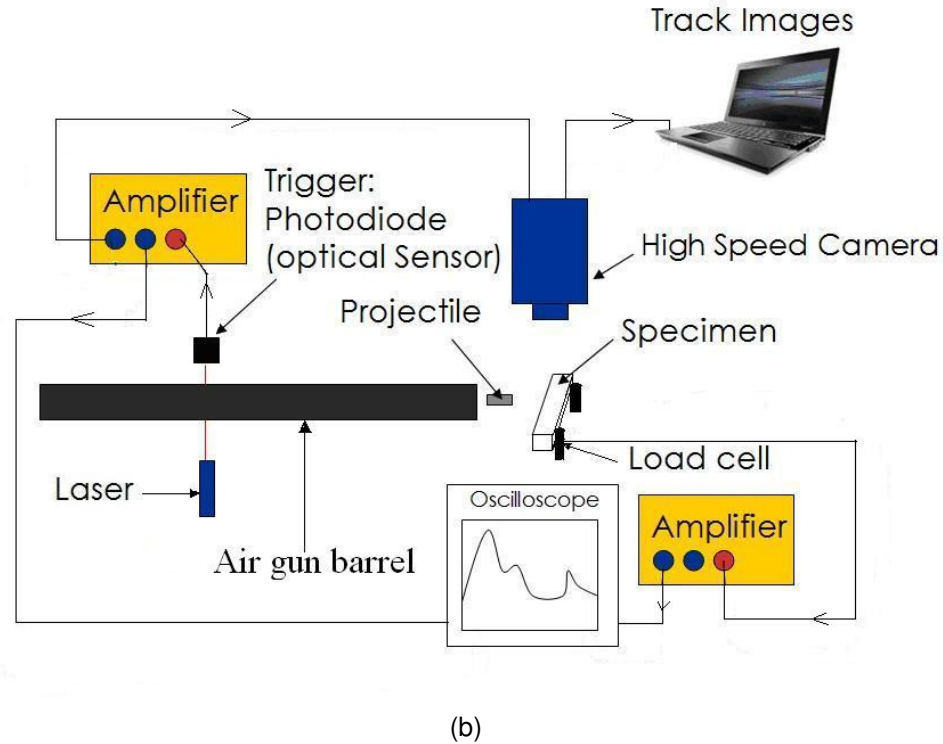


Figure 3.3 (a) Low velocity impact test set-up in three-point bend configuration and (b) circuitry

3.3 Experimental Results

This section discusses results obtained by deformation measurement of Palmetto wood under three-point quasi-static and dynamic bending at multiple length scales. Strain measurement by DIC was performed at several length scales to elucidate the role of hierarchical structure in Palmetto wood in its macro-scale mechanical behavior. The multiscale characterization helped to map the macro-scale behavior from the microscale deformation and to understand the load transfer mechanism through the stronger macrofiber reinforced in porous cellulose matrix. The understanding of the mechanical behavior and the role of macrofiber would be utilized in developing the engineered sandwich composite structures.

3.3.1 Characterization under Quasi-static Load

The quasi-static bending experiments revealed the load transfer mechanisms and the role of macrofiber in load transfer. Whereas the macroscopic measurements help to determine the bulk behavior of the Palmetto wood, the mechanics of the hierarchical structure can only be elucidated by the microscale measurements. Based on the experimental observation failure mechanisms have been identified. This section details the experimental results of the quasi-static three-point bend tests.

3.3.1.1 Deformation measurement at macro-scale

Representative flexural stress-strain response of the Palmetto wood specimen in three-point bending and the fit of a Weibull distribution for the failure response of a bundle of fibers are depicted in Figure 3.4 [69]. The flexural stress, flexural strain and strain energy for a specimen with cross-section 9.5 mm x 9.5 mm and support span of 62.5 mm are calculated using the classical relations for homogeneous isotropic materials given by:

$$\sigma_f = \frac{3PL}{2bh^2}, \quad \epsilon_f = \frac{6\delta h}{L^2} \quad 3.1$$

where P is the applied load, L is the support span, b is specimen thickness, h is specimen height, and δ is the deflection. For these specimen dimensions, the cross-sectional area is nearly 400 times the cross-sectional area of an individual macrofiber, so the global behavior can be considered to be macroscopic. The bulk flexural modulus of this representative specimen was determined to be approximately 500 MPa, and the specimen started to loose load bearing capacity at around 4% elongation with a corresponding nominal stress of about 10 MPa.

The Weibull distribution of the failure response for a bundle of fiber is given by:

$$\sigma = E\varepsilon \exp\left[-\left(\frac{\varepsilon}{\varepsilon_0}\right)^\beta\right], \quad 3.2$$

where ε_0 and β are the Weibull parameters and E is elastic modulus. It has been seen that the flexural behavior of the Palmetto wood can be described by the Weibull fit [68]. The Weibull parameters are chosen as $\varepsilon_0 = 0.05$, $\beta = 1.5$ with elastic modulus (E) as 500 MPa [69]. The strain energy up to the failure initiation has been determined to be 3.0 J/cm².

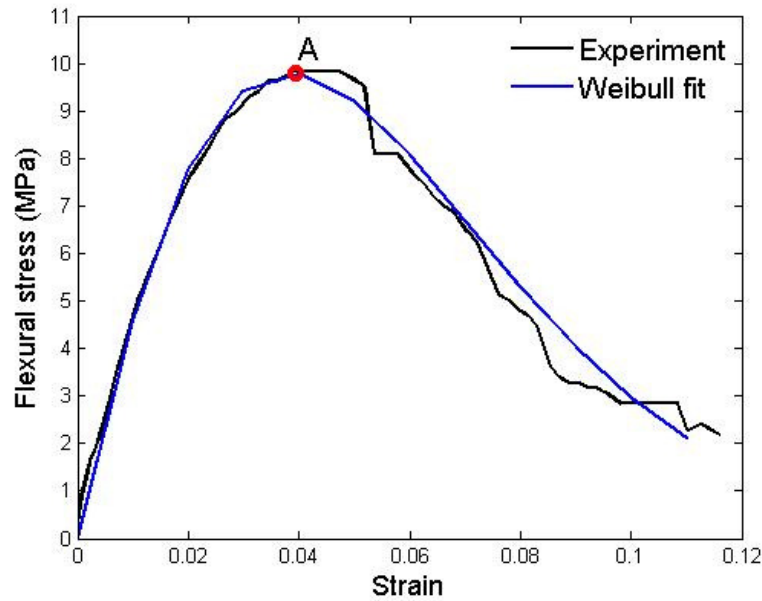


Figure 3.4 Representative quasi-static macroscopic flexural stress strain response for Palmetto wood with a Weibull fit indicating that the failure response conforms to a Weibull distribution

Experiments were performed with several specimens prepared from similar location of the Palmetto trunk. Due to the moisture content and complex structure of the Palmetto wood due to orientation and macrofiber variation, marginal variation was found in the values of modulus, however the scatter for several specimens was marginal and the

qualitative deformation behavior was similar for the specimens. Deviation of around 5% in flexural modulus has been seen from the results of several specimens.

Representative displacement and strain fields obtained using DIC at the macroscale can be seen in Figure 3.5 before the onset of failure corresponding to point A in Figure 3.4. As can be noted from the figure, the specimen can bear a fair amount of load after failure initiation and does not exhibit catastrophic failure, which is preferred for engineering applications where energy absorption is important. As discussed in the earlier study, fiber-bridging is the primary mechanism for Palmetto wood to carry load post-failure [68]. The displacement field is symmetric with respect to the loading point indicating that at the macroscopic scale, the behavior of the wood appears to be homogeneous. The strain field corresponds to the point A, as indicated in the flexural stress-strain response of the specimen. However, the macroscale strain fields reveal a slight asymmetry with respect to the loading point that may arise due to inhomogeneity from the macrofiber distribution in the wood along the specimen length.

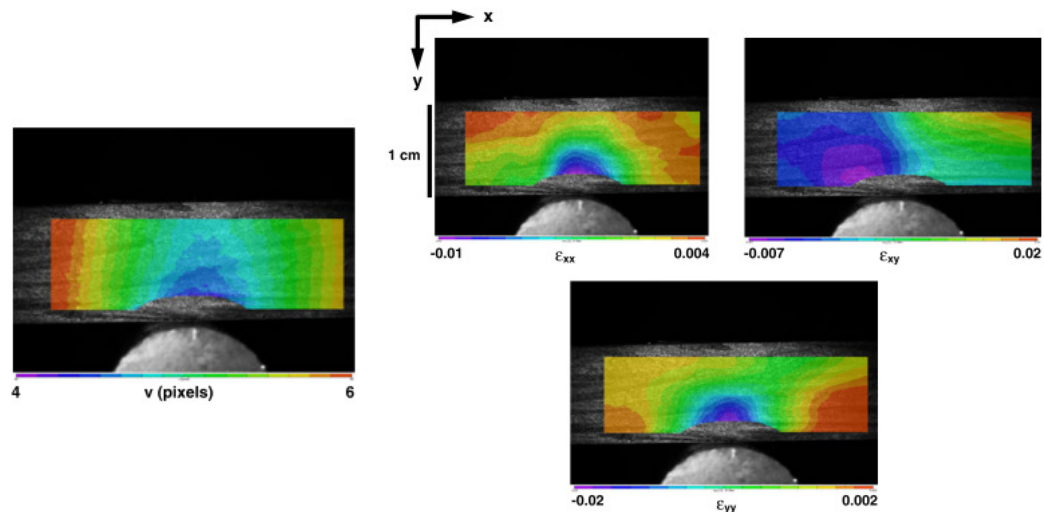


Figure 3.5 Macroscopic (left) displacement (pixels) and (right) strain fields in Palmetto wood obtained under three-point bending before the onset of failure. The fields evidence macroscopically homogeneous behavior of the material. The load level corresponds to point A of Figure 3.4

The bending response of the specimen was evaluated through the classical beam bending theory for homogeneous isotropic material. The vertical displacement along the length of the specimen is extracted from the DIC analysis as shown in Figure 3.6. The displacement field appears to be similar to that in three-point bending of homogeneous isotropic material. A quadratic fit to the displacement is used to obtain the flexural strain. The flexural strain is calculated by the beam bending formula of homogeneous isotropic material. The strain was determined to be 0.007, which matches well with the axial strain of 0.006 directly obtained from the DIC displacement field in the tensile region of the specimen. Thus, it can be concluded that at this length scale, the behavior of the specimens is primarily homogeneous, although there can be some slight asymmetry in the displacement due to the distribution of macrofibers.

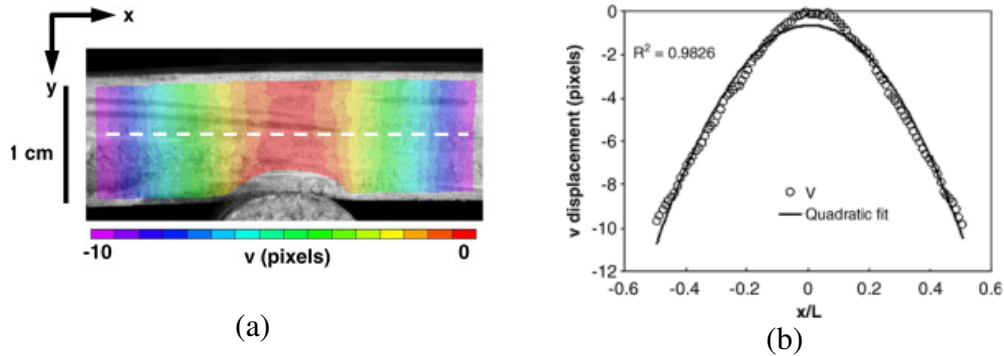


Figure 3.6 (a) Vertical displacement field of the Palmetto wood specimen under quasi-static three-point bend test that resembles typical displacement field in three-point bending for homogeneous isotropic material, and (b) vertical displacement of the specimen along the line (shown in (a)) and quadratic fit used to calculate the strain from beam bending theory

3.3.1.2 Deformation measurement at microscale within elastic regime

Since Palmetto wood is a hierarchically structured material over several length scales, images were taken at multiple magnifications to elucidate on the roles of the porous cellulose matrix and embedded fibers in the failure process. Images were captured at

magnifications that were 10X higher than the macroscale to better quantify the mechanical behavior of the Palmetto wood at what is considered to be the intermediate microscale.

Spatially cyclic strain distribution along the depth consistent with the fiber distribution start to become evident at this magnification (Figure 3.7) and high shear strain between fibers can be more easily discerned as shown in Figure 3.7(a). The images are captured at a loading corresponding to a flexural stress of 1.4 MPa and flexural strain of 0.2 % that are well below the failure initiation and at the compressive side of the specimen approximately 2 mm from the central support at the bottom side of the specimen. The strain field is consistent with a highly inhomogeneous material response, with localized strain that can lead to fiber-matrix debonding or matrix failure. Furthermore, there is significant localization of normal strain in between the fibers within the matrix that could potential lead to pore collapse. Images were also captured on the tensile side (i.e., top side of the specimen) at a distance of approximately 5 mm from the center support to elucidate on the strain distribution. However, the strain analysis of the tensile side of the specimen revealed that the strain distribution at the macrofiber-matrix interface remains the same as was observed in the compression side at microscale, as shown in Figure 3.7(b). High shear strain is noted at the macrofiber-matrix interface and the strains vary cyclically with the distribution of the macrofiber and cellulose matrix. There is a minor difference between the strain distributions in the tensile and compressive regions which might be due to some variability of the macrofiber distribution over the Palmetto wood. Nevertheless, the basic microstructural response is found to be similar. With this, the high shear strain at the macrofiber-matrix interface and similarity in strain distribution is

established irrespective of the global deformation state in either the tensile or compressive region of the specimen.

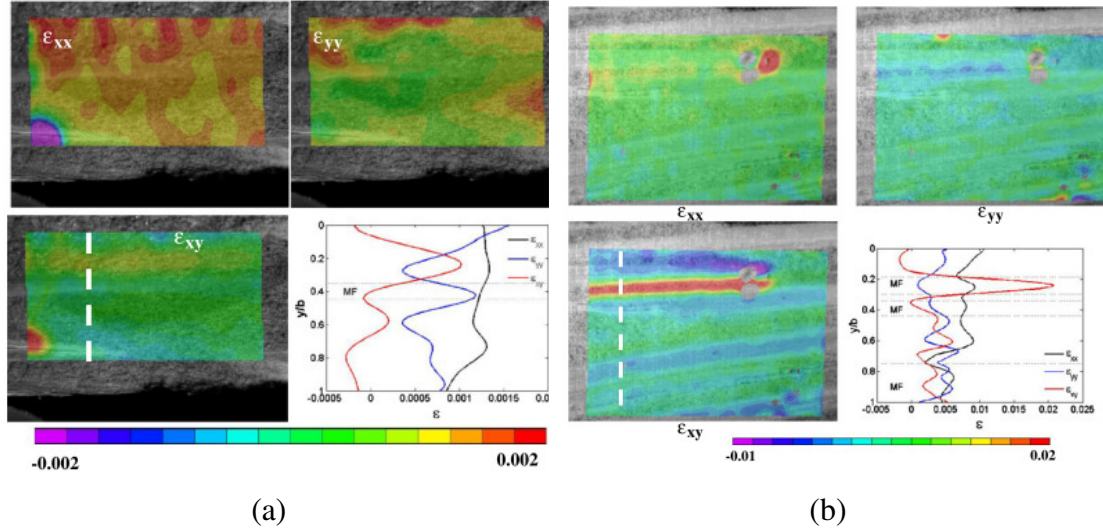


Figure 3.7 Strain contours and strain distribution along depth in (left) compression side and, (right) tensile side of Palmetto wood during three-point bending at intermediate microscale magnification exhibiting more inhomogeneous shear strain distribution consistent with the porous microstructure of the matrix

Microscale strain measurements (shown in Figure 3.8) at a higher magnification, indicated substantially higher strain at the matrix-macrofiber interface than within the macrofiber, which was one order of magnitude less due to the rigidity of the fiber. The strain fields are shown for a flexural stress of approximately 2.1 MPa and globally 0.3% flexural strain, which is in the elastic regime. The displacement field in the specimen, the vertical displacement profile and strain distributions are shown in Figure 3.8(a) and (b). The bending appears similar to a classical bending of a stiff fiber in a compliant matrix, however with asymmetry along the fiber. The asymmetry might occur due to inhomogeneity in matrix-stiffness. The curvature of the macrofiber in local bending at the microscale is used to calculate microscale strain level, and is consistent with the axial strain of 0.003 measured from the microscale DIC displacement fields. The curvature of

the specimen at macroscale and that of the macrofiber at the microscale are found to be approximately similar at equivalent macroscale flexural strain level, which is approximately 0.001 mm^{-1} . Thus, the flexural response translates from the macroscale to the microscale through the mechanical behavior of the macrofiber rather than through the porous cellulose matrix. However, a positive transverse strain occurs in the fiber that might result from the debonding of microfibers within the macrofiber due to local bending of the macrofiber as depicted in Figure 3.8(a).

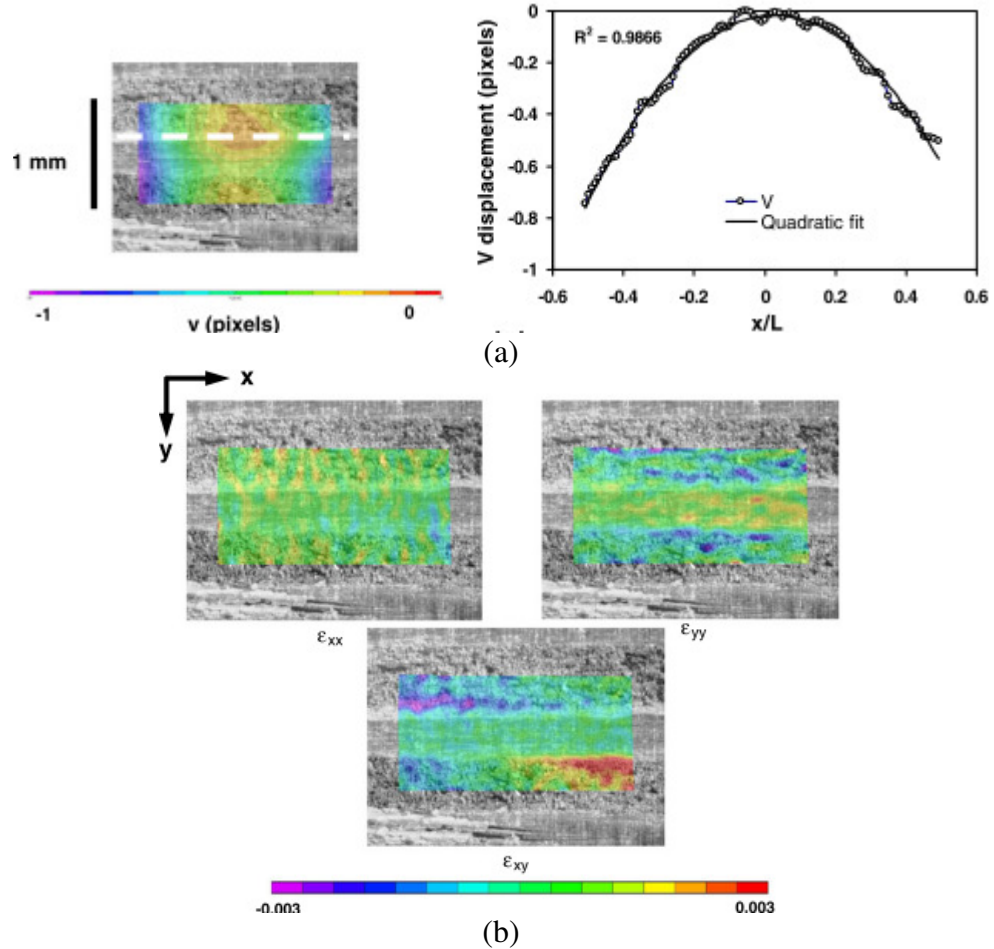


Figure 3.8 (a) Local bending of macro-fiber (b) Strain fields in Palmetto wood at second intermediate microscale obtained near fiber-matrix interface

High interfacial shear strain makes the material prone to debonding. The strain fields in the fiber were more homogeneous and much less significant. This is not unexpected, since the mechanical properties of the macrofiber are significantly greater than those of the porous cellulose matrix, and therefore the response is nearly rigid. To better elucidate the interfacial strain distribution, images were captured at 20X magnification. The strain fields in Figure 3.9 help to understand the difference in strain level in macrofiber and matrix. The strain fields indicate high shear strain at the macrofiber-matrix interface and the normal strains are found to be much higher in the matrix. However, the interfacial mechanics was found to be the same as at the lower magnification, with high interfacial shear and pore collapse in the matrix.

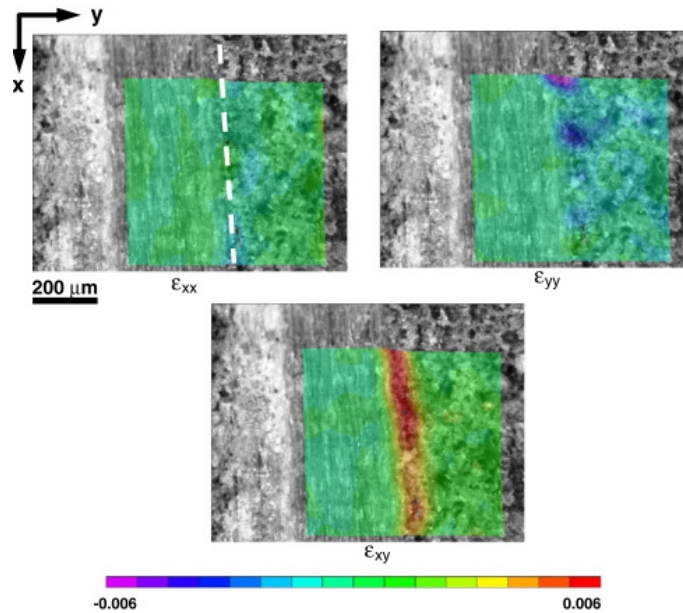
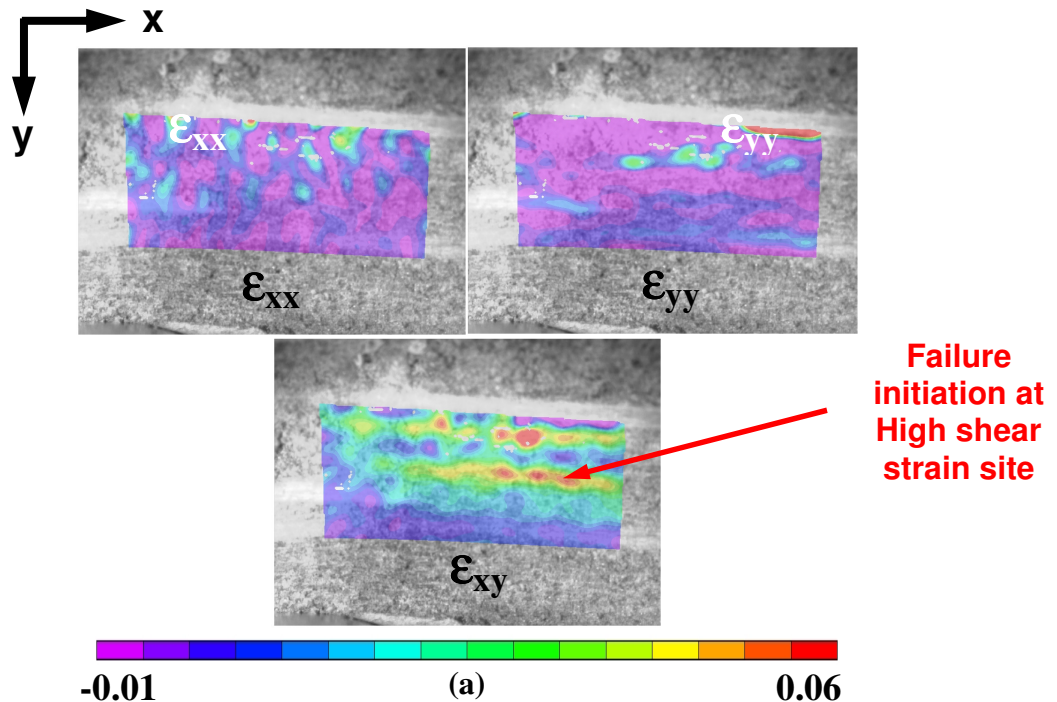


Figure 3.9 Strains measured 200 μm into matrix at microscale indicating concentration of shear strains very close ($\sim 0.25d_f$) to the fiber-matrix interface with associated pore collapse which may allow the shear strain to build up at the interface

3.3.1.3 Deformation measurement at microscale within failure regime

To understand failure initiation, the strain fields were evaluated from the images captured slightly after the maximum stress level (Figure 3.10). The global flexural stress strain behavior obtained from homogeneous isotropic assumption has been depicted earlier. Comparing the strain fields obtained at the microscale and with observations of failure initiation in the images (Figure 3.10 (a) and (b)), it would appear that crack initiation within the cellulose matrix is dominated by shear strain. The strain fields in the pre-failure image can be used to predict the failure initiation. The images correspond to a global flexural stress of 11 MPa and flexural strain of 3%. As can be noted from the strain fields, the shear strain at the failure initiation site is much higher (6%) compared to the normal strains (1%).



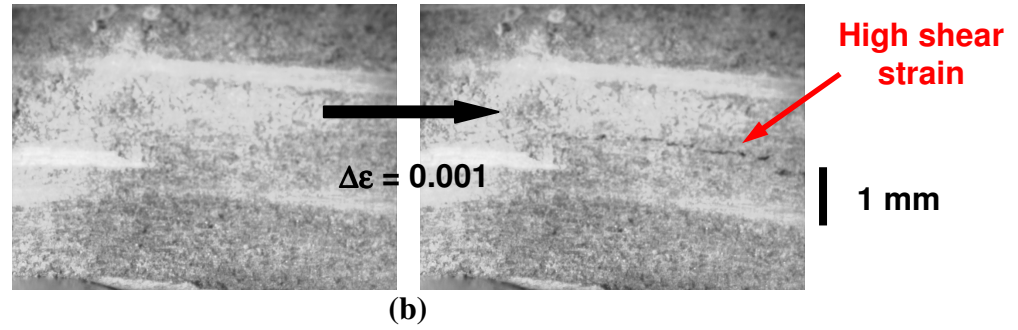


Figure 3.10 (a) Strain fields in the Palmetto wood specimen under quasi-static three-point bend before failure initiation and (b) failure initiation in the by shear cracking in the cellulose matrix after a macro-scale flexural strain increment, $\Delta\epsilon$, of 0.001. The failure initiation corresponds to the high shear strain site

The process of shear cracking in the matrix was evaluated at the highest magnification level of 20X from the macro length scale. While debonding takes place in the matrix-fiber interface due to shear strain, compressive failure at micro-scale level is noted (Figure 3.11) due to crushing of the matrix. At lower global strain levels, the matrix undergoes local crushing indicated by localized compressive strain and shear cracking. However, as the strain increases the pores collapse and coalesce together, giving rise to a shear crack. The evolution of the shear cracking is also shown in Figure 3.11.

As can be noted from the figure, the compressive failure grows faster than the tensile failure site leading to a macro-crack. Also, it is noted that higher compressive strain is accumulated faster as compared to the shear strain (indicated by second strain contours in Figure 3.11), where compressive strain reaches 0.09% while shear strain is approximately 0.06%. The compressive strain was also evidenced to some extent in larger length scale deformation measurement as shown in Figure 3.9. The collapse of the porous matrix reduces the compressive load and generates potential sites for the initiation of shear cracks as the global strain increases. Hence, it is believed that the pore collapse mechanism leads to the shear accumulation. Furthermore, it is most likely the mechanism

by which the flexural response can translate uniformly from the macro-scale to the microscale in the macro-fiber, as was previously discussed.

To map the microscopic to the macroscopic behavior of the Palmetto wood, the strains at each length scale were compared. The evolution of microscale local strains obtained by DIC from the 10X magnification images captured on the tensile and compressive side of the specimen are tracked over the quasi-static bending process with respect to the macroscale flexural strain is depicted in Figure 3.12. The strains are extracted at the points encircled in Figure 3.12 (a), (b) for tensile and compressive region of the specimen. The load levels correspond to points A, B and C in Figure 3.12 (c). The microscale strains are found to steadily increase with the macroscale flexural strain. The microscale transverse and shear strain increased at rates similar to the macroscale flexural strain after failure, and faster than the microscale axial strain, which was approximately half the rate of the macroscale flexural strain. Therefore, the faster increase of the transverse and shear strains is consistent with their dominance in failure initiation. Furthermore, the accumulation of the microscale transverse strain is nearly identical in the compressive and tensile regions. Since this strain is compressive, it is responsible for the pore collapse mechanism and indicates that it is independent of the global bending state, most likely due to the local macrofiber bending previously characterized in Figure 3.8.

The macroscopic shear strain before failure initiation has been measured to be approximately 2% at the failure initiation site (Figure 3.5). However, microscale pre-failure shear strain (in pore collapse) is determined to be as high as 4.5% (Figure 3.11). This is plausible for the hierarchical and inhomogeneous structure of the material at

multiple length scales. A significant accumulation of strain at the microscale is required to initiate macroscopic failure. Hence, the macroscopic stress is limited by the level of the microscale strain. Due to the compliance of the cellulose matrix, the micro-scale strain is not transferred to the higher length scale. The collapse of the cellulose matrix helps it to “absorb” strain locally and redistribute it to impede the initiation of failure. As discussed earlier, the porous media is weaker as opposed to the fiber material and does not transfer strain completely to fiber. The matrix material absorbs the strain, requiring higher strain levels for macroscopic failure to initiate even though microscale failure may initiate earlier, which means microscale failure is actually initiating in the elastic regime.

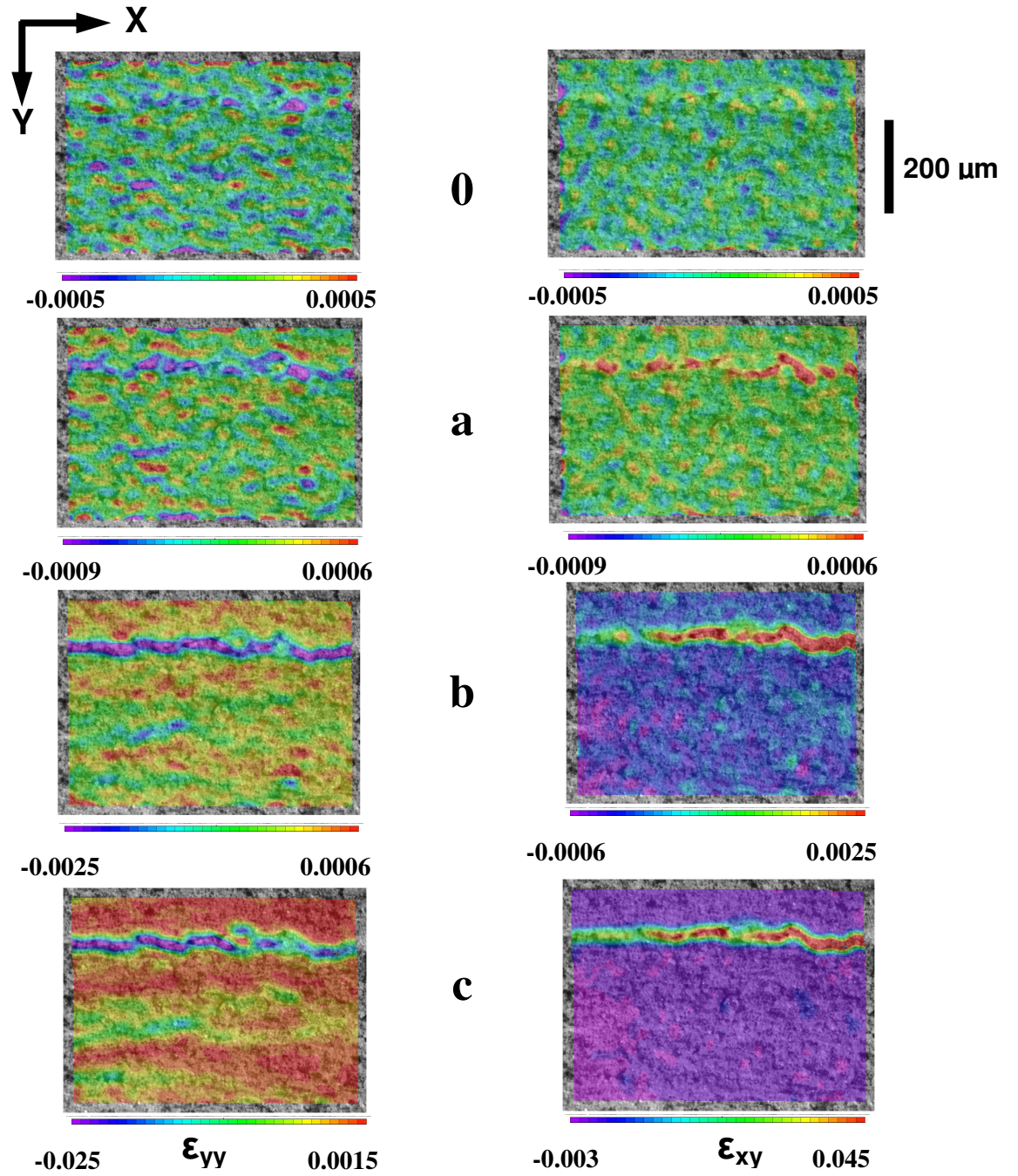


Figure 3.11 Evolution of shear cracking in cellulose material. The pores collapse (a) and coalesce together (b) and accumulate shear strain (c) leading to macro crack (d). The pore collapse mechanism helps for load absorption. The images correspond approximately to the points 0, A, B, C in Figure 3.12(c).

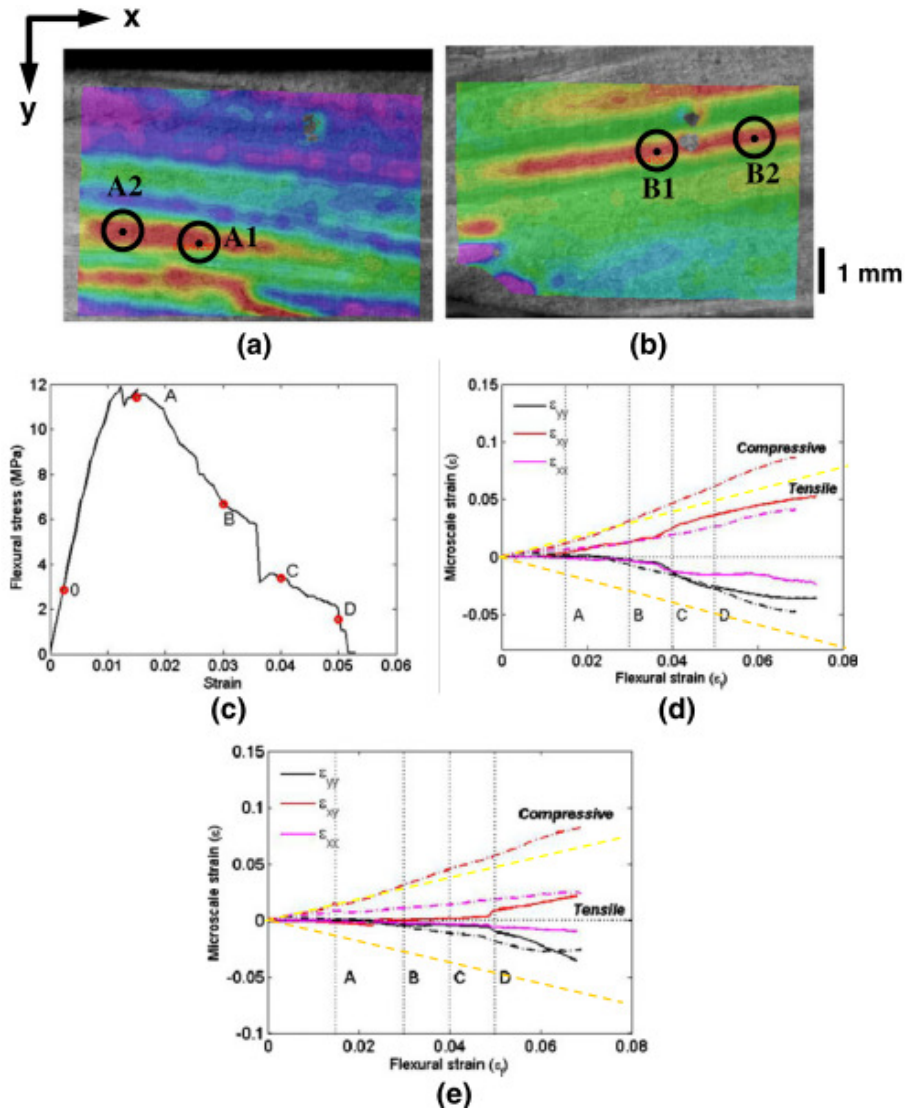


Figure 3.12 Intermediate microscale shear strain field of interfiber matrix in (a) tensile and (b) compressive regions of the specimen, (c) macroscopic stress-strain response, and (d) the evolution of the microscale strains with macro-scale flexural strain (right side) in the tensile (solid line) and compressive (dashed line) regions. The strains were extracted at the encircled points in (a) and (b). The state of deformation corresponding to the points A, B, C and D are shown in the stress-strain response (d). 1:1 correspondence between the magnitudes of the microscale strains and macro-scale flexural strain is denoted by the dashed yellow lines.

3.3.2 Characterization under Low Velocity Impact

3.3.2.1 Flexural stress-strain response under low velocity impact

Low velocity impact tests (strain rate of up to 100 s^{-1}) are performed on the Palmetto wood specimens to characterize the dynamic behavior. By the nano-mechanical characterization [68], it was found that the Palmetto wood has a radially graded distribution of macrofiber over the cross-section. To understand the effect of macrofiber volume fraction, the specimens were prepared from several radial positions of a harvested Palmetto tree as shown in Figure 3.13 and the specimen dimensions were taken large enough compared to the characteristic dimension of constituents (macrofiber diameter). The impact velocity is approximately 30 m/s, similar to that experienced in moving vehicle crashes.

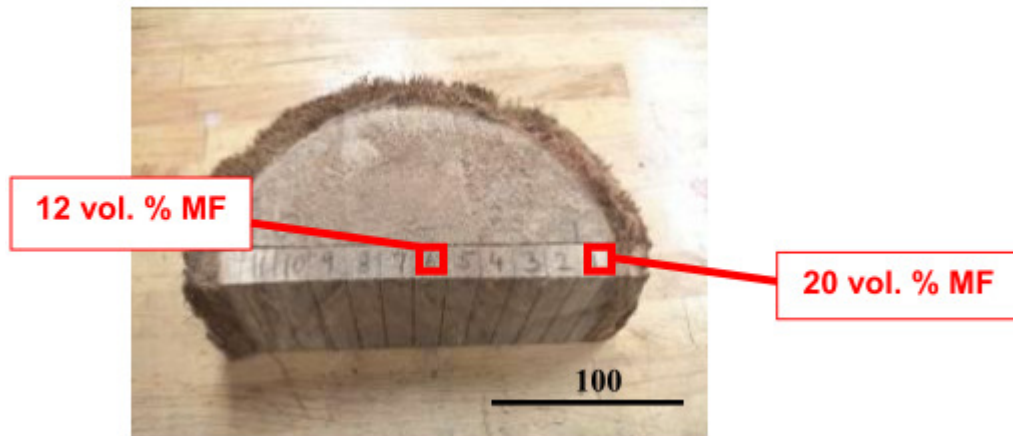


Figure 3.13 Specimens prepared from several radial location of Palmetto wood stem. The specimen prepared from outer region had a higher macrofiber (MF) volume fraction of 20%, whereas that from the inner portion had a lower MF volume fraction of 12%.

In order to obtain the flexural strain from low velocity impact tests, the total displacement of the projectile over time was evaluated from the load cell response obtained from the support through the inertial effects on the acceleration of the projectile. To obtain the total displacement, the acceleration obtained through the equation of motion ($F = m_{proj}a$) was integrated assuming equilibrium between the projectile and specimen, which was found to be reasonable at the time scales associated with the low velocity impact event for these specimens. Thus, the obtained velocity and displacement were then correlated to with those observed from the high-speed camera as depicted in Figure 3.14.

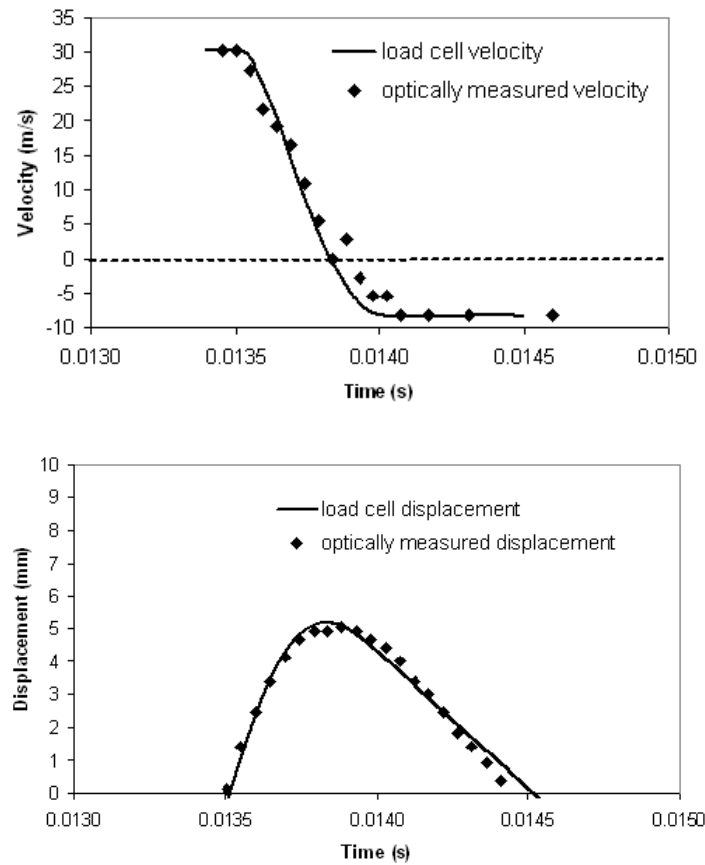


Figure 3.14 Correlation of (Top) velocity and (bottom) displacement obtained from load cell response and optical measurement by high speed imaging

Flexural stress-strain response of Palmetto wood under low velocity impact is depicted in Figure 3.15 and compared to that under quasi-static bending. The flexural stress, flexural strain and strain energy are calculated using the classical relations for three point flexural test as given in Equation:

$$\sigma_f = \frac{3PL}{2bh^2}, \quad \epsilon_f = \frac{6\delta_f h}{L^2} \quad 3.3$$

where P is the applied load, L is the support span, b is specimen thickness, h is specimen height, and δ_f is the deflection at the central load.

It was then observed that the bullet induced significant local indentation as well as bending deformation which varies with macrofiber concentration. To decouple the indentation effect, indentation tests were performed on the similar kind of Palmetto wood specimen by constraining the specimen to prevent from bending. Results for low velocity impact and quasi-static loading can be seen in Figure 3.16. The flexural deflection of the specimen, δ_f , was then found by subtracting the local indentation depth, δ_i , from the total bullet displacement, δ_t (i.e., $\delta_f = \delta_t - \delta_i$) at a given load, which could then be used to determine the flexural strain from Equation (3.3).

In addition to isolating the flexural strain, it was possible to compare the energies associated with indentation versus bending. For the 20 vol. % macrofiber concentration, the dynamic indentation load is approximately 0.8 J, while the total energy absorbed by bending was 5 J, which is the remainder of the projectile energy. Thus, indentation absorbs about 16% of the projectile energy. For the 12 vol. % macrofiber concentration, only 0.35 J was absorbed while the total energy absorbed by bending was still 5 J. Thus, the indentation energy was only 7 % of the total 5 J, which was insufficient to stop the

projectile. Thus, the indentation energy was only half of that of the 20 vol. % macrofibers, which indicates that the macrofiber concentration can also play a critical role in the impact resistance of Palmetto wood through the indentation response.

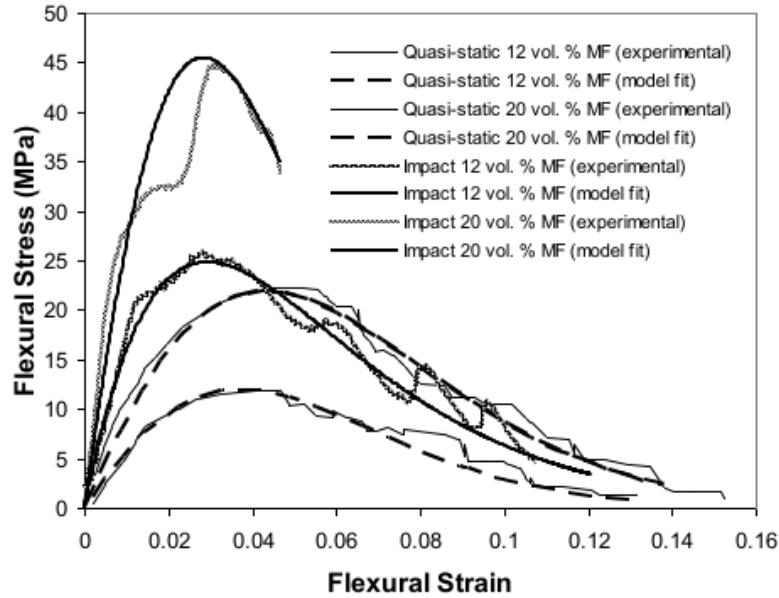


Figure 3.15 Flexural response of 12 and 20 vol. % macrofiber (MF) Palmetto wood specimens under low velocity (approximately 30 m/s) impact and quasi-static three-point bending with Weibull fits

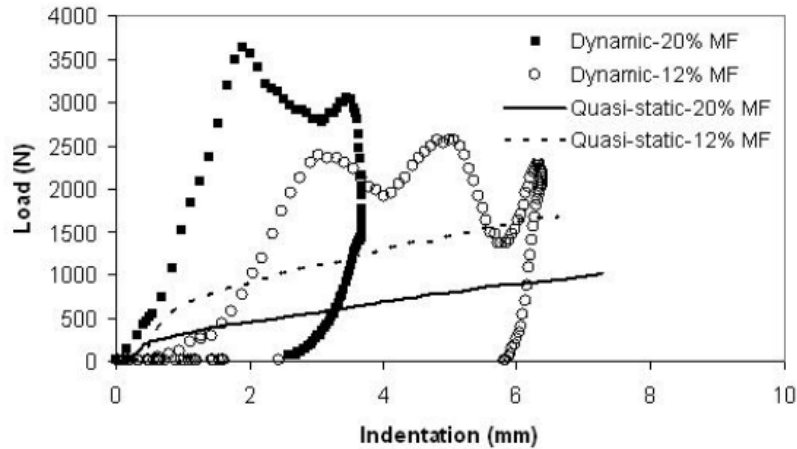
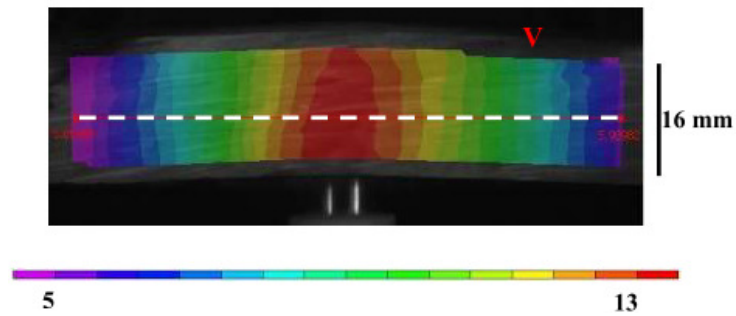
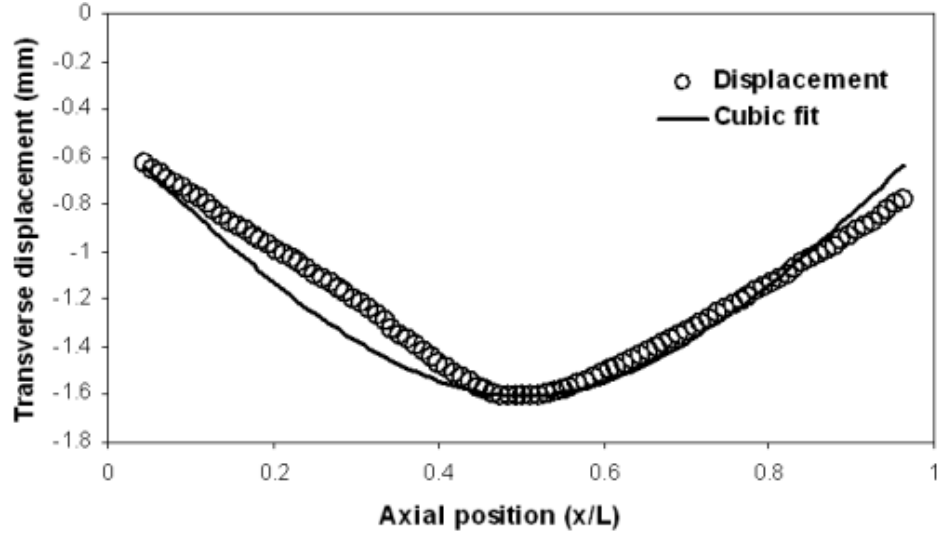


Figure 3.16 Comparison of low velocity impact and quasi-static indentation response of Palmetto wood specimens with different macrofiber (MF) volume fraction.

The flexural strain was also directly measured with lower time resolution from the high-speed images using the displacement fields determined by DIC. An example can be seen in Figure 3.17. The vertical displacement in the Palmetto specimen was captured at a strain level of around 2.7% as shown in Figure 3.17 (a). The vertical displacement and the cubic fit to the deflection are shown in Figure 3.17 (b). The flexural strain obtained from the curvature was around 0.027 that is similar to the value determined by DIC and the flexural response obtained from the load-cell. The bending of the Palmetto wood under impact at macroscale conforms to that of a homogeneous isotropic material as was under quasi-static loading [69]. Since the strain obtained from DIC measurements was found to be consistent with those determined from the load cell, it provided additional confidence in the accuracy of the measured flexural strain from low velocity impact.



(a)



(b)

Figure 3.17 (a) Transverse (vertical) displacement obtained from DIC of the Palmetto specimen under low velocity impact at a flexural strain level 0.027, and (b) displacements obtained along the dashed line and corresponding cubic fit. The strain determined using the curvature from the cubic fit also corresponds to a strain value of approximately 0.027.

In order to assess the effects of strain rate and macrofiber concentration on the mechanical behavior of the Palmetto Wood, a Weibull-based damage model of the stress-strain response for fiber-reinforced polymer composites was used [68, 69]. The Weibull model can be seen in Equation 3.2, and consists of the parameters ε_0 , β and the elastic modulus E , which were determined by fitting the stress-strain curves, as shown in Figure 3.15. The parameters of Weibull fit for dynamic and quasi-static response of the specimens with 20 vol. % and 12 vol. % macrofiber concentrations are shown in Table 3.1. From the Weibull fit, it can be seen that the impact of dynamic loading was to increase the modulus by approximately 200% independent of macrofiber concentration. The critical strain, ε_0 , was also found to be reduced by 30-35% due to dynamic loading, while the evolution of damage described by β did not show substantial differences except

for impact on the 12 vol. % macrofiber specimen. Thus, the Weibull model would indicate that the greatest impact of dynamic loading is to increase stiffness and decrease the strain at which damage begins to evolve. Since the stiffness increases more rapidly than the strain decreases, the end result is a stronger material response. These results are consistent with the fact that quasi-static bending is a slow process (strain rates of 10^{-4} /sec), which gives the macrofiber and the porous cellulose matrix more time to elastically deform in order to minimize local strain energy resulting in lower stiffness and a higher strain level before damage occurs. In contrast, the time scales associated with low velocity impact are orders of magnitude shorter (strain rates of 100/sec), so there is not enough time to minimize the local elastic energy state leading to higher stiffness and a lower strain level for damage initiation.

3.3.2.2 Failure modes under impact

From observation of the failed specimens, it was evident that there was a local crushing due to indentation and a global fiber debonding due to bending that are competing damage mechanisms (Figure 3.18). From the pure indentation response reported in Figure 3.16, it was noted that the dynamic indentation load is significantly higher. Also, the energy absorbed by the local indentation process is significantly larger (almost 200%) under dynamic loading, which significantly decreases the energy available for global bending.

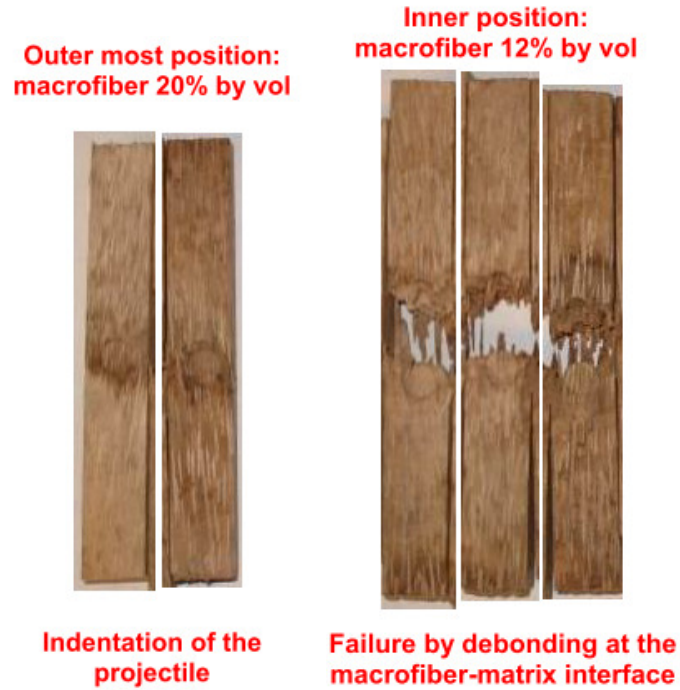


Figure 3.18 Post-failure specimens after macrofiber-interface debonding leading to rupture (right side) and local indentation by projectile (left side) that absorbs all the kinetic energy of the projectile. The transformation of failure mode is attributed to macrofiber concentration in the Palmetto wood.

The variation in energy during indentation was found to depend on the macrofiber and porous cellulose distribution. Comparing the flexural stress-strain curves with the pure indentation loading results, specimens with higher macrofiber volume fraction (20 vol. %) were found to have a much lower indentation resistance relative to flexure, which increases the probability of indentation failure. On the other hand, specimens with lower (12 vol. %) macrofiber volume fraction had much higher indentation resistance relative to flexure, which increased their probability of flexural failure. In the latter case, most of the impact energy would contribute to global bending of the specimen leading to global damage in the specimen, which is consistent with the observation depicted in Figure 3.18.

The volume fraction macrofiber was previously reported to gradually decrease along the radial direction towards the center of the wood stem from the high of 20 vol. % to a

low of 12 vol. % [68]. As can be seen from the reported dynamic mechanical behavior of specimens with different macrofiber concentration, the macrofiber distribution will be the key parameter in controlling the impact resistance of the bulk material. By increasing the macrofiber concentration, the dominant failure mechanism can be transformed from macrofiber debonding due to bending to pore collapse from indentation. This explains why the macrofiber concentration gradually decreases radially towards the center of the wood stem, since the outer portion of the wood has higher indentation resistance while the inner portion is more susceptible to bending failure, which increases the energy absorbed by both mechanisms in order to increase impact resistance. As evaluated in the multiscale characterization of Palmetto wood [69], the strain is highly inhomogeneous at lower length scales due to the difference of mechanical properties of the macrofiber and porous cellular matrix. Hence, the energy absorption is spatially inhomogeneous and leads to a conclusion that local stress-strain curve can not represent the global behavior in terms of strain energy absorption due to the localization of the energy absorption mechanisms.

The strain fields at the initiation of failure in the Palmetto wood specimen under dynamic load is evaluated by DIC of the images captured at higher magnification (around 10X) as depicted in Figure 3.19. The subset size and strain filter used for this correlation to obtain the deformation field were $51 \times 51 \text{ pixel}^2$ and 15 pixels, respectively. The failure initiation is found to occur under high shear and compressive axial strain. However, the failure modes found by the tests with several specimens will be details in next section. As revealed by the DIC, the damage initiation site occurs due to high shear, as well as transverse compressive load. However, the DIC shear strain is much higher

(7%) than the compressive strains (4%), which indicated a higher localized shear resistance relative to compression and thus a propensity for pore collapse followed by shear failure of the macrofibers due to indentation.

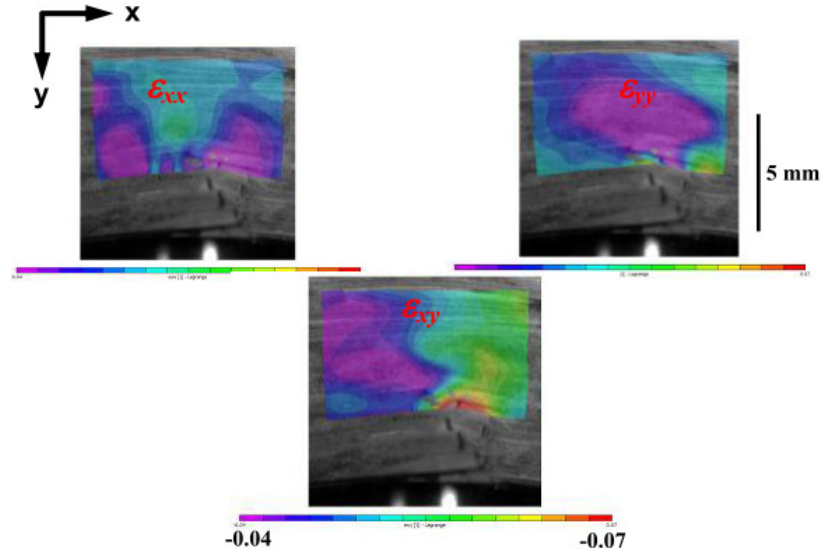


Figure 3.19 Images of deformed Palmetto wood under low velocity impact at a magnification of 10X. The local indentation failure consists of compressive axial strain associated with crushing of the porous cellulose matrix followed by higher levels of shear strain associated with shear cracking of the macrofibers and matrix.

3.3.3 Damage Evolution under Quasi-static and Dynamic Loading

The macroscale damage evolution of the Palmetto wood has been quantified under low velocity impact and compared to that under quasi-static bending. To obtain the damage evolution, same specimen was subjected to several impacts until it lost all its strength. The scalar damage is defined by $D = 1 - \sqrt{E/E_0}$ and is determined experimentally by measuring the reduction of the modulus with strain. The following expression for the evolution of damage with total flexural strain based on strain energy conservation was then fit to the experimental measurements [Figure 3.15],

$$D = D_{\lim} \left[1 - \exp(-A(\varepsilon - \varepsilon_d)) \right] \quad 3.4$$

In this expression, D_{\lim} represents the limiting amount of damage that can occur, ε_d is the strain at which damage initiates, and A is an acceleration factor that describes the evolution of damage with strain. Results from fitting the curves to the experimentally determined damage can be seen in Figure 3.20.

Using Equation (3.4), it was possible to study the effect of the macrofiber volume fraction and loading rate on the damage accumulation. The constants that were determined from Figure 3.20(a) can be seen in Table 3.1. The acceleration factor and limiting amount of damage did not appear to be affected substantially by loading rate or macrofiber concentration. However, the strain at which damage begins to accumulate did decrease by 15 – 30 %, which was similar to what was observed with the Weibull model fit.

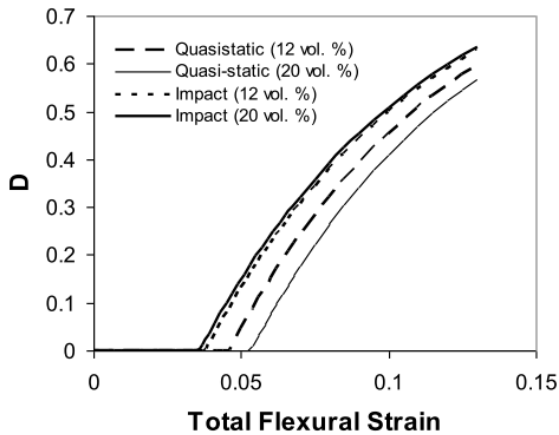
In addition to the damage that accumulates with flexural strain, the mechanism of plasticity due to pore collapse must also be accounted for. Therefore, the plastic flexural strain, ε_p , was related to the total flexural strain through a form of the conventional power law hardening relationship as follows,

$$\varepsilon_p = \varepsilon \left[1 - \exp(-B(\varepsilon - \varepsilon_y)^p) \right] \quad 3.5$$

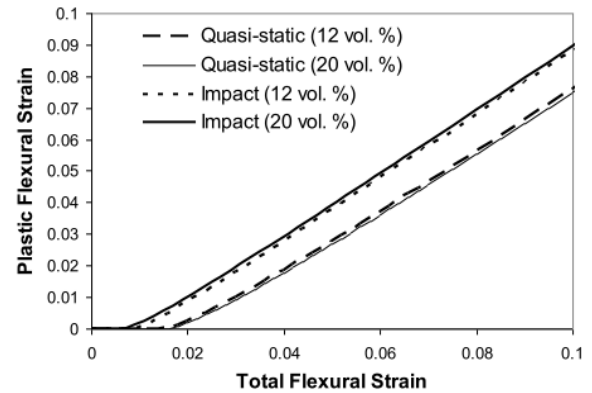
where ε_y is the yield strain and p and B are related to the power law hardening exponent and coefficient, respectively. The plastic strain could be determined experimentally by measuring the permanently deformed shape of the specimen. The evolution of macroscopic plastic strain with respect to the total strain could then be determined and

Equation (3.5) fit to the data. The resulting fits can be seen in Figure 3.20(b), and the constants determined from the fit can be seen in Table 3.1.

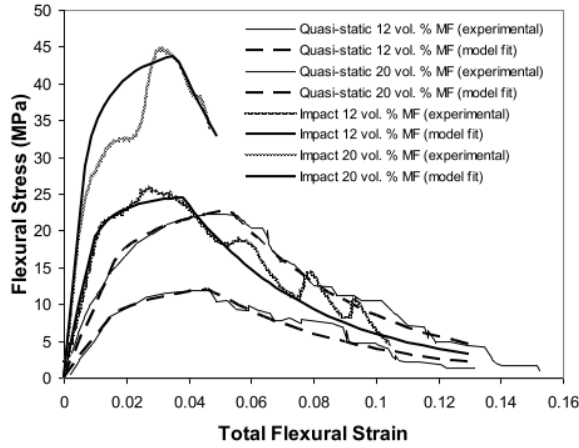
From the constants that were determined, it can be seen that the hardening exponent does not appear to vary with macrofiber concentration and loading rate. Instead, the hardening coefficient appears to increase by approximately 50% as the loading rate increases. The yield strain also substantially decreases by 40-50% as the loading rate increase, but does not vary as substantially with macrofiber concentration. This would tend to be consistent with the previous comment on the time required for the local strain energy level to reach a critical level that result in a strain rate dependency for the pore collapse mechanism responsible for plasticity.



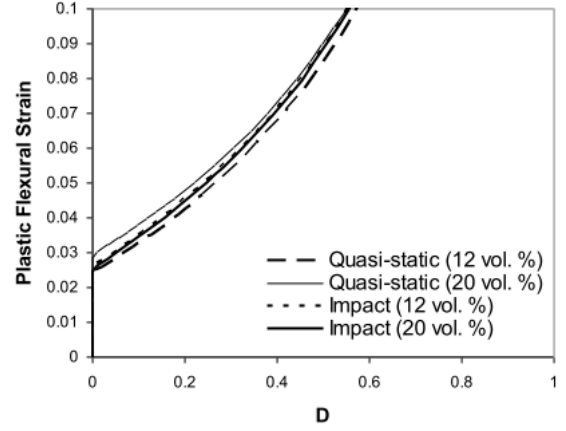
(a)



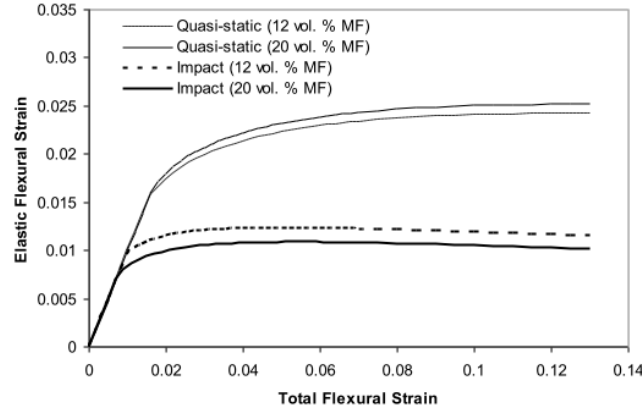
(b)



(c)



(d)



(e)

Figure 3.20 (a) Damage evolution with total flexural strain, (b) evolution of plastic flexural strain with total flexural strain, (c) Flexural stress-strain curves with new model fit, (d) evolution of plastic flexural strain with damage, and (e) evolution of elastic flexural strain with total flexural strain for Palmetto wood of 12 and 20 vol. % macrofibers (MF) under quasi-static and low velocity impact three-point bending.

In order to better understand the observed dependency of the plastic deformation on strain rate, Equations (3.4) and (3.5) were combined to determine the constitutive response of the Palmetto wood as follows,

$$\sigma = E_0 (1 - D)^2 (\epsilon - \epsilon_p) \quad 3.6$$

The resulting fits to the experimental data can be seen in Figure 3.20(c). The undamaged moduli that were determined from these fits can be seen in Table 3.1. It was previously determined that for quasi-static loading these values increased with macrofiber concentration according to the rule-of-mixtures. As the loading rate increases, these values increase substantially by approximately 300%, a higher increase than was observed with the Weibull model fit. The sensitivity of these values to loading rate is similar to that observed in polymeric materials. Given the fibrous nature of Palmetto wood, it is natural to assume that the dependency is related to the viscoelastic behavior of the material. Thus, the moduli could be associated with the rubbery and glassy response of the Palmetto wood at low and high loading rates respectively.

The increasing stiffness of the Palmetto wood with loading rate also provides insight into the variation of the plastic deformation response of the Palmetto wood with loading rate. As the Palmetto wood stiffens, the associated stress increases substantially with decreasing strain. Thus, the critical loads at which plastic strain initiates occur at much lower strain levels. Using the yield strain and the elastic modulus, the corresponding yield stress can be determined. It can be seen that the yield stress will increase from 8.3 MPa to 18.0 MPa, an increase of 116%, as the loading rate increases for 12 vol. % macrofibers and from 15.6 MPa to 28.7 MPa, an increase of 84%, as the loading rate increases for 20 vol. % macrofibers. Thus, pore collapse occurs at approximately 100% higher stress levels with increasing loading rate, and approximately 70% higher stress levels with increasing macrofiber concentration, which is reasonable given the nature of

this mechanism. Thus, the observed plastic deformation response of Palmetto wood is consistent with the plastic deformation mechanism.

In order to understand the comparative evolution of plastic deformation and damage in Palmetto wood, the damage was plotted against the plastic flexural strain in Figure 3.20(d). It can be seen that the relationship between plastic strain and damage accumulation appears to be independent of macrofiber concentration and loading rate. Given that previous investigations using DIC identified that pore collapse at the macrofiber-porous cellulose matrix interface precedes macrofiber debonding, these results appear consistent with the previously identified relationship between these failure mechanisms. Visible evidence of the differences in flexural deformations and the corresponding level of damage can be seen in Figure 3.21.

It was also possible to use the new damage model to track the evolution of the elastic flexural strain with total flexural strain. The results can be seen in Figure 3.20(e). It is clear from these results that the strains tend to increase linearly until reaching a plateau value of around 2.5% for quasi-static loading and around 1% for impact loading independent of macrofiber concentration, a decrease of 60% with increased loading rate. Thus, it would appear that there is a critical level of elastic strain that can be sustained before additional deformation requires the accumulation of plasticity and damage, and is consistent with the idea that so there is not enough time to minimize the local elastic energy state as the loading rate increases which reduces the global critical level.

The resulting relationship between stress and strain in Equation (3.6) can also be used to compare the resulting energy absorption of Palmetto wood. It can be seen that the density of energy absorption increases with strain rate from 0.75 to 1.75 J/m³ for 12 vol.

% macrofibers and from 1.55 to 2.68 J/m³ for 20 vol. % macrofibers. Thus, nearly doubling the volume fraction of macrofibers nearly doubles the energy absorption, while increasing the loading from quasi-static to low velocity impact increases the energy absorption by approximately 75 to 133%.

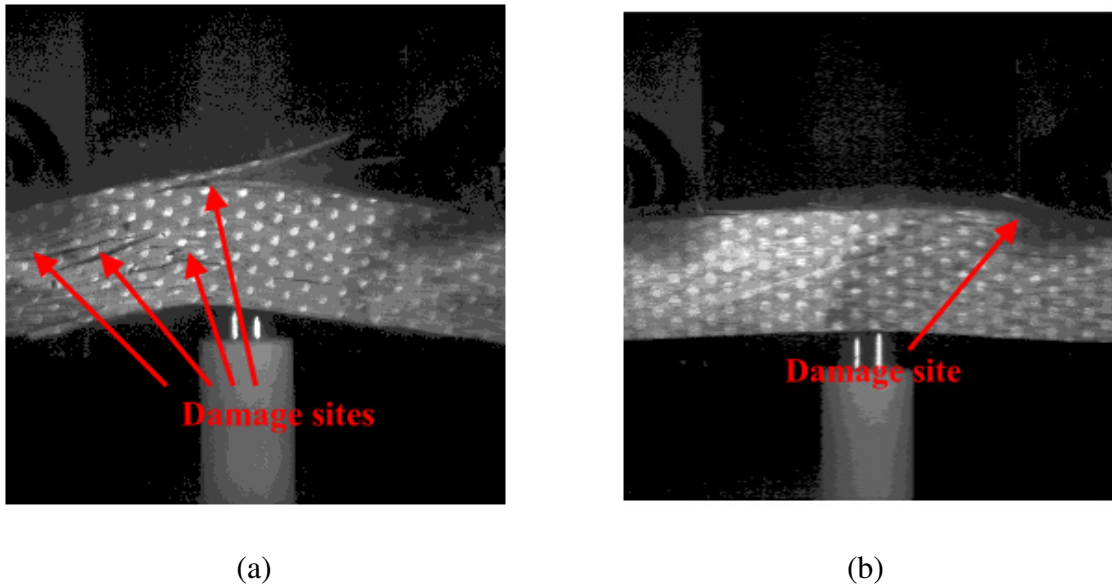


Figure 3.21 Impact-induced damage in Palmetto wood due to debonding at the macrofiber-porous cellulose matrix interface for (a) 12 vol. % and (b) 20 vol. % macrofiber concentrations. The specimen with 20 vol. % macrofibers absorbs the projectile and has lesser flexural deformation (3.8% flexural strain) compared to 12 vol. % macrofiber (11% flexural strain). Also, the specimen with a lower macrofiber concentration (a) has a significantly higher number of damage sites than the later (b)

Loading condition/vol. % MF	Weibull model			New damage model with plasticity						
	E (MPa)	ε_0	β	E (MPa)	ε_y	ε_d	D_{lim}	A	B	p
Quasi-static/12	600	0.05	1.6	550	0.015	0.046	0.9	13	6	0.4
Quasi-static/20	950	0.058	1.6	975	0.016	0.052	0.9	13	6	0.4
Impact/12	2100	0.032	1.1	2000	0.009	0.038	0.9	13	9	0.4
Impact/20	3000	0.038	1.6	4100	0.007	0.036	0.9	13	9	0.4

Table 3.1 The modulus, E , and Weibull parameters (ε_0, β) obtained by fitting the flexural stress-strain curves and the modulus, E , and damage initiation strain (ε_d) obtained from the new damage model for the Palmetto Wood specimens.

3.4 Discussion of Results

3.4.1 Characterization under Quasi-static Bending

DIC analysis has been performed at multiple length scale to understand the failure mechanism in Palmetto wood under three-point bending under quasi-static load and low velocity impact. Several possible modes of failure are: (i) tensile failure on the tension side, (ii) buckling (wrinkling) on compression side or (iii) inter-layer delamination due to shear. Multiple length scale deformation measurements are performed under quasi-static load. Two types of cracking are noted in the specimens, namely macro-fiber-matrix debonding and matrix shear cracking. Both are found to be dominated by interlayer shear and transverse compression.

At the macro-scale, specimens can be prepared from the Palmetto wood that exhibit more homogeneous material behavior as evidenced by homogeneous strain fields. The macro-scale bending can be mapped to that of a homogeneous isotropic material.

However, highly inhomogeneous deformations due to the fiber reinforcement and matrix response can be distinguished at the microscale. The periodicity of fiber and matrix is evident from the periodic nature of the shear strain distribution along the depth in specimen. High shear strain is found at the macro-fiber-matrix interfaces of both globally tensile and compressive sides of the specimen. The fiber, being mechanically superior, does not deform as a porous matrix material (as expected), giving rise to shear strain concentrations at the fiber-matrix interface.

When obtaining microscale deformation measurement, macro-fiber has been noted to deform like a beam embedded in a compliant matrix giving rise to a classical bending profile. The compressive load is not transferred to the subsequent fiber as the inter-fiber matrix absorbs the load through a collapse mechanism. For this reason, crushing of the material at loading point does not affect the far-field behavior of the specimen, and also enables the material to sustain higher normal load in the direction perpendicular to fiber alignment.

The tensile load is primarily carried by the fibers. Since the fibers are both stronger and more rigid the tensile region deforms less than the compressive zone. Failure at both the macro-fiber-matrix interface and cellulose matrix is seen to be dominated by interlayer debonding due to shear strain. The wavy nature of shear strain along the width indicates high shear in the macro-fiber-matrix interface. The shear strain at potential failure sites appears to increase steadily until failure. Strain at the microscale is seen to be higher than measured at the macro-scale. This is acceptable as the microscale since local failure initiation does not immediately leads to macroscopic failure of the specimen because of local redistribution of the load within the multiple-laminate nature of wood.

Damage in the material occurs via a multi-step failure process. The difference in mechanical properties of compliant matrix and comparatively rigid macro-fiber results high shear strain concentration at the interface. At the highest magnification scale, the pore collapse mechanism and accumulation of strain by pore collapse is found. The shear cracking is noted to be initiated by the pore collapse at the sites undergoing high shear and compressive strain.

3.4.2 Characterization under Low Velocity Impact

As previously demonstrated, the insight into the structure-property relationship of Palmetto wood can be used as biological inspiration for the development of polymer composites [1]. The results in this study expand the insight into the development of more impact resistant polymer composites, especially for sandwich composite structures. It can be seen that inserting as little as 12 to 20 vol. % macrofibers into a foam core may significantly enhance the stiffness, strength, and energy absorption. The interaction between the macrofibers and the porous cellulose matrix can also significantly increase energy absorption as the loading rate increases.

For impact resistant polymer composites, it is anticipated that the characteristics of the macrofiber will also contribute to the performance enhancement. Pultruded carbon fibers are very similar in structure to the macrofibers in Palmetto wood. Their mechanical properties are also significantly better. Thus, it is anticipated that reinforcing standard foams with 12 to 20 vol. % pultruded carbon fibers will produce similar benefits to those observed with Palmetto wood. Furthermore, interfacial adhesion will also play a critical role. Thus, the chemistry of the foam should be compatible with the pultruded

carbon fibers, or a compatibilizer with adhesive should be used at the interface of the pultruded carbon fiber with the foam matrix.

3.5 Summary

This chapter establishes the technical feasibility of using the Palmetto wood as a template to enhance the mechanical properties of advanced composite materials by hierarchical structure and establishes the characterization methodology to understand the mechanics principle of hierarchical structure across multiple length scales.

The quasi-static mechanical behavior of palmetto wood, a hierarchically structured natural material, has been investigated by three-point bend testing with the neutral axis of the specimen along the fiber orientation. Strain fields for quasi-static loading have been determined using DIC at multiple length scales using different optical magnifications to elucidate on the roles of the porous cellulose matrix and embedded fibers in the failure process. The natural texture of the specimens was found to be adequate for image correlation.

It was determined from the quasi-static DIC results at the macro-scale that the material behaves fairly homogeneously with a slight asymmetry due to the presence of the fibers. The macro-scale bending behavior complies well with the classical beam bending theory. However, microscale measurements at a magnification difference of 10X-20X relative to the macro-scale revealed inhomogeneous deformations due to differences in the properties of the macro-fibers and porous cellulose matrix. The shear and transverse strains exhibited significantly greater variability than the axial strain. The variability in shear strain coincided with debonding at the fiber-matrix interface or cracking within the

matrix due to shear strain. The variability in transverse strain was primarily within the matrix and coincided with pore collapse.

It is postulated that the pore collapse mechanism acts as a load absorber that significantly reduces the energy available for fiber-matrix debonding, and enables the flexural response to translate from the macro-scale to the microscale in the macro-fiber. DIC measurements obtained at the highest magnification revealed that there was no further elucidation that could be obtained for the load transfer mechanism. However, the pore collapse mechanism and shear strain accumulation is elucidated. The microscale transverse normal strain and shear strains monotonically increase along with the macro-scale flexural strain at a faster rate than the longitudinal strain, indicating their dominance in the failure process. The microscale mechanical behavior was consistent in both the compression and tension regions of the three-point bend specimen, indicating that the failure process was not sensitive to the sign of the stress state.

Low velocity impact experiments were performed to evaluate the dynamic behavior of the dry Palmetto wood for comparison with previous quasi-static three-point bending measurements. Under low velocity impact, the dynamic damage was found to be dominated globally by axial loading induced by bending leading to localized, shear-dominated debonding at the macrofiber-porous cellulose matrix interface, as well as compressive loading induced by indentation under the projectile leading to local crushing of the porous cellulose matrix. Through the changes in macrofiber concentration, it was also determined that the dynamic failure mode of the Palmetto wood can be transformed from the shear dominated debonding by axial loading to the crushing of the porous cellulose matrix and shear cracking of the macrofibers and matrix by local indentation.

The relative energy absorption by indentation increased from 7% to 14% with the increase in macrofiber concentration from 12 vol. % to 20 vol. %. This explains why the macrofiber concentration gradually decreases radially towards the center of the wood stem, since the outer portion of the wood has a high indentation resistance while the inner portion absorbs more energy through bending.

In order to better understand the influence of macrofiber concentration and loading rate on the mechanical behavior of Palmetto wood, two models of the stress-strain response were fit to the experimental data. The first was a model based on Weibull statistics developed for fiber-reinforced polymer composites. From the Weibull fit, it was determined that increasing the loading rate increased the modulus by approximately 200% independent of macrofiber concentration. The critical strain, ϵ_0 , was also found to be reduced by 30-35% due to dynamic loading, while the evolution of damage described by β did not show substantial differences.

Since the Weibull model combined effects of all the damage mechanisms, a new model was developed that separated the evolution of damage from plastic deformation. It was determined that the yield stress associated with the previously identified pore collapse mechanism increases by approximately 100% as the loading rate increased, and by approximately 70% as the macrofiber concentration increased. The stiffness also increases by approximately 300%, which is higher than what was observed with the Weibull model fit. In contrast, the damage evolution with plastic deformation exhibited a stronger dependence on macrofiber concentration than strain rate, consistent with the pore collapse mechanism at the macrofiber-porous cellulose matrix interface preceding macrofiber debonding mechanism that was observed using DIC. It was also possible to

use the new damage model to track the evolution of the elastic flexural strain with total flexural strain, which indicated there is a critical level of elastic strain that can be sustained before additional deformation requires the accumulation of plasticity and damage due to pore collapse and macrofiber debonding. The combined behavior of the pore collapse and macrofiber debonding mechanisms resulted in an increase of energy absorption that nearly doubled with doubling the macrofiber concentration and increased by 75-133% as the loading rate increased from quasi-static to low velocity impact.

The present study helps in understanding the failure mechanism of a novel hierarchically-structured natural material that serves as a template for developing biologically-inspired polymer composites. The results from this study can provide guidance to previous efforts in using Palmetto wood as biological inspiration for the development of polymer composites. In particular, it indicates that macrofiber reinforcement of foam cores can lead to more impact resistant sandwich composite structures using as little as 12 to 20 vol. % macrofiber reinforcement.

However, there are several issues like fabricating the bioinspired sandwich with proper length scales that include the size of the foam pores, size of the pultruded carbon rod, adhesive material and processing. These parameters would significantly affect the sandwich behavior.

In the next chapter, fabrication and characterization of mechanical behavior of sandwich structures with bioinspired core has been described.

Chapter 4 Fabrication and Characterization of Bioinspired Sandwich Structures through Reinforcement in Core

In this chapter, development and characterization of sandwich composite structures with bioinspired core has been detailed. The understanding of load transfer mechanisms and the role of macrofiber in the porous cellulose matrix of Palmetto wood has been utilized to modify the core of traditional sandwich composite structure. Using the structural template of Palmetto wood, as inspiration, reinforcements have been embedded in the core of foam core sandwich composite structures to translate the load transfer and energy absorbing mechanisms in the core of the sandwich composite. The fabrication of the sandwich composite structures with bioinspired core is detailed in Section 4.2, and the experimental results are presented in Section 4.3 followed by the discussion in Section 4.5.

4.1 Motivation

Palmetto wood, a naturally occurring hierarchically structured composite, had been assumed to be a novel bioinspiration to develop synthetic sandwich composites that will have enhanced mechanical properties, energy absorbance capability as well as damage resistance. The unique mechanical behavior of Palmetto wood in the protective structures during Civil and Revolutionary war has been the motivation for using Palmetto wood as bioinspiration.

The multiscale structural characterization of Palmetto wood revealed its hierarchical structure as well as structural characteristics and its potential as a novel bioinspiration [68]. Following by the structural characterization, load transfer and failure mechanisms

have been investigated at multiple length scales under quasi-static three point bend to reveal the roles of macrofiber and porous cellulose matrix in the load transfer mechanism [69]. As discussed in the previous Chapter, the pore collapse and shear dominated debonding were found to be the key failure mechanism. The damage evolution in the Palmetto wood has been characterized under unloading-reloading. The dynamic behavior of Palmetto wood has also been characterized under low velocity impact in three point bend configuration [70]. The characterization of dynamic behavior revealed that the failure mechanism dominates the dynamic behavior similar to the quasi-static behavior. Damage modeling of the Palmetto wood revealed the slower damage evolution under the dynamic load than that under quasi-static loading. The deformation measurement to characterize the mechanical behavior of Palmetto wood at multiple length scales and loading rates have been accomplished by using the Digital Image Correlation (DIC) on the images captured at several magnifications and it was possible to relate the microscale deformation to the macroscale deformation behavior.

Motivated by the enhanced mechanical behavior of the Palmetto wood by virtue of its hierarchical structure and macrofiber reinforcement in the porous cellulose structure, effort has been made to translate the load transfer and failure mechanisms into an engineered sandwich composite structure with bioinspired core using macroscale reinforcement of pultruded carbon rods in the foam core. The pultruded carbon rods are made of carbon fibers similar as the macrofibers in Palmetto wood are made of fibrils. The sandwich composite specimens with bioinspired foam core are the main interest in the present study. To achieve hierarchical structure as well as enhanced strength at the interface, the interface in sandwich composite structures are engineered by using nano-

enhanced epoxy as adhesive. The main objective of the characterization is to translate the failure mechanisms of Palmetto wood into the synthetic sandwich composite structure and quantify the effect of reinforcement in the core. To this goal, global flexural behavior along with damage evolution in the sandwich composite structures has been studied. The response of the sandwich composite structures with reinforcement in the core has been analyzed in the context of the mechanical behavior of Palmetto wood, the bioinspiration for the structure of the sandwich composites in this study.

4.2 Materials, Fabrication and Characterization Technique

The materials used to prepare the sandwich composite specimens with bioinspired core are Rohacell soft foam, epoxy carbon woven fabric laminates from DragonPlate, pultruded carbon rods from The Composites Store and epoxy resin 105 and slow hardener 206 from West System. The core of sandwich composite specimens was reinforced by pultruded carbon rods to mimic the hierarchical structure of the Palmetto wood. The facesheets of carbon fiber strips (Composites) were glued to the core using epoxy based adhesive. West system epoxy resin 205 with 106 slow hardener has been mixed by 5:1 ratio by weight.

This epoxy based adhesives has been used as to glue the soft foam, and facesheets of carbon strips. The foam and facesheets were manually attached by the adhesives detailed above. For another class of specimen, reinforcement of carbon rods have been used by penetrating the carbon roads in the soft foam core after dipping them in the adhesive to achieve better adhesion with the foam. The glued and reinforced specimens were cured in a closed chamber at 80° C for around 30 hrs under a dead weight.

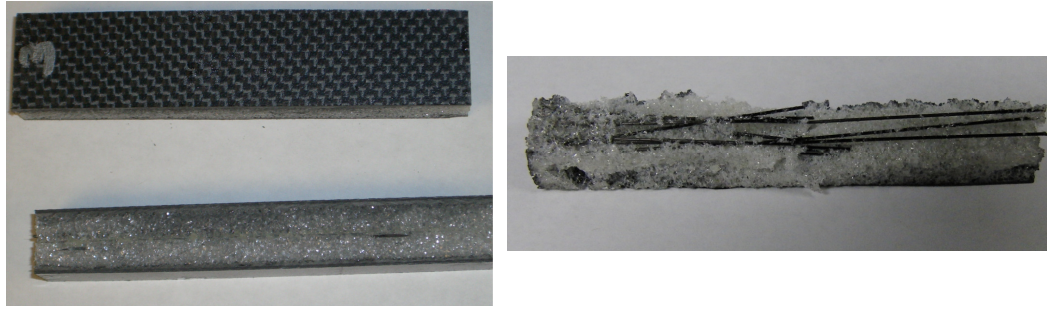


Figure 4.1 (left) Sandwich structure with bioinspired core developed using Palmetto wood as a template and (right) post-mortem of the inside structure of sandwich

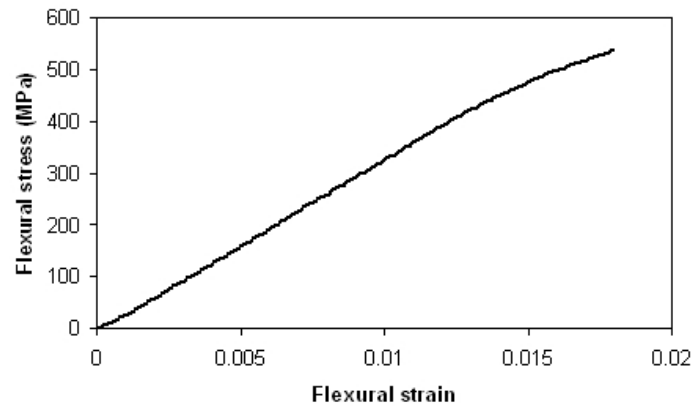
Mechanical behavior of the sandwich composite structures with reinforced core has been characterized and compared with that of sandwich composite structures without any reinforcement in the core. Three-point bend tests (Section 3.2.1) have been performed to characterize the flexural behavior of the sandwich composite specimens under quasi-static load and low velocity impact. As discussed earlier (Section 3.2.1), the quasi-static flexural tests have been performed in the Imada MX-500 load frame aided with load cell and caliper to measure the load and displacement. Continuous real time imaging has been performed to capture the deformation and determine the displacement and strain fields by DIC of the images captures during the test. The low velocity impact test has been performed in the experimental set-up that has been discussed earlier in detail (Section 3.2.2).

4.3 Experimental Results

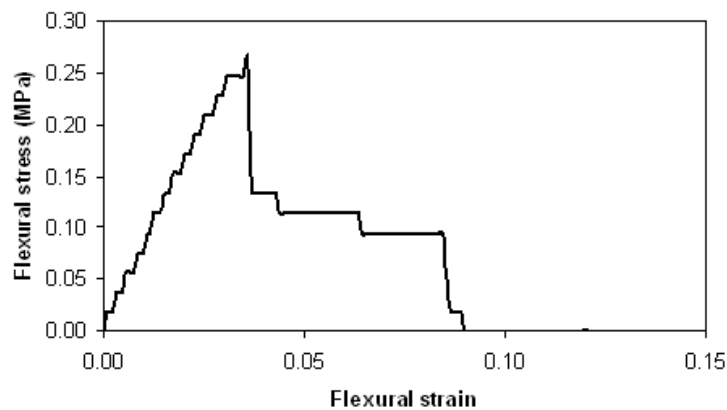
Quasi-static flexure and low velocity impact tests in three-point bend configuration have been performed to characterize the mechanical behavior of the composite sandwich specimens with reinforcement of pultruded carbon rod in the foam core.

4.3.1 Characterization under Quasi-static Bending

The flexural response of the constituent facesheet and foam core used to fabricate the composite sandwich structures has been shown in Figure 4.2. The flexural modulus of the facesheet is determined to be around 32200 MPa and that of the polymeric foam core is around 8 MPa. The failure mode in the polymeric foam core under quasi-static flexure is found to be due to axial tension on the tensile side under the indenter as was identified in flexural test of GFRP/PVC foam core sandwich composite structure by Valenza et al. [99]. The failure of in foam occurs at around 3% global flexural strain.



(a)



(b)

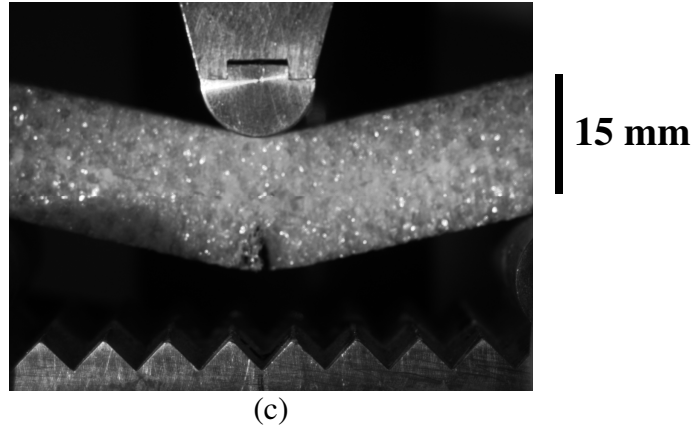


Figure 4.2 Flexural properties of (a) facesheet, (b) foam core and, (c) failure initiation in foam core

Representative macro-scale flexural response of the composite sandwich structures has been depicted in Figure 4.3 for three kinds of foam core to compare their flexural strength. In conventional composite sandwich structures, the core is assumed to act mainly as a separator increasing the shear strength of the sandwich structure. However, the bioinspired core exhibits its potential to increase the flexural strength of the composite sandwich compared to the one with conventional core. In our laboratory fabrication, the bio-inspiration in the composite sandwich core was realized by penetrating pultruded carbon rods in the foam core. Reinforcement of pultruded carbon rods in the polymeric foam core increases the flexural stiffness and energy absorbance through the increase in interface by virtue of higher stiffness of the pultruded carbon rod and localized deformation at the new reinforcement-foam core interfaces. The effect of the carbon rod was found to increase the flexural stiffness from 90 N/mm to 230 N/mm leading to increase in the flexural strength of the sandwich structure. It has been noted that the volume % of pultruded carbon rod reinforcement for this composite sandwich with bioinspired core was only around 0.90 vol%. However, since, the foam core and reinforcement interface was also glued by the adhesive, the interfacial adhesive also

contributed in the response. The results show that use of nano-enhancement at the interfaces as well as bioinspired core provides the best mechanical behavior of the composite sandwich structure.

The effect of increase in volume fraction of carbon rods has been depicted in Figure 4.3. An increase in pultruded carbon rod reinforcement from 0.90 vol% to 2.45 vol% leads to an increase of around 100% in the flexural stiffness. However, it is evident that there is a limit on the increasing amount of the carbon rod. The natural inspiration of this engineering material, namely, the Palmetto wood has a hierarchical structure from the macrofiber to the bulk wood and has excellent interfacial strength at the macrofiber-cellulose interface. The interfacial strength at the carbon rod and foam core interface and collapse of the foam cell due to penetration of the carbon rod may impose a limitation on the strength enhancement in these composite sandwich structures. Thus, beyond an amount of reinforcement, the core would appear as a bundle of carbon rods and would be highly stiff as the cost of lesser failure strain and catastrophic nature of failure. As far as the weight of the sandwich material is concerned, the nano-enhancement and bioinspired core increase minimal amount of weight causing to maintain a close stiffness to weight ratio compared to that of the composite sandwich structures without any nano-enhancement and reinforcement of carbon rod.

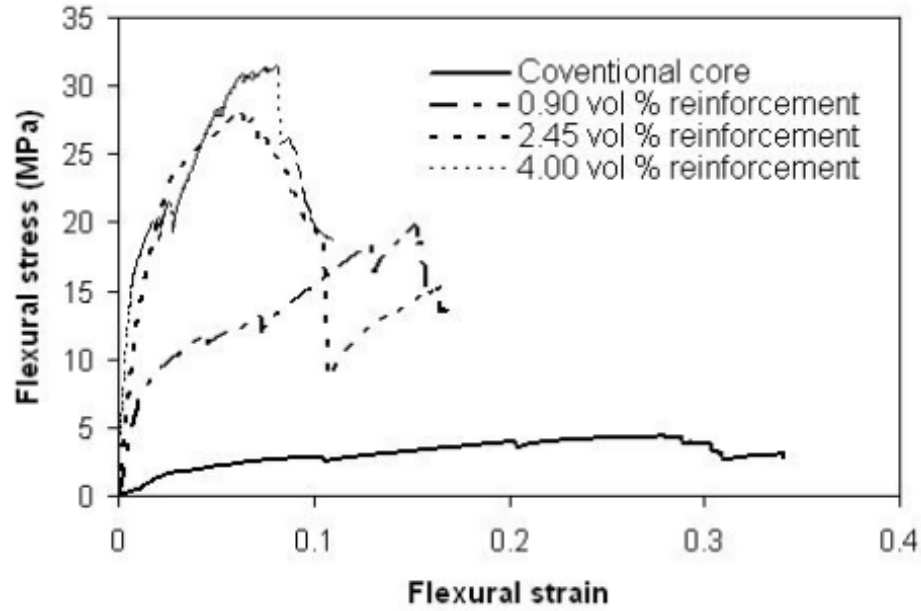


Figure 4.3 Global flexural response of sandwich composite structure under quasi-static load

The global flexural response of the sandwich composites with and without reinforcement in the foam core has been modeled using the Weibull fit that has been found to well describe the behavior of bundles of fibers, natural composite like Palmetto wood. However, the bilinear type of behavior of sandwich composites with conventional core and that with very low reinforcement can not be described well with the Weibull model. The Weibull fit to the global stress-strain response of the sandwich composite structures are depicted in Figure 4.4 and the Weibull parameters are listed in the Table 4.2. As depicted in the figure, the Weibull model underestimates the flexural stiffness of the sandwich with bilinear flexural behavior. However, for the sandwich composite with higher reinforcement vol %, the behavior tends to be more like a bundle of fiber and the Weibull model can be successfully used to quantify the mechanical behavior.

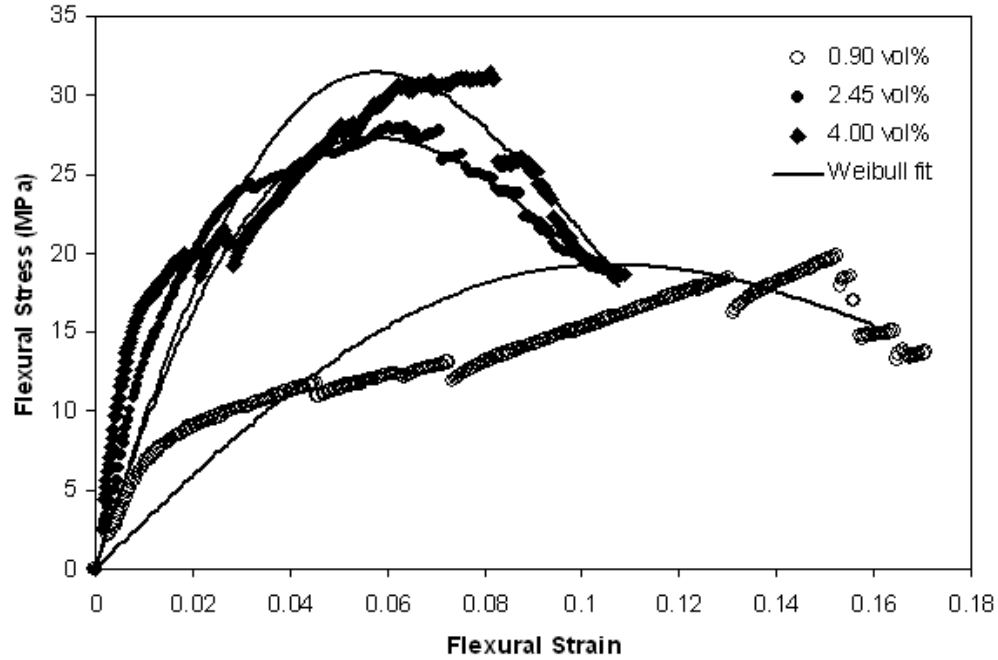


Figure 4.4 Weibull fit to the global flexural response of sandwich composite structures under quasi-static load. Since the Weibull model has been found to be useful for a bundle of fibers, the bilinear type response of the sandwich structures can not be captured well

Experiments were performed with several specimens to ensure reproducibility and variation in the material response over different specimens. Due to fabrication limitations, relative location and alignment of pin reinforcements in the specimens vary. Approximately 5-10% variation in the global flexural modulus was observed for the specimens tested.

The macroscale strain fields developed in the composite sandwich structure during flexural deformation is characterized by DIC technique as depicted in Figure 4.5. The strain fields obtained from the images at macro-scale appears similar to that in conventional sandwich structure. As evident from the strain fields, the compressive and shear strains are leading. The flexural strain (0.6 %) is significantly low as compared to the compressive and shear strains, which are of magnitude 7 % and 3 %, respectively.

The failure initiation is observed to occur by the accumulation of compressive strain below the indenter and shear strain at the facesheet-foam core interface.

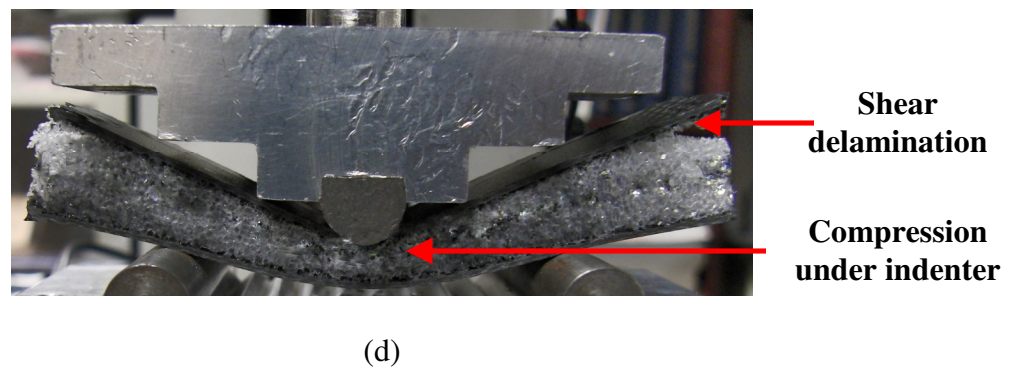
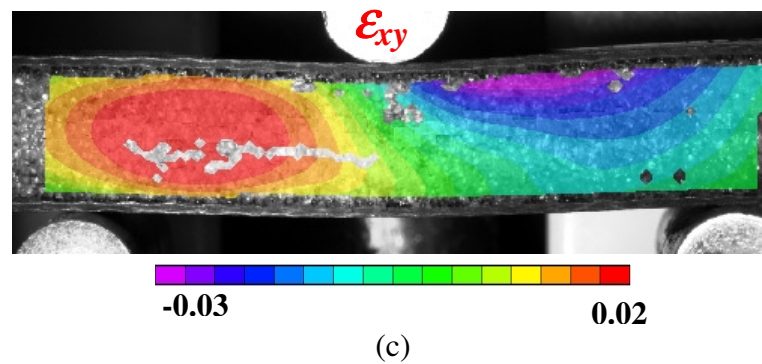
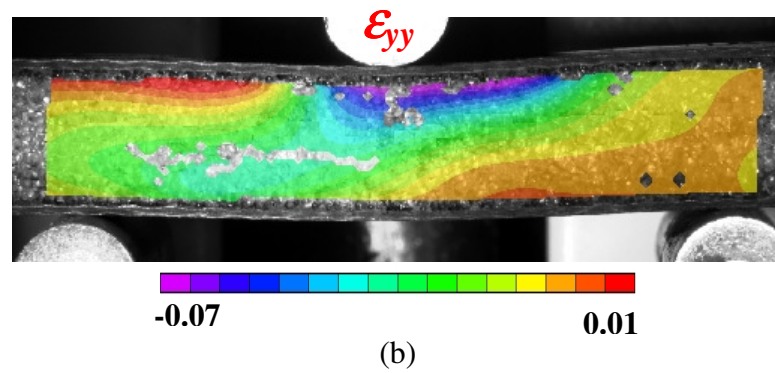
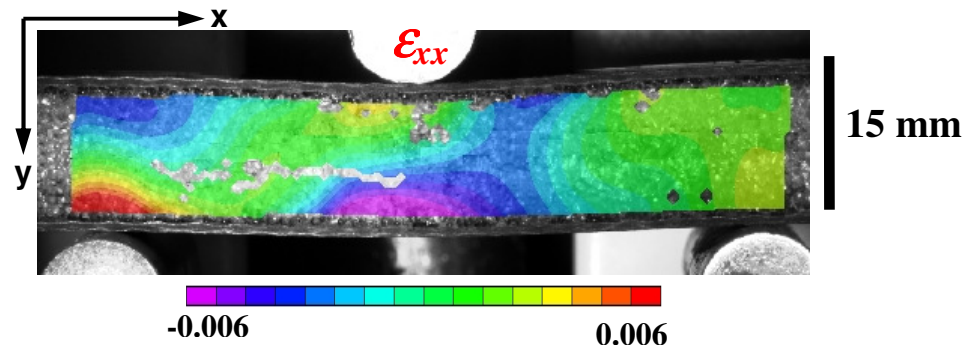


Figure 4.5 Macroscale (a) flexural, (b) compressive and (c) shear strain fields in the sandwich core corresponding to around 130 N load (Point A in *Figure 2*) and (d) failure mode by pore collapse in foam core under indenter and shear dominated debonding at the facesheet-foam core interface

Several investigations determined the failure modes in sandwich structure. One of the leading failure mechanisms in sandwich composites is interfacial failure. Using DIC technique the evolution of strain fields has been studied. In the sandwich with conventional core, the failure modes are found to be shear dominated delamination at the facesheet and core interface as well as bending/kinking failure of the facesheet under compression. The core has been noticed to undergo transverse compression causing increase in energy absorption. Whereas in the sandwich composite with conventional core, transverse compression was significant, in the bioinspired core, the transverse compression has been reduced by the added stiffness due to reinforcement. The shear dominated delamination at the facesheet-foam core interface is shown in Figure 4.5 (d).

To elucidate the deformation and load transfer mechanism at the interface of carbon rod reinforcement and foam and around the reinforced carbon rod, imaging at higher magnification has been performed during flexural test. The carbon rod reinforcement in foam core of the sandwich composite structure is shown in Figure 4.6 (a). The strain fields obtained by DIC of the images captured during three-point bend test of the specimen are depicted in Figure 4.6 (b-c). The image corresponds to the tensile side of the specimen around the central area between loading indenter and right support. It is noted that the foam core near the stiffer pultruded carbon rod is deformed under compression and shear. During the bending, the soft polymeric foam deforms more than the stiffer carbon rod reinforcement and the carbon rod along with flexural deformation exhibits rigid rotation. Thus, the carbon rod compresses the foam around it. The

pultruded carbon rod being mechanically stronger, the foam undergoes higher amount of compressive and shear strain at and around the carbon rod – foam core interface.

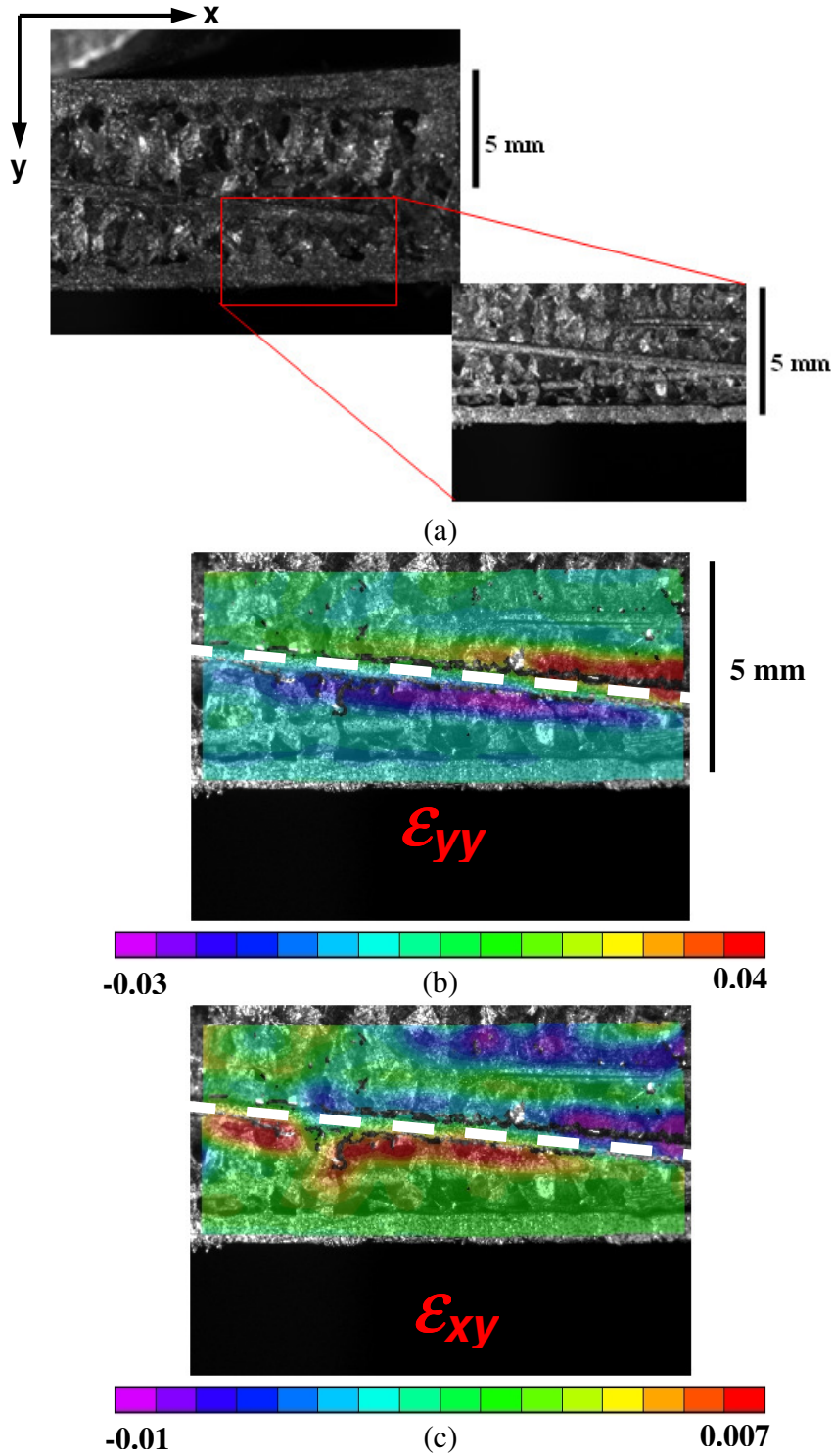


Figure 4.6 (a) Image of the core of the bioinspired sandwich composite structure at magnification of around 5X and (b) compressive and shear strain fields at the carbon rod

– foam core interface and under flexure at high magnification. Dotted white line represents the reinforced pultruded carbon rod in foam core. Shear and compressive strains are dominant around the carbon rod.

The use of reinforcement in the foam core of the sandwich composite increases the energy absorbance due to its increased interface in the core and localized deformation. However, since the equivalent bending stiffness (EI_{eq}) of the composite depends on material properties as well as size and position of the reinforcements, the effect of bioinspiration in the foam core of the composite sandwich structure also depends on size and properties of reinforcement (carbon rod). Detail computational model is required to explore the effects of size and properties of reinforcement and foam core on the mechanical behavior of bioinspired sandwich composite structures.

Loading condition/ Reinforcement	Weibull model parameters		
	E (MPa)	ε_0	β
QS/No reinforcement	-	-	-
QS/0.90 vol%	300	0.15	2.0
QS/2.45 vol%	930	0.075	1.5
QS/4.00 vol%	950	0.08	1.8
Dyn/No reinforcement	120	0.11	1.0
Dyn/0.90 %	780	0.02	0.6

Table 4.1 The modulus, E , and Weibull parameters (ε_0, β) obtained by fitting the flexural stress-strain curves for the sandwich composite specimens under quasi-static and dynamic load.

4.3.2 Characterization under Low Velocity Impact

The dynamic behavior of the composite sandwich structures has been characterized by low velocity impact at a global flexural strain rate of around 450/sec. The global flexural response of the sandwich composite specimens under low velocity impact is depicted in Figure 4.7. Only one amount of reinforcement has been considered for the dynamic characterization. To determine the dynamic load displacement response, acquired load cell data was smoothed to exclude noise in the data. As discussed earlier, the velocity and displacement history were obtained from the load cell response by integrating the equation of motion ($F_{Loadcell} = m_{bullet} a$) of the bullet shot at the specimen assuming equilibrium between the bullet and the sandwich composite specimen. The displacement and velocity were also obtained by high speed imaging and differentiating the displacement history. The displacement and velocity obtained from load cell and optical measurement were then correlated to determine the load – displacement response of the specimen. The load – displacement response was then converted to flexural stress – strain using the relations for flexure.

To quantify the flexural response of the sandwich under low velocity impact and compare with that of the quasi-static response, the Weibull model has been then fit to the flexural response of the specimen. The experimental flexural response and the resulting fit are depicted in Figure 4.7. The Weibull parameters used for the fit are listed in Table 4.1. As evidenced from the flexural response the bioinspiration increases the stiffness, strength and energy absorption of the composite sandwich structure. The flexural stiffness of the sandwich without reinforcement in the core has been determined to be around 120 MPa, whereas the stiffness of sandwich composite with 0.90 vol %

reinforcement in the core is around 185 MPa. Thereby the reinforcement in the core could be increased by around 60 % using a reinforcement of 0.90 vol % in the foam core. However, compared to the impact velocity, the specimen strength was low thus leading to high deformation of the specimen. The failure initiation of the sandwich without reinforcement was found to be around 10% compared to that of the sandwich with reinforcement in core being 7 %. The Weibull parameters obtained from the dynamic flexural response of the sandwich composite structures reflect only marginal improvement in the global behavior and the parameters are comparable in terms of numerical value. It has been seen that the bioinspired core enhances the impact resistance and energy absorbance of the specimen in a manner that is similar to the Palmetto wood. The global flexural response has been used to study the damage evolution characteristics that would be discussed later.

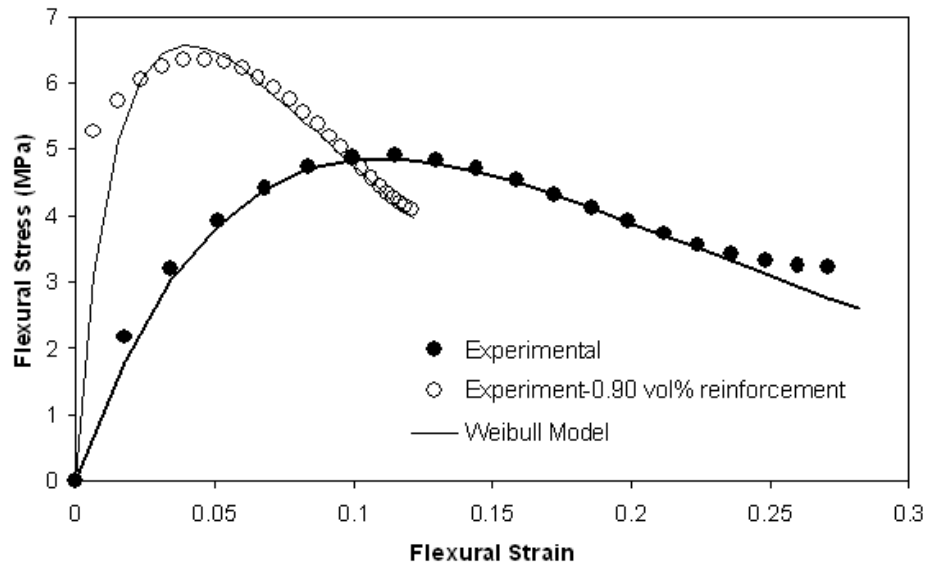


Figure 4.7 Flexural response of sandwich composite with and without reinforcement to the in the core under low velocity impact and Weibull fit to the experimental data

The displacement and strain fields have been determined by using DIC of the images captured during the test. However, the capability of multiscale DIC at higher magnification has been limited due to the trade off of resolution and imaging speed (fps). Thus imaging at specimen length scale only was possible. At the specimen length scale the deformation fields have been found to be like that of homogeneous beam under bending, however, high strain is accumulated near the indenter due to the effect of local deformation of the soft foam.. Thus, the deformation fields of the sandwich composites are not shown. The images of a sandwich composite specimen at undeformed and deformed state are shown in the Figure 4.8.

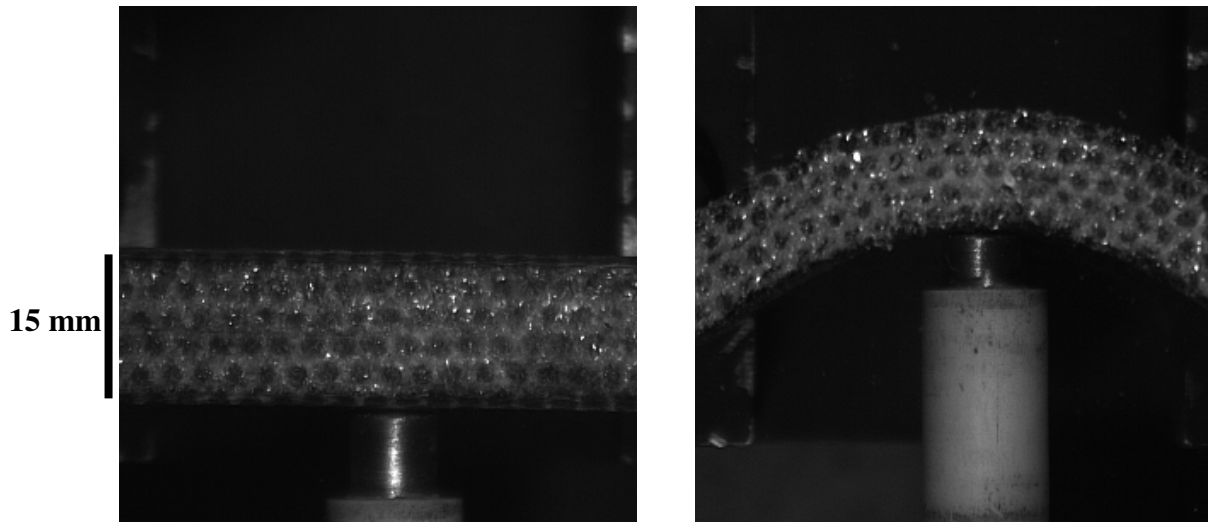


Figure 4.8 (Left) Undeformed and (right) Deformed sandwich composite specimen under low velocity impact

4.3.3 Damage Modeling of the Sandwich with Bioinspired Core

The damage evolution in the composite sandwich structures has been determined based on the definition of damage parameter $D = 1 - \sqrt{E/E_0}$, where E_0 is the initial modulus and E is the degraded modulus due to damage and is determined experimentally by

measuring the reduction of the modulus with strain. The damage model developed to study the damage evolution to account for the plastic deformation and pore collapse in the porous core in Palmetto wood has been employed to the global response of the sandwich composites. The evolution of damage with total flexural strain based on strain energy conservation has been used to describe the experimental measurements as given by,

$$D = D_{lim} \left[1 - \exp \left(-A (\varepsilon - \varepsilon_d) \right) \right], \quad 4.1$$

where D_{lim} represents the limiting amount of damage that can occur, ε_d is the strain at which damage initiates, and A is an acceleration factor that describes the evolution of damage with strain. Results from fitting the curves to the experimentally determined damage can be seen in Figure 4.9 and the parameters are listed in Table 4.2.

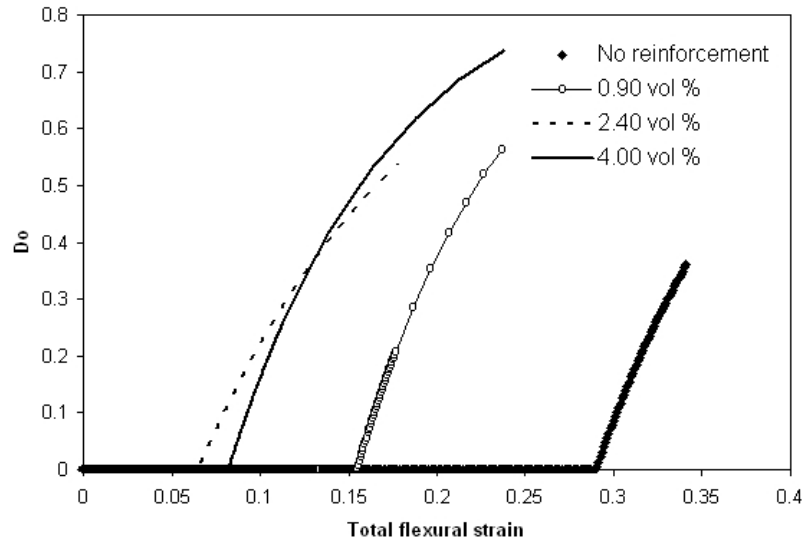


Figure 4.9 Damage evolution with total flexural strain in the sandwich composite specimens under quasi-static bending

The damage evolution parameters reveal that the damage initiation strain is reduced by the increase in reinforcement. A reinforcement of 0.90 vol% of carbon rod in the sandwich composite core reduced the damage initiation strain from around 0.30 to 0.15. Using Equation (4.1), the effect of volume fraction of reinforcement and loading rate on the damage accumulation are studied. The acceleration factor and limiting amount of damage did not appear to be affected substantially by the volume fraction of the macroscale pultruded carbon rod reinforcement and loading rate.

As discussed in the previous Chapter, a model was developed to account for the mechanism of plasticity due to pore collapse of the porous material in the study of damage behavior of Palmetto wood. The plastic flexural strain, ε_p , was related to the total flexural strain through a form of the conventional power law hardening relationship as

$$\varepsilon_p = \varepsilon \left[1 - \exp\left(-B(\varepsilon - \varepsilon_y)^p\right) \right], \quad 4.2$$

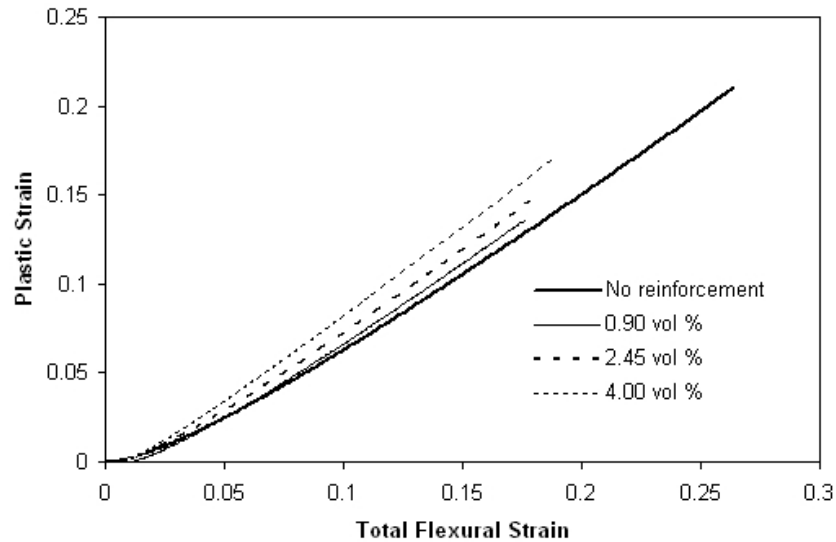
where ε_y is the yield strain and p and B are related to the power law hardening exponent and coefficient, respectively. The plastic strain could be determined experimentally by measuring the permanently deformed shape of the specimen. The evolution of macroscopic plastic strain with respect to the total strain has been determined and is depicted in Figure 4.10 (a), (b). The evolution of plastic strain with total global flexural strain is linear like that of Palmetto wood and the rate is not much affected by the volume fraction of reinforcement.

Similar to the damage modeling of Palmetto wood, Equations (4.1) and (4.2) were combined to determine the constitutive response of the composite sandwich material in

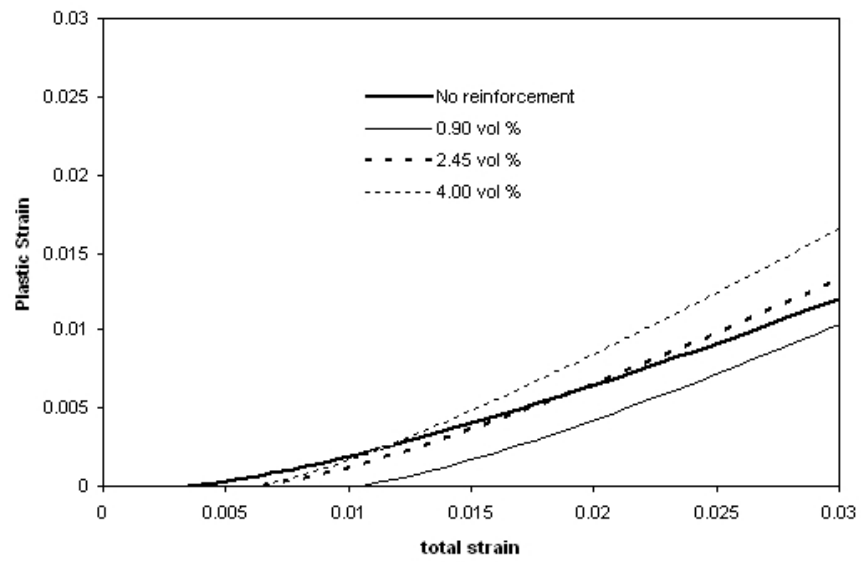
order to better understand the observed dependency of the plastic deformation on strain rate.

$$\sigma = E_0 (1 - D)^2 (\epsilon - \epsilon_p) \quad 4.3$$

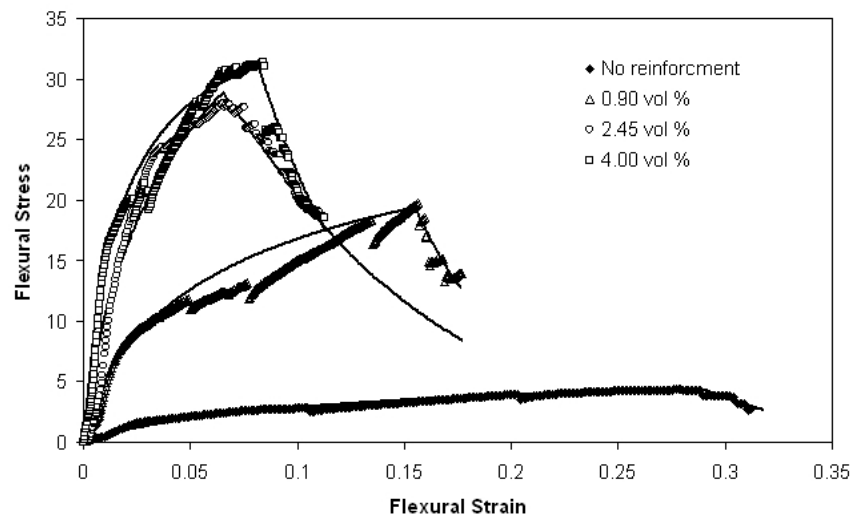
The constitutive relation in Equation 4.3 is then fit to the experimental stress-strain response. The resulting fits to the experimental data can be seen in Figure 4.10 (c). The flexural modulus and the fitting parameters of the damage model are listed in Table 4.2. As depicted in the figure, the flexural modulus is increased by the increase in reinforcement and the damage resistance is also enhanced. The damage model can be fit to the experimental data more accurately than the Weibull model to the bilinear behavior of the sandwich composite structures with conventional core and lower volume fraction of reinforcement, thereby allowing more precise determination of the damage parameters.



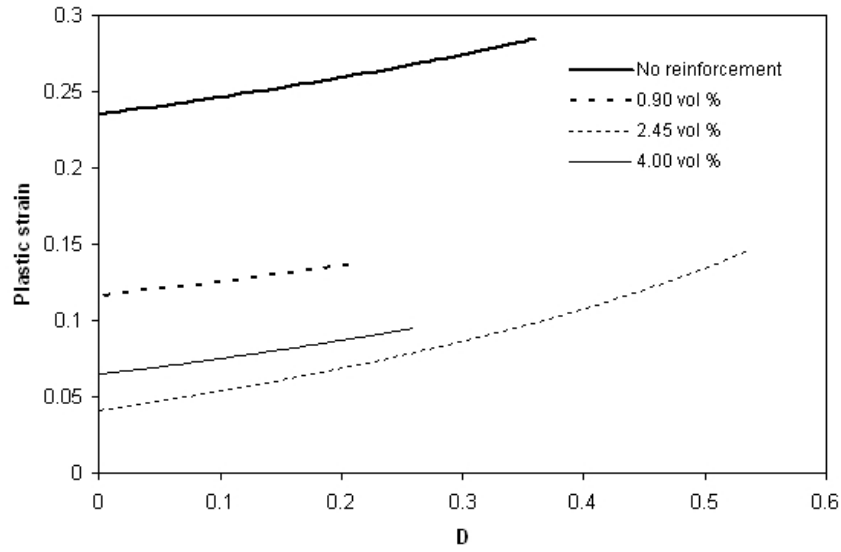
(a)



(b)



(c)



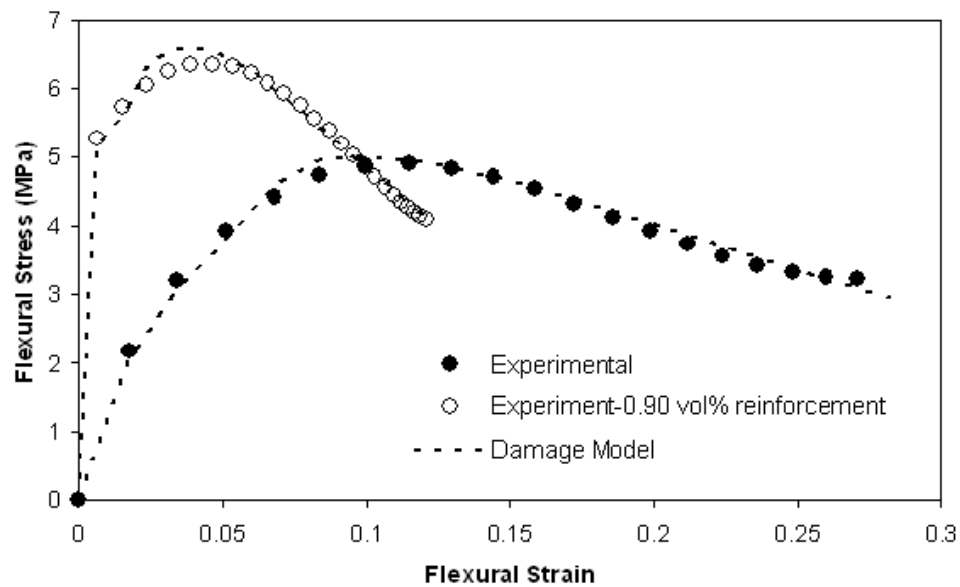
(d)

Figure 4.10 Damage evolution characteristics of sandwich composite specimens: (a) evolution of plastic strain with total global strain, (b) closer look at the plastic deformation, (c) fit of the damage model to the experimental response, and (d) damage evolution with the plastic strain

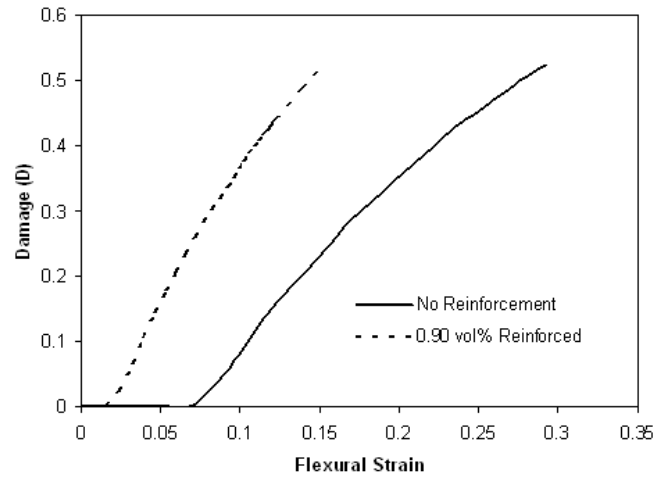
Loading condition/ Reinforcement	Weibull model			New damage model with plasticity						
	E (MPa)	ε_0	β	E (MPa)	ε_y	ε_d	D_{lim}	A	B	p
QS/No reinforcement	-	-	-	80	0.003	0.290	0.9	10	3.0	0.45
QS/0.90 vol%	300	0.15	2.0	500	0.010	0.155	0.9	12	3.5	0.40
QS/2.45 vol%	930	0.075	1.5	1200	0.006	0.065	0.9	8	4.0	0.43
QS/4.00 vol%	950	0.08	1.8	1780	0.006	0.082	0.9	11	5.6	0.42
Dyn/No reinforcement	120	0.11	1.0	120	0.03	0.075	0.9	4	1.55	0.3
Dyn/0.90 %	780	0.02	0.6	800	0.01	0.02	0.9	6.5	4	0.3

Table 4.2 The modulus, E , and Weibull parameters (ε_0, β) obtained by fitting the flexural stress-strain curves and the modulus, E , and damage initiation strain (ε_d) obtained from the damage model for the sandwich composite specimens

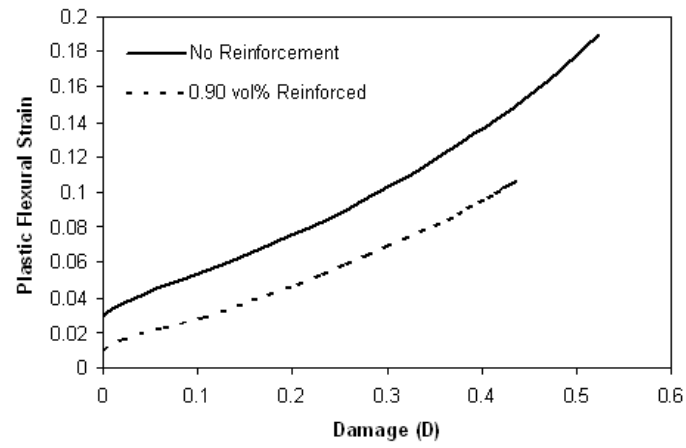
The damage model developed herein is also employed to the dynamic response of the sandwich structure with bioinspired core under low velocity impact. The resulting fit of the damage model to the experimental stress-strain response is depicted in Figure 4.11 (a). The damage evolution with total global flexural strain is depicted in Figure 4.11 (b). The evolution of plastic strain and the stress-strain response obtained from the damage model fit is depicted in Figure 4.11 (a). It is seen that the dynamic behavior in the context of damage evolution and damage resistance of the sandwich composite is not substantially different from that under quasi-static response, however, the strain at which the damage initiate and plastic strain accumulates is marginally affected.



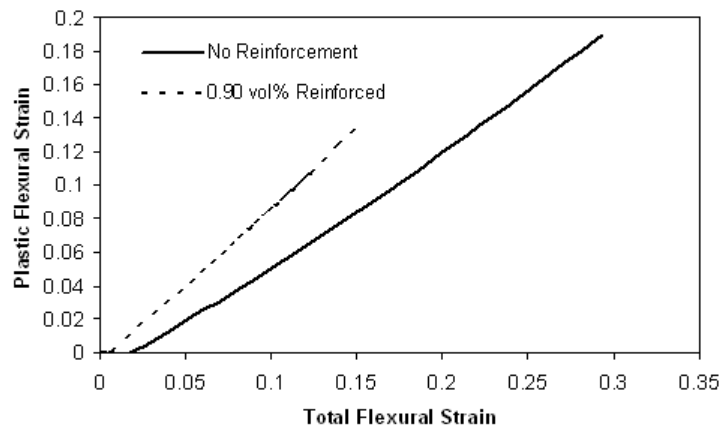
(a)



(b)



(c)



(d)

Figure 4.11 Dynamic damage behavior of the sandwich composite structures obtained from the damage model

4.4 Discussion of Results

Using the structural template of Palmetto wood, sandwich composite structure have been fabricated by reinforcement of pultruded carbon rod in the polymeric foam core and carbon fiber facesheet. The flexural mechanical behavior of the sandwich composites with different amount of reinforcement in the core has been characterized under quasi-static loading and low velocity impact and has been compared to that of the sandwich composite structure without reinforcement in the core. While the global flexural behavior was determined from the load cell data and displacement measured from the experiment, the deformation fields have been evaluated employing DIC to the images captured during the deformation. Single mode Weibull model has been used to study the flexural response of the sandwich composite structures. A damage model developed to account for the plastic deformation in the material has been used to relate the damage evolution with plastic deformation and determine the damage evolution parameters. The parameters obtained from the Weibull model and damage model has been used to quantify the effect of reinforcement and loading rate on the flexural behavior of the sandwich composites.

The quasi-static flexural response shows that the reinforcement in the foam core of the sandwich composite can increase the flexural modulus of the sandwich composite significantly compared to that of the sandwich without reinforcement in the core. An increase of more than 100% in the flexural modulus could be achieved by using reinforcement of pultruded carbon rods in the sandwich composite. However, with the increase in flexural stiffness and maximum load bearing capacity, the failure initiation strain is reduced. Thereby, a better combination of flexural stiffness and deformation characteristics can be achieved by tuning the reinforcement in the core. The deformation

fields obtained by DIC revealed that the deformation behavior at macroscale on the external face of the specimen is similar to that under bending, however, at the reinforcing rod and foam core interface, more localized deformation occurs. Thus by increased interface and localized deformation at the interfaces due to the reinforcement in the core, energy absorption capability is increased.

The dynamic behavior of the sandwich composite structure has been characterized at a strain rate of around 450/sec by low velocity impact. The results show that the flexural stiffness under low velocity impact is significantly increased (by around 50%) by using the carbon rod reinforcement in the core. The reinforcement in the core increased the strength of the sandwich as well as energy absorption capability.

The damage model developed to relate the scalar damage variable defined by degradation is modulus and plastic deformation in the material has been used to quantify the damage evolution characteristic. It has been seen that the increase in reinforcement decreases the damage initiation; however, the damage evolution remains qualitatively similar with very marginal affect. The plastic deformation with the global bending of the specimen could be extracted using the damage model and the evolution of the plastic strain was found to remain unaffected with the reinforcement.

The behavior of the sandwich composites have been compared with that of the Palmetto wood and it has been depicted that the flexural behavior of the sandwich composite structures can be tailored to achieve a required behavior of flexural stiffness and damage evolution by tuning the reinforcement in the foam core of the sandwich.

4.5 Summary

The present chapter discusses the fabrication of the sandwich composite structures with reinforcement in the foam core in order to enhance of the mechanical behavior by using the principles of deformation behavior of Palmetto wood. Sandwich composite structures have been fabricated with bioinspired cores though the reinforcement of pultruded carbon rod in the polymeric foam core to realize the enhancement in mechanical behavior. The flexural behavior of the sandwich composites has been characterized under quasi-static load and low velocity impact and the effects of the reinforcement in the core have been investigated. Three point flexural tests have been performed under quasi-static load and low velocity impact. The facesheet foam core interfacial adhesive has been nanoenhanced. The experimental results show that nano-enhancement increases the stiffness of sandwich structures. The macroscale reinforcements of pultruded carbon rod in the core of the sandwich composite help to increase the flexural stiffness. The increase in volume fraction of the macroscale reinforcements has been employed to transform the behavior of sandwich to that of a Palmetto wood. The damage model developed to characterize the plastic deformation in the Palmetto wood has been employed to the flexural response of the sandwich structures with foam core and bioinspired core. It has been noted that the behavior of the bioinspired core has been tuned to that of Palmetto wood compared to the foam core sandwich structure.

Chapter 5 Finite Element Modeling of Sandwich Structures

In this chapter, the computational modeling of the mechanical behavior of the sandwich composite structure is discussed. The sandwich composite structures have been fabricated and experimental characterization has been performed to understand the mechanical performance, energy absorption and damage resistance using the reinforcement in the porous polymeric foam core of sandwich composite. The experimental characterization showed that the mechanisms for enhanced mechanical behavior of Palmetto wood due to the reinforcement of macrofibers in the porous cellulose matrix can be translated to the engineering sandwich composite structures by using longitudinal reinforcement of pultruded carbon rods in the foam core of sandwich composite. Finite Element Analysis (FEA) has been performed to investigate the effects of reinforcement on the global flexural behavior and local deformation fields of the sandwich composite structures under quasi-static load. The effect of reinforcement amount was varied to verify the experimental observations. This chapter details the motivation for computational model, modeling and the results obtained from the FEA of the model of sandwich composite structures with reinforcement in foam core.

5.1 Motivation

The engineered sandwich composite structures have been fabricated in Laboratory following the hierarchical structure of Palmetto wood, where the mechanically stronger macrofibers are reinforced in the soft porous cellulose matrix. However, Laboratory fabrication and experimental characterization has limited scope to further investigate the

whole parametric domain of the design space of the materials. The reinforcement size, amount and the core material characteristics would significantly impact the interaction of the constituents of the sandwich composite structure, thereby affecting the global properties of the sandwich composite. The FEA can verify and validate the experimental observations of the global behavior and the local deformation characteristics. To study the effect of constituent materials and the effect of the geometric and material properties of the reinforcement on the sandwich composite behavior in detail, a parametric study through computational model is necessary. In the present work, the effect of reinforcement on the sandwich composite has been studied to verify the experimental observations using homogeneous isotropic properties of the constituents.

5.2 Finite Element Analysis (FEA)

The Finite Element Analysis (FEA) is performed in commercially available software Abaqus 6.10 (SIMULIA, PROVIDENCE, RI). For initial investigation of the effect of the reinforcement in the core of the sandwich composite structure, the cellular foam core has been modeled as homogeneous isotropic continuous media. Cylindrical rods have been placed inside the core to represent the reinforcement of pultruded carbon rods. The material properties of the foam and facesheet have been experimentally determined for the simulations. The amount of rod has been increased to vary the reinforcement volume fraction to study the effect of reinforcement on the global behavior and verify experimental observations. The global behavior was studied through the homogenization of the reinforced core. The local deformation field was investigated using the detail model of the rods to compare with the full field experimental deformation measurements by Digital Image Correlation (DIC). The interfaces at facesheet-core and reinforcement-

core have been assumed to be in perfect contact through the TIE option available in Abaqus. The simulations have been performed with reduced size of the sandwich composite compared to the experimental specimens. The model has been meshed by 8-noded linear brick element. The out-of-plane degrees of freedom have been constrained to obtain plane strain condition. Schematic diagram of the simulation model is depicted in Figure 5.1.

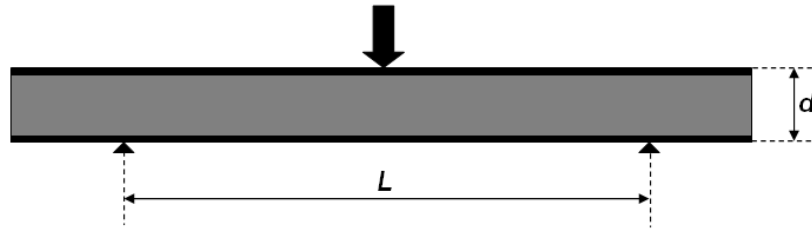


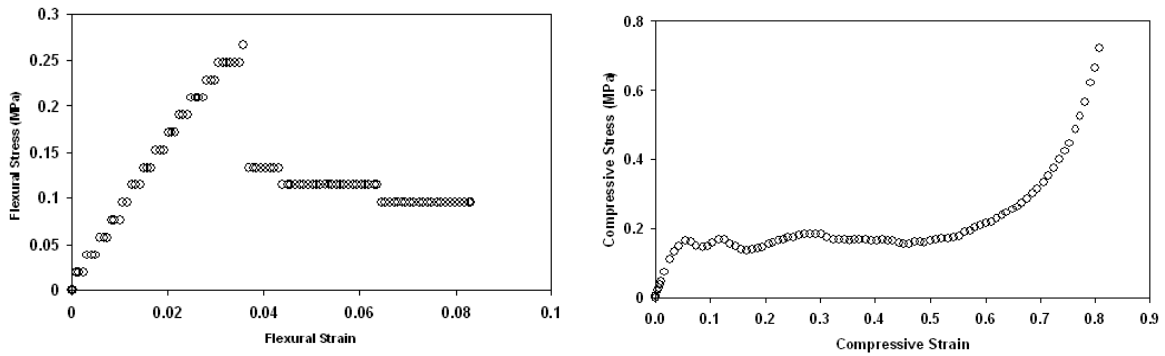
Figure 5.1 Schematic of the FE simulation of flexure of sandwich composite structures

5.3 Material Properties, Mesh and Model validation

5.3.1 Material Properties

The model for the FEA of the sandwich composite structure has been developed based on the isotropic continuum assumption of constituent carbon fiber facesheet, polymeric foam core and pultruded carbon rod reinforcement. The material constants have been determined experimentally. The experimental response of the foam material under flexure and compressive load are shown in Figure 5.2. The moduli of the foam core, facesheet were experimentally determined to be around 7 MPa and 32200 MPa. The pultruded carbon rods have a tensile modulus of around 100 GPa. However, since in the fabricated specimens, the alignment of the pultruded carbon rods has not been perfect and

foam material might have been damaged during penetration of the carbon rods, the effective bending stiffness of the carbon rod has been reduced. Therefore, the reduced modulus of carbon rod was estimated to be 70 GPa. The material properties of the foam has been assumed to be elastic perfectly plastic with a yield stress of 0.20 MPa. The experimentally determined flexural response of the facesheet material and the plastic behavior of the facesheet material used in the simulation have been depicted in Figure 5.3. The simulation of sandwich composite structure has been performed using perfect bonding at the core-facesheet interfaces. The material properties have been listed in Table 5.1.



(a)

Figure 5.2 Experimentally determined properties of foam material under (a) flexure and (b) compression

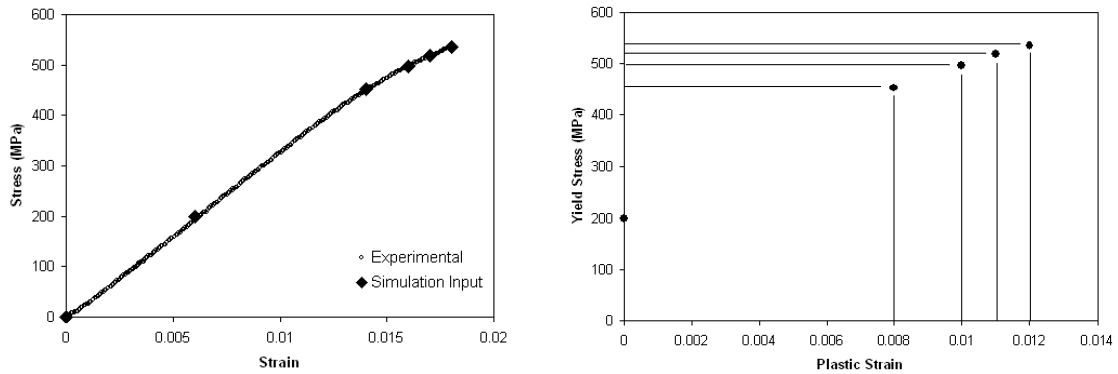


Figure 5.3 Properties of facesheet material (a) experimental and (b) simulation input for plastic deformation

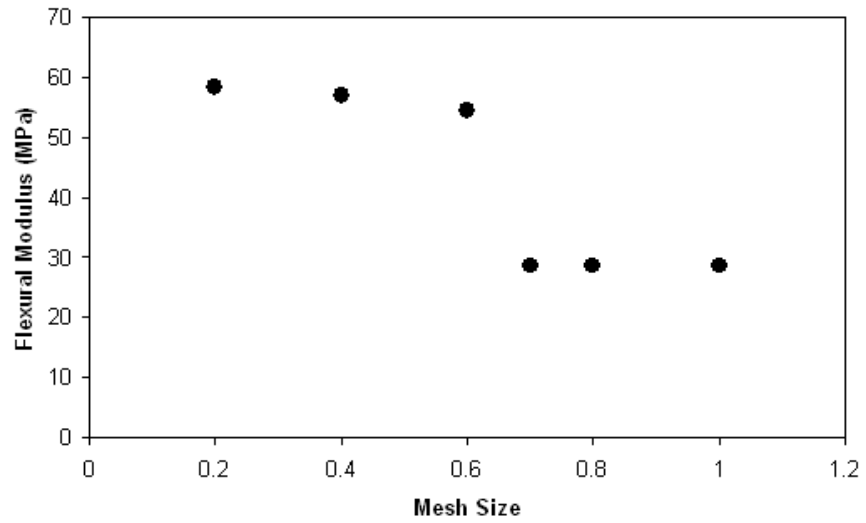
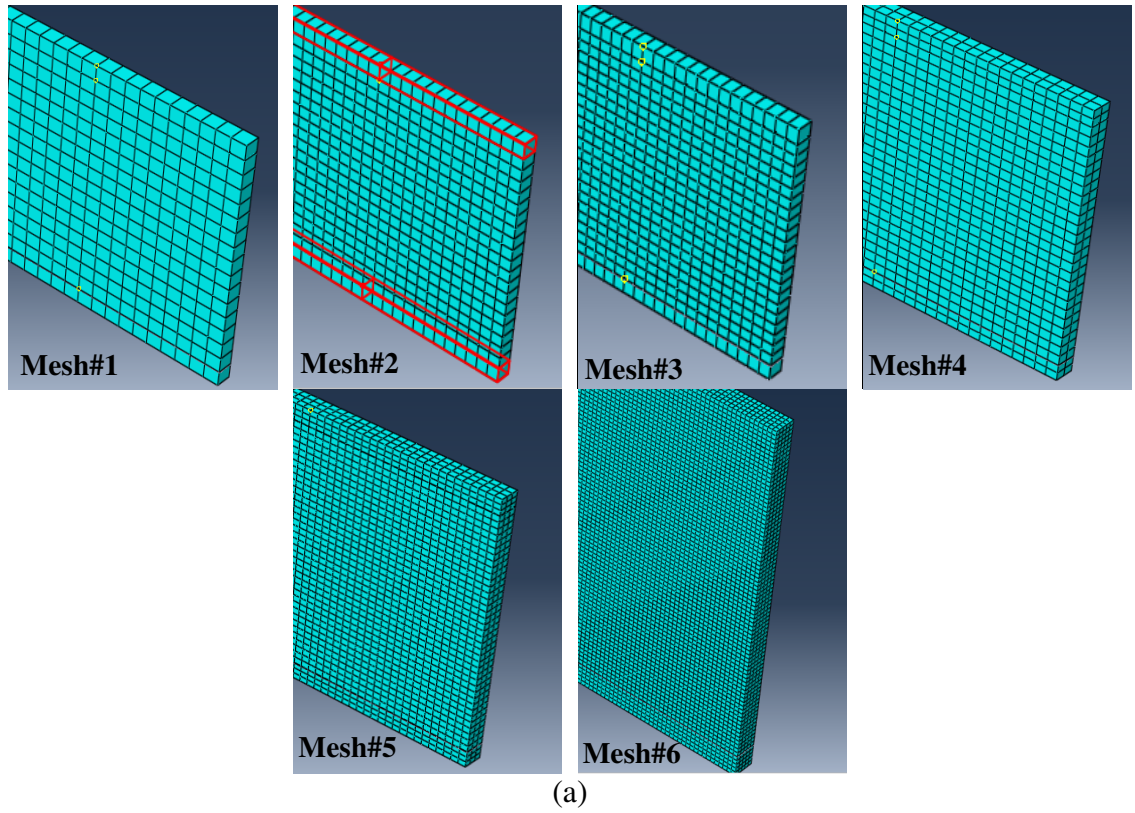
Core properties (Elastic –perfectly plastic)		Facesheet properties (Elastic – plastic)		Reinforcement properties (Elastic perfectly plastic)	
Elastic Modulus	Poisson's ratio	Elastic Modulus	Poisson's ratio	Elastic Modulus	Poisson's ratio
7 MPa	0.3	32200 MPa	0.3	70 GPa	0.3
Yield Stress		Yield stress	Plastic strain	Yields Stress	
0.20 MPa		200 MPa	0	100 MPa	
		452 MPa	0.008		
		497 MPa	0.01		
		519 MPa	0.011		
		535 MPa	0.012		

Table 5.1 Material properties of foam core, facesheet and reinforcement used in the simulation

5.3.2 Mesh Convergence

The mesh convergence study has been performed by changing the mesh size and a converged mesh size has been used to perform the simulations. The model has been discretized using linear 8 noded brick element. The effect of mesh size on the flexural modulus has been depicted in Figure 5.4 by showing the calculated flexural modulus with respect to mesh size. The mesh detail for different mesh densities are listed in Table 5.2. The jump in the response due for the cases Mesh#3 and Mesh#4 arises due to the

discretization of the facesheet in more elements in the thickness and width direction. The simulations have been performed with a reasonable mesh size for precise results.



(b)

Figure 5.4 (a) Mesh density in the sandwich composite model and flexural modulus for different mesh density

Mesh #	Element Size	Total Elements	Flexural Modulus (MPa)
1	1.0	1360	28.66
2	0.8	2142	28.65
3	0.7	2622	28.65
4	0.6	7772	54.50
5	0.4	26400	57.01
6	0.2	170000	58.26

Table 5.2 Mesh details and flexural modulus determined from the simulation

5.3.3 Model Validation

The simulation of the conventional sandwich composite structure without any reinforcement in the core was performed using experimentally determined properties of the foam and facesheet to compare with the flexural response obtained from experiments. The global flexural response was determined from the applied displacement at the central loading point and reaction forces at the supports. The flexure stress-strain response was calculated using the engineering relations $\sigma_f = \frac{3PL}{2bd^2}$ and $\epsilon_f = \frac{6Dd}{L^2}$, where P, D are reaction force and loading point displacement, L is the support span and bXd is the cross section (width X height) of the sandwich composite beam as shown in Figure 5.1. The simulation has been performed using linear 8-noded brick element with elastic-perfectly plastic foam and elastic-plastic facesheet properties as listed in Table 5.1. It has been seen that with sufficiently fine mesh, 8-noded element with reduced integration scheme offers similar accuracy as 20-noded element. The flexural response obtained from the simulation was found to closely match with that obtained from the experiment. The

present study has been limited to elastic plastic deformation and damage initiation to avoid the complexity of estimation of properties for damage evolution that requires detail experimental characterization of the constituent materials.

The strain fields obtained from the simulation in the sandwich composite material under flexure is depicted in Figure 5.6. The strain fields correspond to around 2 MPa of global flexural stress level. The qualitative behavior of the deformation fields are seen to closely match with that obtained from the experimental measurements using DIC. Thus the homogeneous isotropic assumption and continuum modeling was found to be useful to numerically verify the response of the composite sandwich and thus, in modeling the effects of reinforcements on the global as well as local deformation behavior.

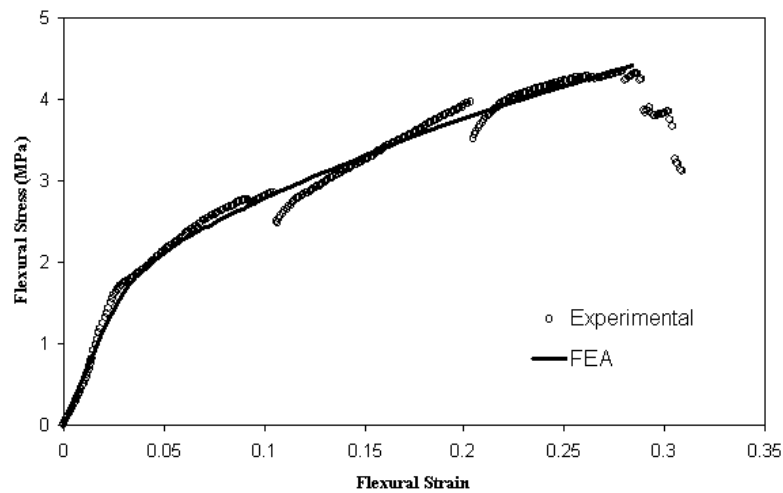


Figure 5.5 Comparison of flexural response obtained from experiment and FEA of sandwich composite structure

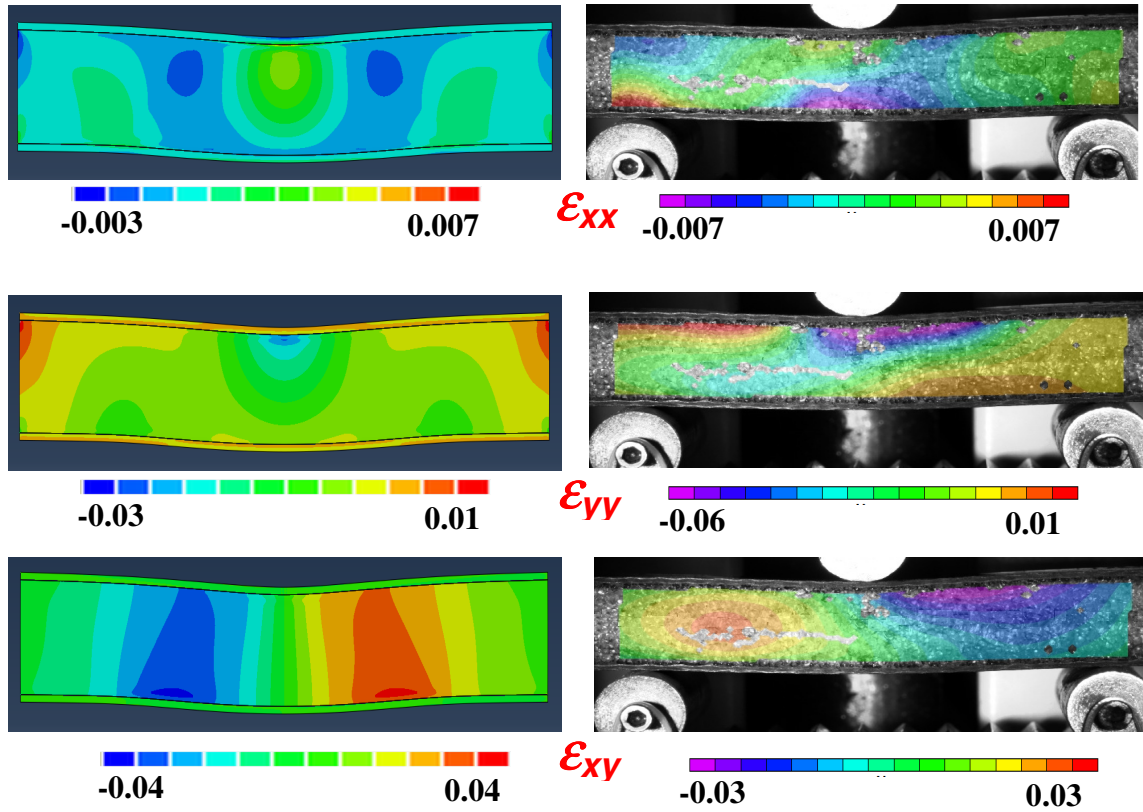


Figure 5.6 Strain fields in the sandwich composite obtained from FEA and experiment

5.4 Global Flexural Response from FEA: Effect of Reinforcement

5.4.1 Effect of Reinforcement on Global Flexural Response

The simulations were performed with the experimentally determined facesheet and foam core material properties to quantify the effect of reinforcement in the core on the global flexural modulus of the sandwich composite structure. Displacement control simulation was performed to evaluate the global flexural response of sandwich structure with similar core properties and different reinforcement amount. A uniform displacement was applied at the top facesheet of the sandwich composite beam. The force-displacement data was obtained from the global applied displacement at the top and the reaction forces obtained from the supports at the bottom. The load-displacement response

was then transformed to flexural stress-strain response using engineering relations of flexure.

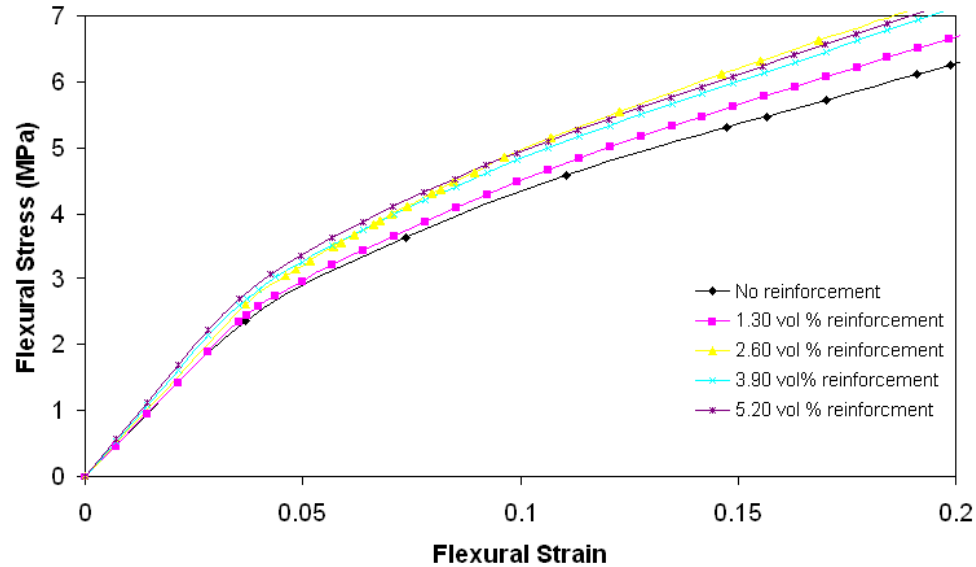


Figure 5.7 Flexural response of the reinforced sandwich composite structure with several vol % of reinforcement

These simulations have been performed assuming perfect contact between the reinforcing rod and the foam core. From the simulations, it is seen that the effect of reinforcement amount on the increase of global flexural stiffness is minimal for the presented amount of reinforcement unlike the experimental observations.

The results obtained from the simulations show that the reinforcement in the foam core increases the global flexural modulus by only around 10% from the base sandwich composite structure (Figure 5.7) unlike that measured in experiments. The sandwich composite structures had been a complex system to model numerically due to the high difference in the properties of the constituents. It is believed that the effect of the reinforcement could not be captured well due to cushioning effect of the soft foam core arising from the very high difference in the modulus of the reinforcement and foam

material. To overcome the complexity, a homogenization methodology has been adopted to capture the effect of reinforcement on the global flexural response of the sandwich composites with reinforcement in the core.

5.4.2 Variation of Flexural Modulus with Volume Fraction

The schematic of cross-section of a sandwich composite with reinforcement in the core is depicted in Figure 5.8.

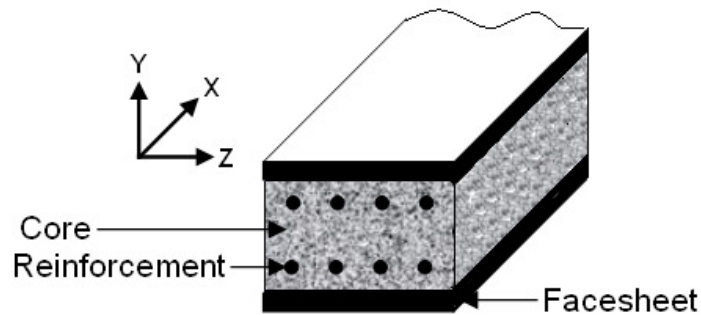


Figure 5.8 Schematic of the cross-section of a reinforced sandwich composite

However, for the sandwich composite structures prepared in laboratory with reinforcement in the core has misalignment as well randomness in position. Apart from that the epoxy adhesive layer at the foam core – reinforcement rod contributes to the stiffness. Thus, modeling sandwich composite with reinforcement of pultruded carbon rods requires significant effort. For the purpose of parametric study, simulations have been performed with the assumption of aligned reinforcement and perfect contact between the reinforcement and foam core without any physical dimension of the adhesive layer.

It has been experimentally seen that the increase in reinforcement volume fraction increases the flexural stiffness of the sandwich. To study the effect of reinforcement volume fraction in the flexural stiffness, simulations are performed to determine the

global flexural stiffness of the sandwich composites with different volume fraction. For these simulations, the properties of foam core, facesheet and reinforcing carbon rod are maintained same and the amount of volume fraction has been increased. The sandwich for the basis of comparison has no reinforcement and the flexural stiffness is 60 Mpa. The flexural stiffness of several sandwich structures with different volume fractions is determined from the simulation of three point beam bending. The normalized flexural stiffness with respect to the volume fraction is depicted in Figure 5.9. Apart from the amount of reinforcement, the size of the reinforcing rod was also considered. As seen from the Figure 5.9, to achieve an increase by 40-50% in the flexural modulus, depending on the size of the reinforcement 10-15 vol % reinforcement is required. Similar observations were made in the characterization of the Palmetto wood. It was determined that the Palmetto wood had a radial distribution of the macrofiber from 12 – 20 vol % fractions, leading to significant increase in the flexural modulus. It can be noted from the simulation results that the dependency of the global flexural modulus on the reinforcement vol % and size of the reinforcement is very closely linear.

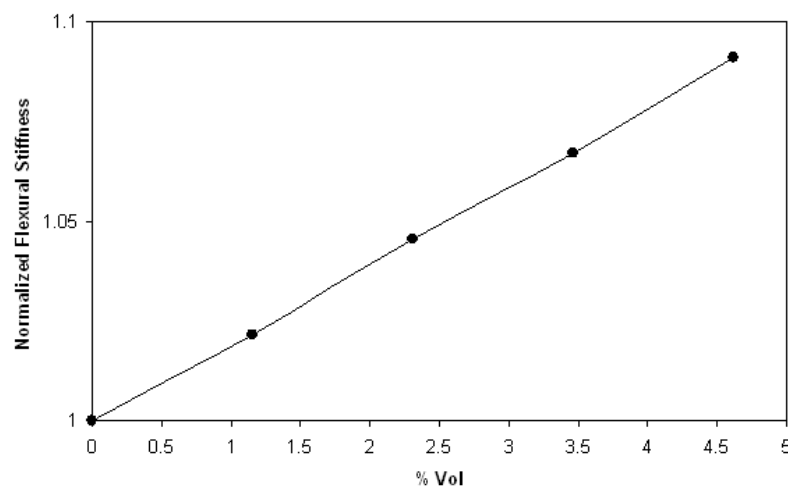
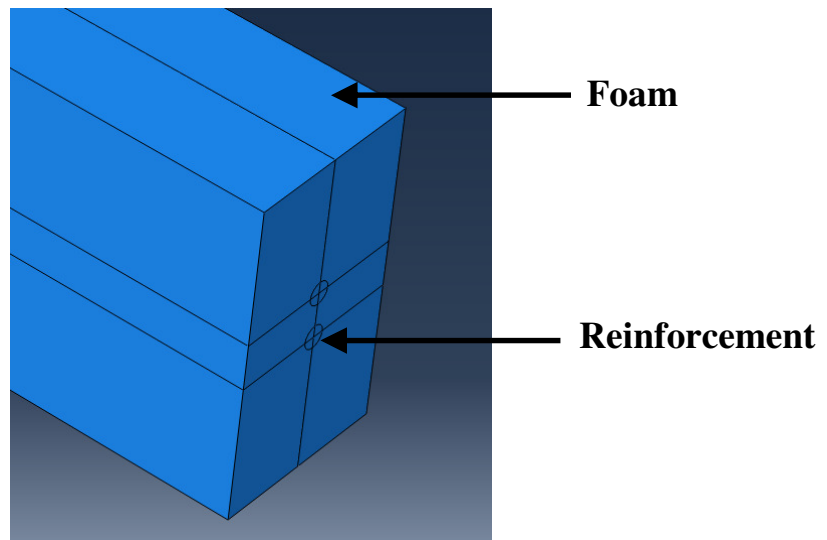


Figure 5.9 Effect of vol % of reinforcement on global flexural modulus

5.5 Modeling of Foam Core with Reinforcement for Homogenization of Properties

As discussed earlier, it was found that the effects of carbon rod reinforcement were not well-captured in the FEA due to high difference in material properties. To properly capture the effect of the reinforcement in the core, only the foam core with the reinforcement of pultruded carbon rod has been studied through simulation. The reinforcing rods have been systematically placed symmetrically measured from the central line of the sandwich to best match the fabricated sandwich composites. The simulation has been performed based on the 'homogenization' concept to determine the global response of the core as a homogenous material taking into effect of the reinforcement using representative core with reinforcement (Figure 5.10 (a)). Thus, the misalignment of the carbon rods in the foam core also can be taken care of. The properties of the reinforced core have been thus determined and used in the simulation of flexure of the sandwich composite structure with reinforcement in the core. Herein the foam properties were assumed to be elastic-perfectly plastic and the rod properties to be elastic. The flexure response of the representative foam core with 0.9 vol % and 2.45 vol% reinforcement has been depicted in Figure 5.10 (b). The global flexural modulus is found to increase to 25 MPa by reinforcement of around 0.9 vol% and to 55 MPa by reinforcement of around 2.45 vol% of pultruded carbon rod compared to the foam modulus of 7 MPa. The flexural response obtained from the simulation of the core with reinforcement has been then used as the material property of the homogenized core of the sandwich composite structure. It can be noted that in this approach the effect of reinforcement of the mechanically stronger reinforcement in the soft foam can be well captured on the elastic-plastic deformation of the foam. Thus equivalent homogenized

global flexural response was determined for the cores that were studied experimentally for the simulation of flexure of sandwich composites.



(a)

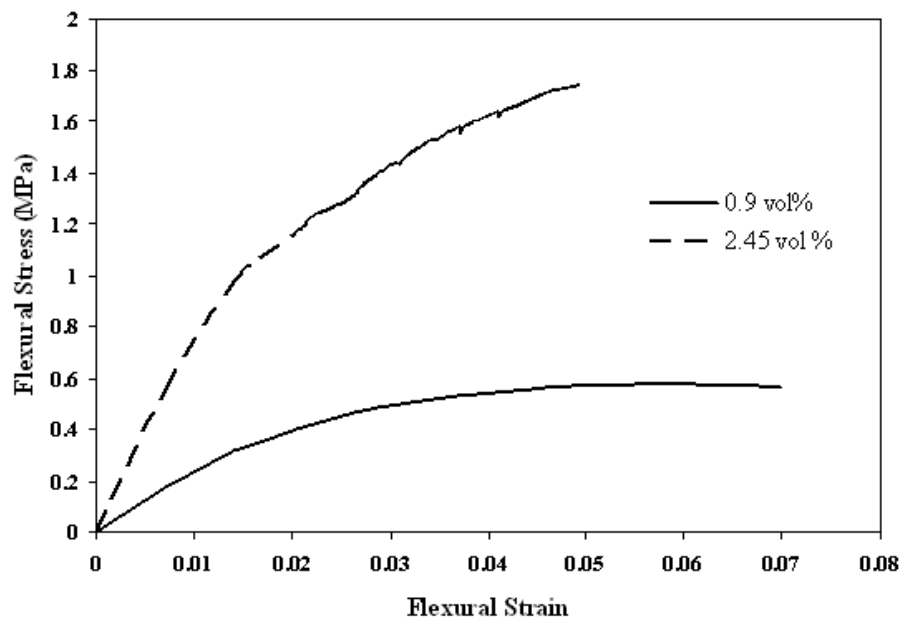


Figure 5.10 (a) Representative foam core with reinforcement and (b) flexural response of the reinforced core to determine the homogenized behavior

5.6 Flexural Response of the Reinforced Sandwich from FEA and Experiment

Simulations have been performed with reinforcement in the foam core with the amount of reinforcement being similar to the ones in experimental characterization. A sandwich model with lesser width has been used for the simulation to reduce the computational cost. To eliminate the out of plane deformation, plane strain condition was obtained by restricting the out of plane degrees of freedom. The properties of reinforced foam core material have been determined by the homogenization of the reinforcement in the foam core estimated from the flexural simulation of the foam core with reinforcement as discussed in the previous section. A representative reinforced sandwich composite and its homogenized model is depicted in Figure 5.11. In the simulation, a displacement has been applied at the central position of the sandwich model and reaction force at the supports has been extracted. The force displacement response has been transformed to the flexural stress-strain response using engineering relations. The present model assumes isotropic properties of the reinforced core. Since, the out-of-plane deformation was restricted to obtain plane strain condition; the out-of-plane properties would not affect the deformation behavior greatly.

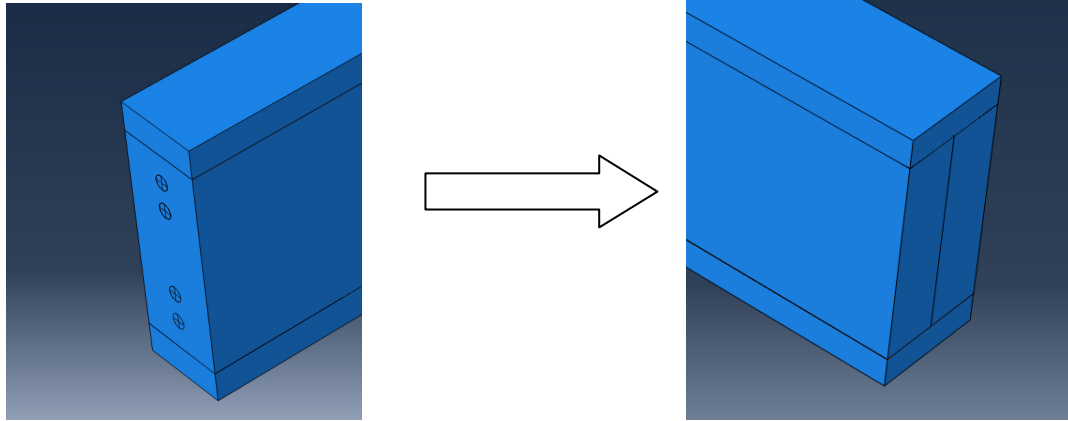


Figure 5.11 Model sandwich composite with reinforcement in the core and homogenized core

The flexural response of the reinforced sandwich composite using homogenized properties with 0.90 vol % and 2.45 vol % reinforcement in the core had been determined from the simulation results with equivalent homogenized core properties. The homogenized properties of the core estimated by the simulation of the reinforced foam core have been listed in the Table 5.3.

Thus it was then possible to determine the effect of the reinforcement on the global flexural behavior of the sandwich composite structures with reinforcement in the core. The flexural behavior measured experimentally and that obtained from simulation have been depicted in the Figure 5.12. The global behavior of the sandwich composite structure is found to match very closely with the experimental measurement. It can be noted that a 0.90 vol% of reinforcement in the sandwich score increases the global flexural stiffness to around 600 MPa and 2.45 vol% reinforcement increases the same to around 1100 MPa.

Sandwich composite	Effective Elastic modulus of core (Mpa)	Yield stress (Mpa)
No reinforcement	7	0.20
0.90 vol %	25	0.55
2.45 vol %	55	1.10

Table 5.3 Properties of the foam core estimated from finite element simulation

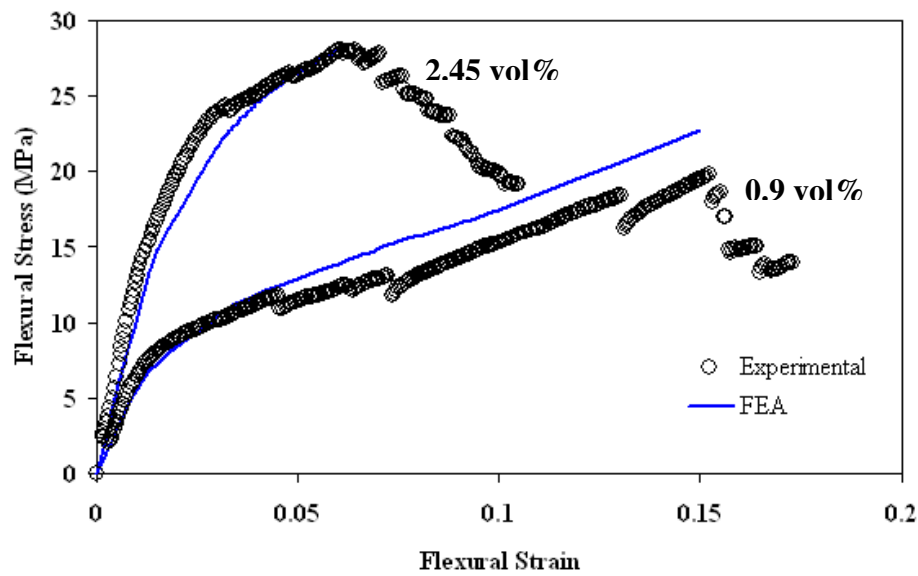


Figure 5.12 Flexural behavior of sandwich composite structure using homogenized properties of the reinforced core in simulation and experiment

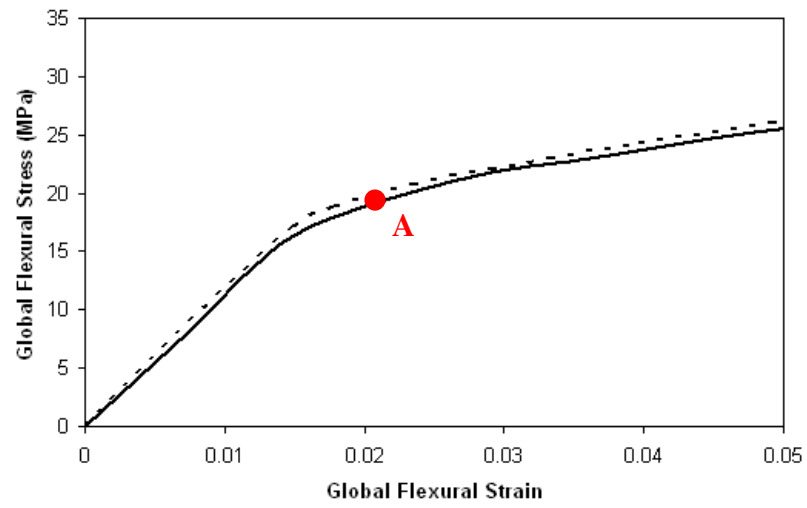
5.7 Effect of Reinforcement on Local Strain Fields

Previous experimental studies showed that the reinforcement in the sandwich core increases the stiffness as well as strain energy absorption capability by localized deformation at lower length scales at the interfaces in between the reinforcement and porous soft core. The multiscale experimental characterization of the deformation behavior revealed that the local deformation plays an important role on the mechanical behavior. To elucidate the localized deformation, the inhomogeneous strain fields in the

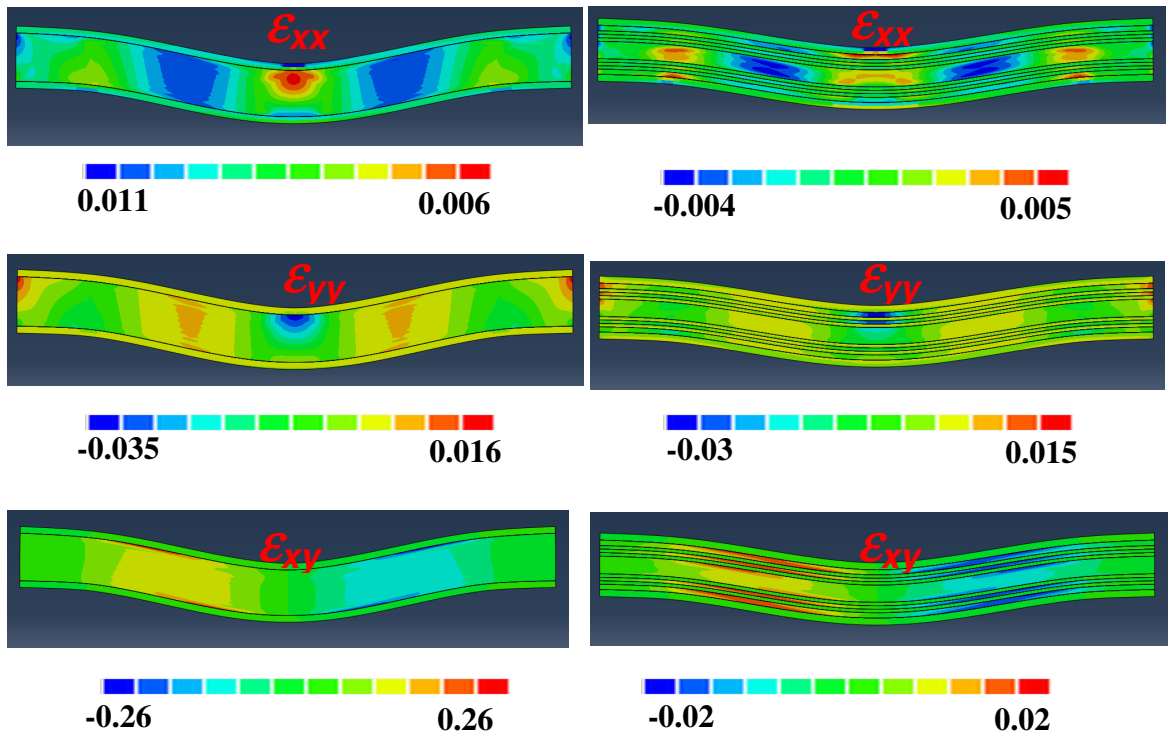
sandwich beam due to reinforcement have been investigated using a detail model of reinforcement in the core to compare with the deformation fields observed experimentally by DIC. The mesh has been created using 8noded linear brick element. This simulation can not capture the global flexural response, however, is useful for the insight of the local deformation fields. The strain fields obtained from the FEA of the flexural response of sandwich composite structures with and without reinforcement in the core have been elucidated. It is observed that the strain fields are concentrated in the soft core sandwich structures and high concentration of shear strain occur at the facesheet-foam core interface, thereby leading to delamination and local crushing failure of the foam core. The reinforcement of comparatively stiffer material in the core of the sandwich composite increases the interfaces of property mismatch and create several sites for localized deformation. Thus, more interfaces diffuse the strain energy leading to an increase in energy absorbing capability and damage resistance.

The simulation results have been used to study the effect of reinforcement on local the deformation behavior in the sandwich composite structures under quasi-static flexure. The global flexural response is depicted in Figure 5.13 (a) for the sandwich without any reinforcement and with around 2.45 vol% reinforcement. The global flexural response shows only marginal effect of the reinforcement. The local strain fields developed in the sandwich composite with around 2.45 vol% reinforcement of rods has been compared with the sandwich composite with same constituent properties but without the reinforcement. The simulations of the sandwich and reinforced sandwich were performed with perfect contact at the interfaces, and elastic-perfectly plastic core, elastic-plastic facesheet and linear reinforcement. The global flexural modulus was found to be

increased by only around 10 % due to the reinforcement of around 2.45 vol % of reinforcement. However, the local deformation characteristics have been significantly affected. The planar strain fields under at a load level of around 21 Mpa are depicted in Figure 5.13 (b). The strain fields obtained from the detail discrete model the reinforced sandwich composite are similar to that observed in experiment as shown in Figure 5.13 (c). The longitudinal flexural strain is found to be decreased minimally; however, the compressive and shear strains are affected more. The reinforcement reduced the local compressive strain to 0.03 from 0.035. In the sandwich without any reinforcement the localized shear strains occurred only at the facesheet-foam core interface. The reinforcements of rod in the core of the sandwich increased the interfaces, thereby increasing the sites of localized shear deformation. The maximum local shear strain was around 0.02, whereas the same for the sandwich without reinforcement was 0.26. Thus, the reinforcement reduced the magnitude of the local strain, and by virtue of increased interfaces, the deformations are more diffused.



(a)



(b)

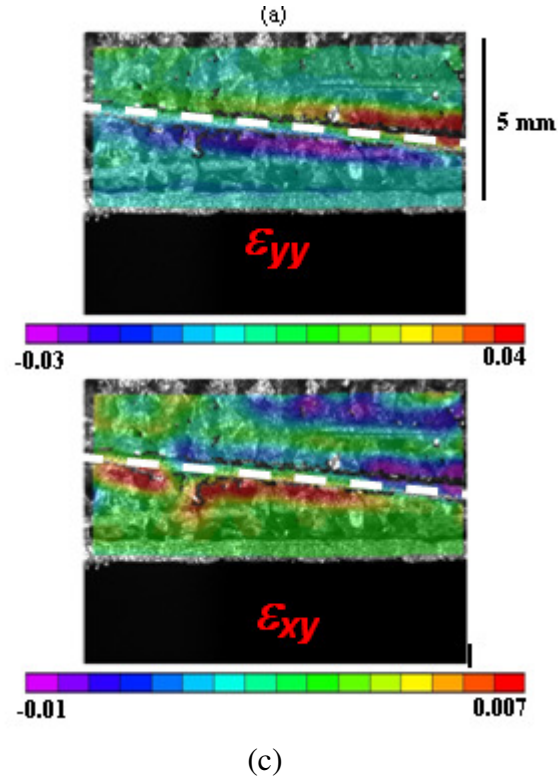


Figure 5.13 (a) Global flexural response and (b) effect of reinforcement on the local deformation fields in sandwich composite under flexure. The strain fields correspond to a global flexural stress level of around 21 MPa (Point A) (c) experimental observations of strain concentrations at the reinforcement - foam core interface in sandwich composite structure

5.8 Effect of Reinforcement on Damage Initiation

The effect of the reinforcement in the damage initiation and the strain fields developed prior to damage initiation has been studied through simulations using consistent foam core properties and reinforcement. The simulation results of the sandwich composites are compared for the response of the sandwich with foam properties calibrated from the experimental response with and without reinforcement. The damage initiation criteria were identified to match experimentally observed damage initiation.

The flexural simulation was performed without any reinforcement with the foam properties corresponding to the sandwich with 2.45 vol% reinforcement to study the

effect of reinforcement in the core on damage initiation characteristics. The damage initiation has been incorporated through the ductile damage and shear damage model available in ABAQUS [100, 101]. The ductile damage initiation criteria was set based on the equivalent plastic strain and stress triaxiality, and the shear damage initiation criteria was set based on the equivalent plastic strain and shear ratio. The ductile damage criterion is a phenomenological model for predicting the onset of damage. The damage initiation occurs when the equivalent plastic strain reaches a critical amount. The model assumes that the equivalent plastic strain at the onset of damage ϵ_D^{pl} is a function of stress triaxiality and strain rate $\epsilon_D^{pl}(\eta, \dot{\epsilon}^{pl})$. The stress triaxiality is defined by $\eta = -p/\sigma_{Mises}$, p is the pressure stress, σ_{Mises} is the Mises equivalent stress, and $\dot{\epsilon}^{pl}$ is the equivalent plastic strain rate. The criterion for damage initiation is met when the following condition is satisfied:

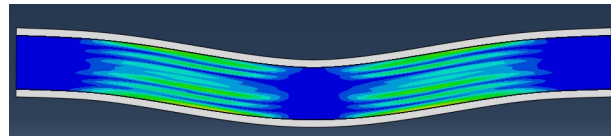
$$\omega_D = \int \frac{d\bar{\epsilon}^{pl}}{\epsilon_D^{pl}(\eta, \dot{\epsilon}^{pl})} = 1 \quad 5.1$$

where ω_D is a state variable that increases monotonically with plastic deformation. Similarly, the shear damage criterion is a phenomenological model for predicting the onset of damage due to shear band localization. The model assumes that the equivalent plastic strain at the onset of damage, ϵ_s^{pl} is a function of the shear stress ratio and strain rate $\epsilon_s^{pl}(\theta_s, \dot{\epsilon}^{pl})$, where $\theta_s = (q + k_s p)/\tau_{max}$ is the shear ratio, τ_{max} is the maximum shear stress, and k_s is a material parameter. The criterion for shear damage initiation is met when the following condition is satisfied:

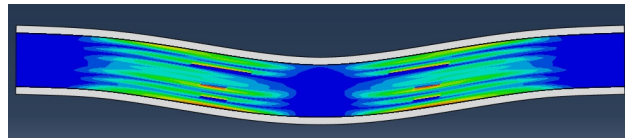
$$\omega_s = \int \frac{d\bar{\epsilon}^{pl}}{\epsilon_s^{pl}(\theta_s, \dot{\bar{\epsilon}}^{pl})} = 1 \quad 5.2$$

where ω_s is a state variable that increases monotonically with plastic deformation proportional to the incremental change in equivalent plastic strain.

It is found that the reinforcement in the sandwich composite core decreases the global damage initiation strain since local strain concentration sites at the interfaces increase. The damage initiation sites in the sandwich composite with and without reinforcement have been depicted in Figure 5.14. The value 1 corresponds to the damage initiation with respective deformation as discussed in Equations 5.1 and 5.2 . It can be noted from the damage initiation sites map that for the sandwich without reinforcement the damage initiates at the facesheet-foam interface due to high concentration of strain. On the other hand, the strain energy is distributed over several interfaces between reinforcement and foam core thereby leading to lower local strain. However more local damage initiation occurs at the plane of reinforcement as can be seen from the Figure 5.14.

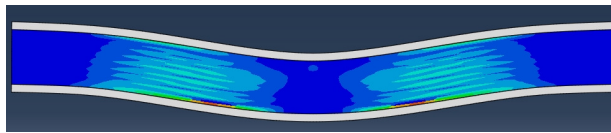


Ductile Damage

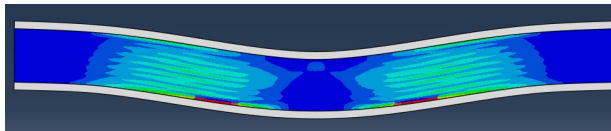


Shear Damage

(a)



Ductile Damage



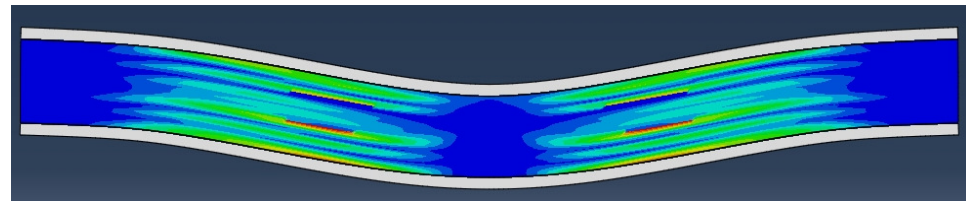
Shear Damage



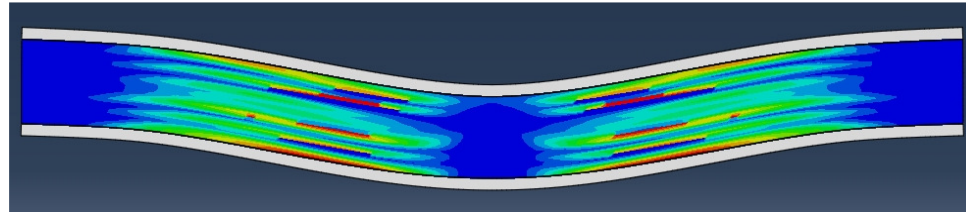
(b)

Figure 5.14 Damage initiation sites in the sandwich composite (a) with reinforcement and (b) without reinforcement. The value 1 corresponds to damage initiation, and 0 corresponds to no damage as discussed in Equation 5.1 and 5.2

Using the FEA it is possible to diagnose the damage initiation sites in side the sandwich composite in the vertical plane of reinforcement and at the external face that can be only experimental diagnosed by DIC. The comparison of the damage initiation sites at the external face and the inside plane of reinforcement can be seen in Figure 5.15 due to ductile damage and shear damage criteria. As seen, more damage initiates at the plane of the reinforcement right at the interface in line with the bending plane. Damage accumulation and global damage evolution occurs when further microscale damage accumulates as shown in Figure 5.15. It is also worth noting that the shear damage is the leading mechanism for damage accumulation due to the shear strain concentrations at the interface that has been earlier observed in the experimental measurements in the natural composite, Palmetto wood as well as engineered composite sandwich with reinforcement in the core.

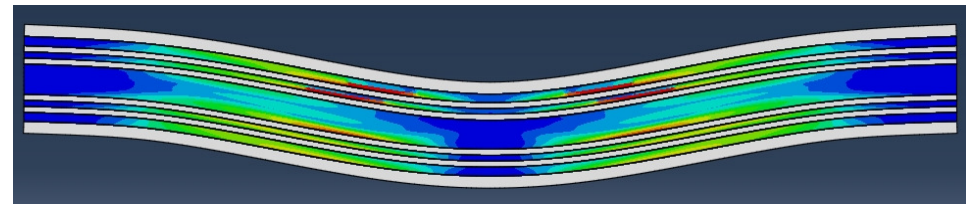


Ductile Damage

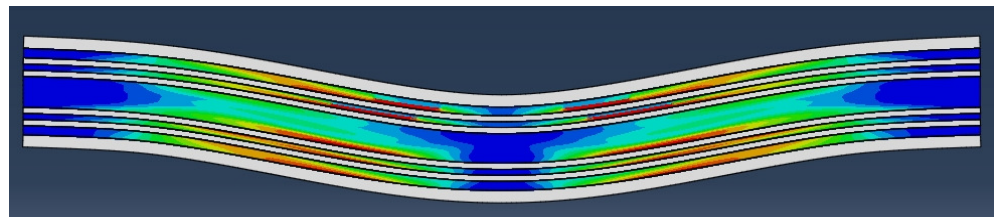


Shear Damage

(a)



Ductile Damage



Shear Damage



(b)

Figure 5.15 Damage initiation sites (a) in the front face and (b) in the vertical plane of reinforcement in sandwich composite with reinforcement

5.9 Discussion of Results

FEA has been performed to numerically investigate the flexural behavior of the sandwich composite structures based on the continuum properties of the constituent materials. The material properties for the simulation have been determined experimentally. The preliminary model of the sandwich without any reinforcement in the core has been validated with the experimentally determined properties and global flexural response.

The simulation of the sandwich with reinforcement in the core has been performed with systematically placing the reinforcing rods in the core based on the amount of the reinforcement volume fraction. The simulation of the experimental response has revealed that the, the core properties had been affected by the reinforcement. Since, the sandwich composite structures fabricated for experimental characterization has an epoxy based adhesive in the core-reinforcement interface, diffusion of the epoxy adhesive in the open cell foam core resulted in increase its stiffness along with increasing the stiffness of the whole sandwich. To obtain the flexural response of the sandwich with reinforcement in the core, the core properties have been estimated. Therefore, it has been possible to quantify the effect of the reinforcement in terms of modification of the core material property as well as global flexural response.

The effect of solely reinforcement on the flexural response has been studied by systematically varying the reinforcement amount. It has been found that in an ideal situation of reinforcement without any adhesive, the effect of the reinforcement is significantly less. An increase of around 50 % in the global flexural modulus would require around 15-20 % of volume fraction in the core. The increase in the global flexural

response by the reinforcement in the core has been numerically found to be linear with the volume fraction of the reinforcement. The size effect of the reinforcing rod (diameter) has been numerically studied by varying the size of the reinforcing rod. The simulations show that the larger reinforcement causes requirement of lesser reinforcement, however, the effect is similar by virtue of the volume fraction amount. The linear dependency is justified by using the engineering relation for the bending stiffness for a composite beam.

The flexural behavior and deformation characteristic due to reinforcement in the core has been compared with that of the sandwich composite without reinforcement in core. The experimentally observed effects of the reinforcement of stiffer material in the soft core have been verified. The strain fields determined by FEA in the core of the sandwich due to the reinforcement confirms that the strain concentration are diffused at several interfaces between reinforcement and core, thereby increasing energy absorbing capability and damage resistance.

The model based on FEA presented here does have limitation that it does not capture microstructural features of the foam, does not incorporate any interface properties. The study has been performed only until damage initiation. The global flexural response has been captured using homogenization technique. However, The present approach to model the flexural behavior of the reinforced sandwich composite structures can be extended to any composite structures with arbitrary reinforcement and alignment using homogenization technique based on Representative Volume Element (RVE). The approach presented here uses homogenization of the reinforcement properties to incorporate the effect of reinforcement properties in the core of the sandwich composite.

Therefore, theoretically any reinforcement geometry and property can be handled by this technique.

5.10 Summary

This chapter presents the numerical study of the global flexural behavior of the sandwich composite structures with reinforcement in the core developed by bioinspired template. The effect of longitudinal reinforcement in the core on the global flexural behavior and local deformation behavior of sandwich composite structures under quasi-static flexure has been numerically investigated. Simplified Finite Element simulations have been performed to (i) to validate the continuum assumption of the constituent material properties, (ii) to verify the effect of reinforcement of pultruded carbon rod on the flexural behavior of the sandwich composite structure.

A parametric study has been performed by systematically varying the reinforcing amount and size of reinforcement to estimate the effect of the reinforcement vol % and reinforcement size on the global flexural modulus of the sandwich composite structure with reinforcement in the core.

The effect of reinforcement in the sandwich composite structures on the local deformation behavior in the core has been explored by comparing the deformation fields obtained from simulation with and without reinforcement in the core. The damage initiation characteristics have been studied by the damage initiation sites in the numerical simulations.

Chapter 6 Structural Battery: *Multifunctional Sandwich Structure*

6.1 Motivation

Palmetto wood, a hierarchically structured natural composite, had been assumed to be a novel bioinspiration to develop synthetic sandwich that will have enhanced mechanical properties, energy absorbance capability as well as damage resistance.

The multiscale structural characterization of Palmetto wood revealed its hierarchical structure as well as structural characteristics and its potential as a novel bioinspiration [22]. Following by the structural characterization, load transfer and failure mechanism were investigated at multiple length scale under quasi-static three point bend to reveal the roles of macrofiber and porous cellulose matrix in the load transfer mechanism [69]. The pore collapse and shear dominated debonding were found to be the key failure mechanism. The damage evolution in the palmetto wood was characterized under unloading-reloading. The dynamic behavior of Palmetto wood had been characterized under low velocity impact [70]. The characterization of dynamic behavior revealed that the failure mechanism dominates the dynamic behavior similar to the quasi-static behavior. Damage modeling of the palmetto wood revealed the slower damage evolution under the dynamic load than that under quasi-static loading. The deformation measurement to characterize the mechanical behavior of Palmetto wood at multiple length scales and loading rates was accomplished by using the Digital Image Correlation (DIC) on the images captured at several magnifications.

Motivated by the structure of Palmetto wood, a bioinspired core has been developed using macroscale reinforcement of carbon rods in the foam. The sandwich specimens with bioinspired foam core are the main interest in the present study. Motivated by the

enormous strength enhancement by nano-reinforcement, the interface in present sandwich structures are strengthened by using nano-enhanced epoxy.

Significant efforts have been dedicated to achieve multifunctionality in a single system combining several functional properties based on the requirement and potential applications. Integration of multiple capabilities in a single system will reduce the usage/need of multiple systems for to serve all the functionalities, as well as increase the system performance. Motivated by the need of combining mechanical and electrical power storage capabilities, a material system is designed to achieve electro-mechanical functionality in order to store electrical energy while providing structural support (i.e., a structural battery).

A model structural battery is depicted in the Figure 6.1. In the proposed design, the plate configuration was wisely chosen to achieve better structural characteristics as opposed to the cylindrical configuration of the conventional batteries. It is hoped that the enhancement in structural properties will be possible to harvest from the concepts of sandwich structures that have been successfully developed for high strength to weight properties. Figure 6.2 demonstrates the mapping of the electrical functionality of each part of the sandwich to a Zn-carbon battery. The proposed metrics for comparing the properties of the multifunctional material system are considered to be weight, static and dynamic mechanical behavior, and energy density.

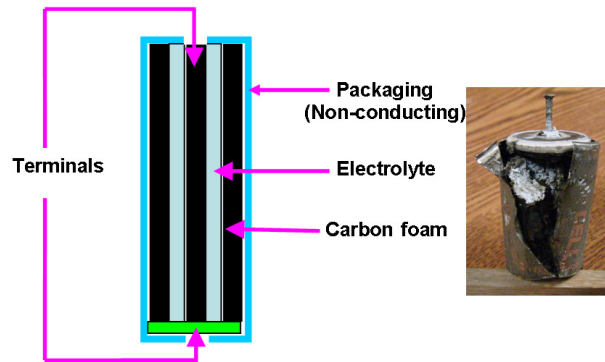


Figure 6.1 Proposed model sandwich structure for a structural battery. The material system is designed to be a lightweight battery with enhanced structural support

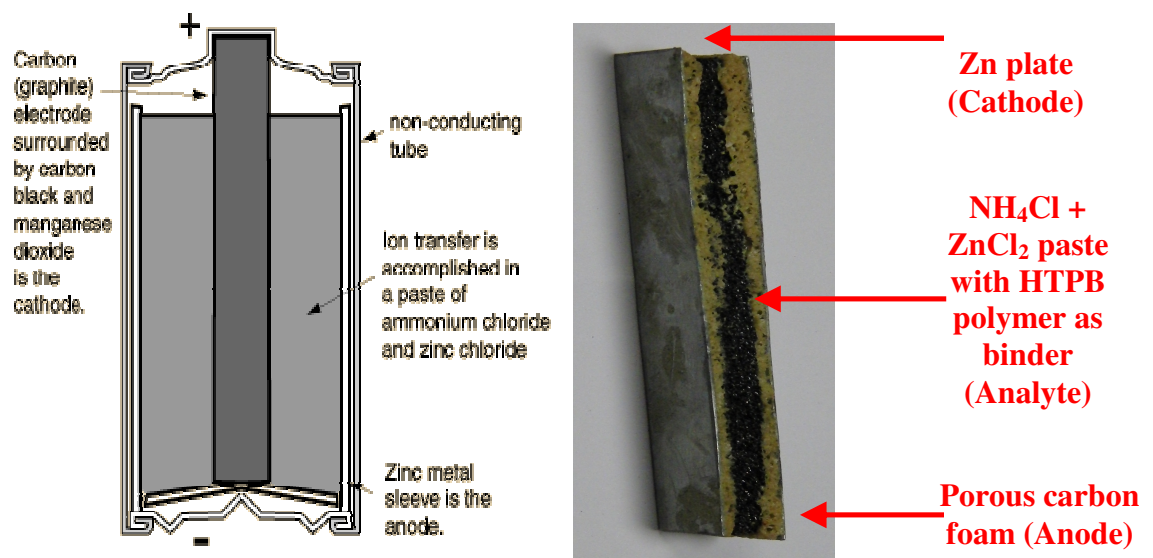


Figure 6.2 Mapping of the multifunctional sandwich (structural battery) and a Zn-Carbon battery

6.2 Materials, Fabrication and Characterization Technique

Prototype multifunctional sandwich specimens were fabricated using carbon foam (CF17) as a core material attached to two copper coated fiberglass facesheets by a paste made of NH_4Cl and ZnCl_2 , which also acts as electrolyte. To enhance the adhesive properties, the electrolyte (NH_4Cl and ZnCl_2) was mixed with PAPI and MDI polymers in electrolyte to polymer weight ratio of 3:1. The PAPI and MDI acted as binder of the salts. To achieve better binding and stronger interface DITBA and TITBA has been used

in the interfacial adhesive. Another material system developed with the same electrolyte-adhesive composite utilized 0.04” thick zinc (Zn) sheets instead of the copper coated fiberglass.

The copper coated fiberglass or Zn sheets have been manually glued to the carbon foam using the NH_4Cl and ZnCl_2 salts and the polymers as adhesive. The adhesive was prepared by hand-mixing the MDI and PAPI polymer, DITBA and TITBA binder and the two salts. The interface was cure in open air for around 10-12 hours.

The beams specimens of multifunctional sandwich have been tested under three-point bend test and have been characterized by their electrical performance. The flexural response of the fabricated sandwich was obtained by quasi-static three-point bend test performed in Imada MX-500 load frame. The load on the specimen and displacement at the central loading point were obtained by a load cell and caliper attached to the load frame.

6.3 Experimental Results

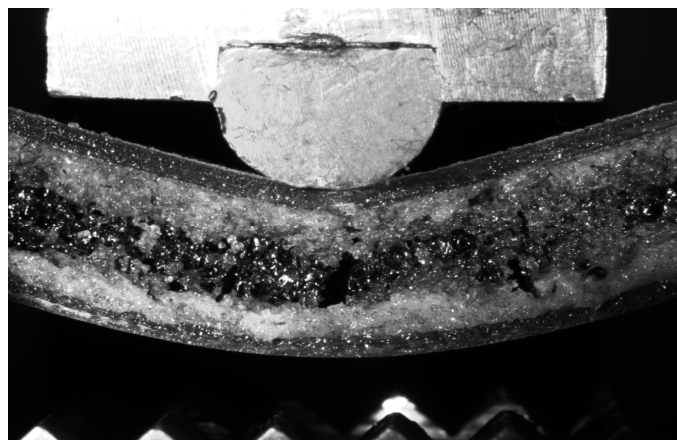
6.3.1 Mechanical Characterization

The structural battery specimens fabricated in sandwich composite form from carbon foam core and (i) Zn and (ii) fiberglass facesheet are characterized under quasi-static flexural load and the interface strength of the batteries have been characterized to understand the effect of the interface ingredients. The flexural responses of the sandwich structural battery with Zn facesheet and fiberglass facesheet have been depicted in the Figure 6.3. The specimen sustained flexural stress of around 20 MPa and 16% flexural strain with effective elastic modulus being 125 MPa. The flexural responses of the multifunctional specimens are compared with that of only the facesheets, unbonded and

without core (for both the copper coated fiberglass and Zn facesheet specimens) without any bonding in between them. The responses match very well indicating that the electrolyte-adhesive composite with the carbon foam core contributes slightly to an increase in strength at larger deformations for the copper-coated fiberglass facesheet specimens while there is a more significant enhancement in strength for the softer Zn facesheet specimens. These preliminary results indicate that there is a significant tradeoff in structural support using Zn facesheets to obtain the 100% gain in voltage. The contribution of the facesheet and carbon foam core in the load bearing capacity and the effect of carbon foam core failure has been further diagnosed by corresponding to the deformation observed in the specimen and the strain fields obtained by DIC.



(a)



(b)

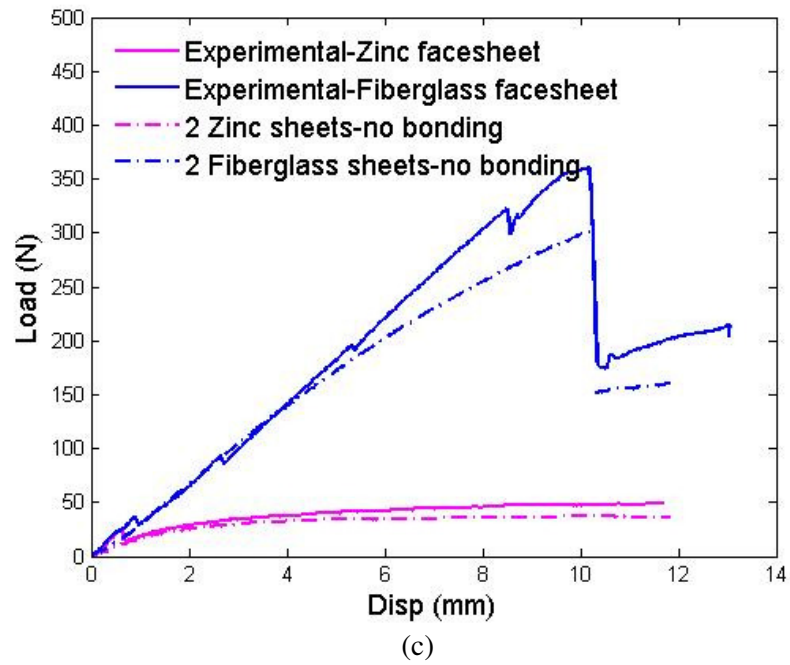
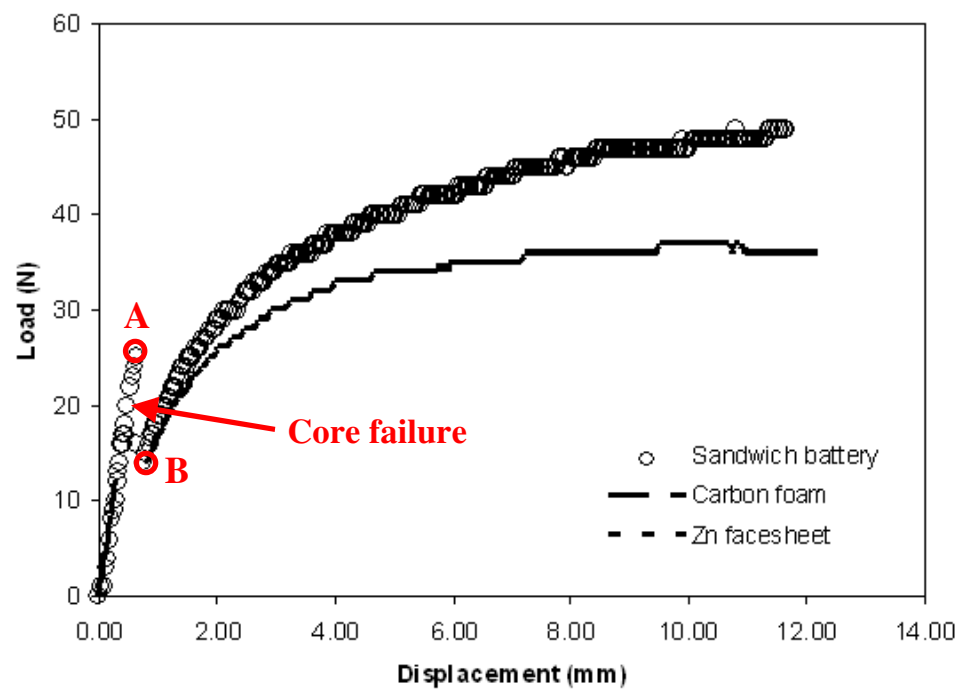
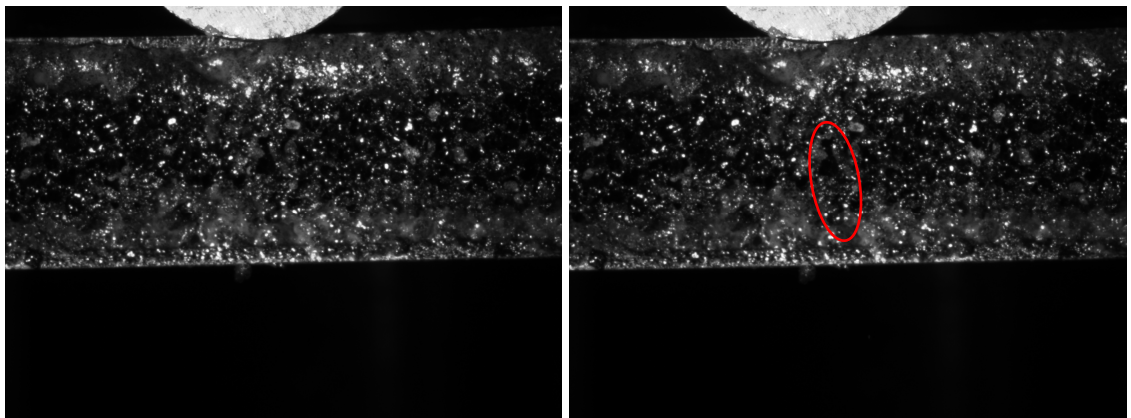


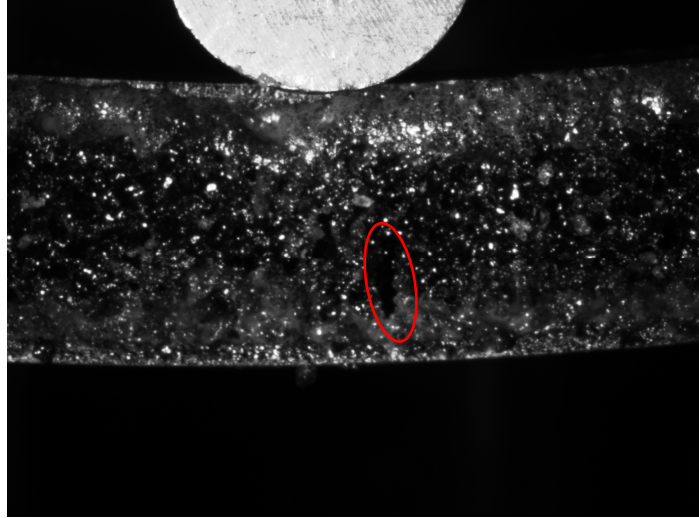
Figure 6.3 (a) A structural battery, (b) three-point bend test on a multifunctional sandwich specimen, and (c) the flexural responses of the multifunctional specimens and the behavior of just the facesheets, unbonded and without core (both copper coated fiberglass and Zn facesheet specimens)

The flexural behavior of the Zn facesheet sandwich structure has been explored further with the aid of DIC and observation of failure of the ceramic carbon foam. The flexure response of the sandwich is depicted in Figure 6.4 and the contribution of the carbon foam and the facesheets are details. The figure shows the flexural behavior of the carbon foam core and two Zn facesheets without bond are depicted in the same figure. It can be observed that in the initial deformation carbon foam contributes the stiffness of the sandwich. Once the failure of the carbon foam occurs, an instantaneous load drop is noted and further stiffness is achieved by the sandwich battery due to the contribution of the facesheets. The difference in behavior of the sandwich and the unbonded Zn facesheets occur due to their separation by the carbon foam core.

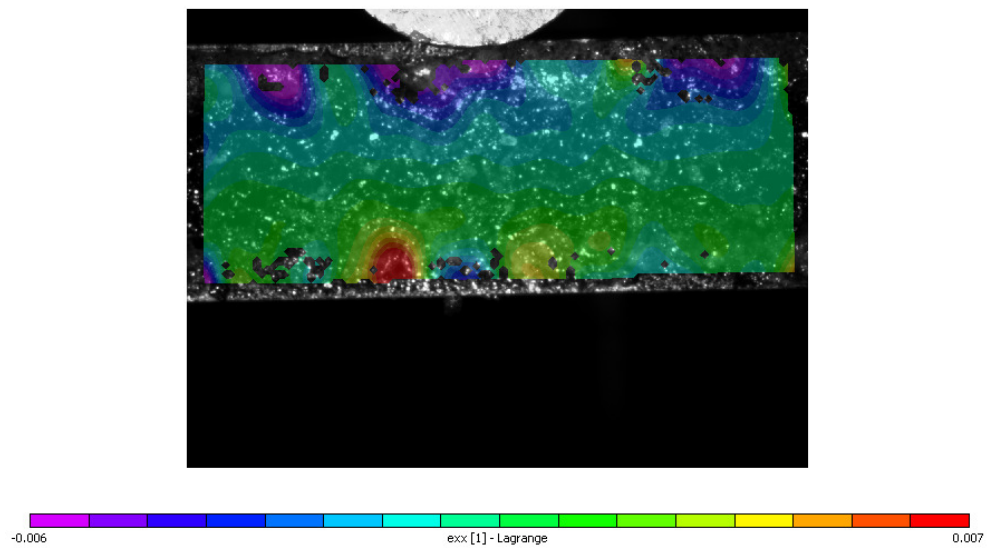


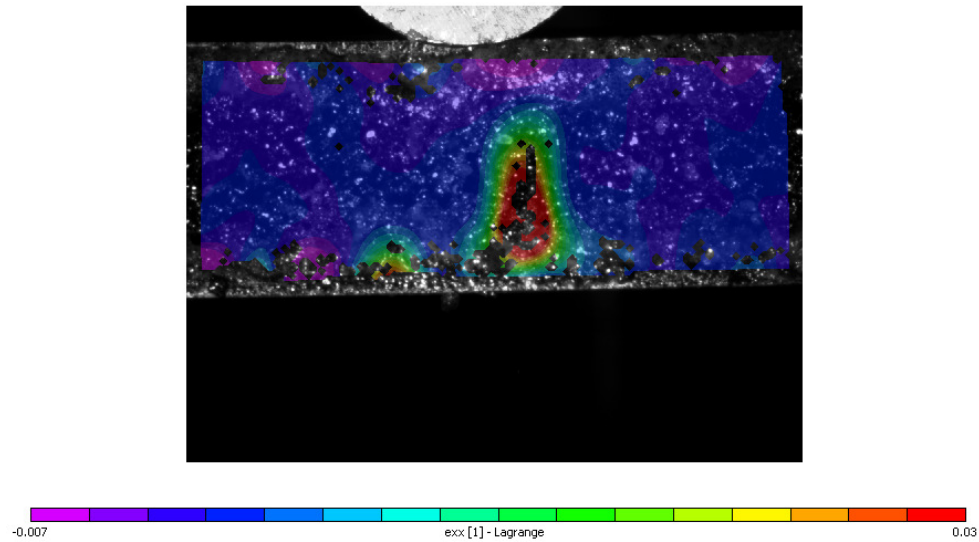
(a)





(b)

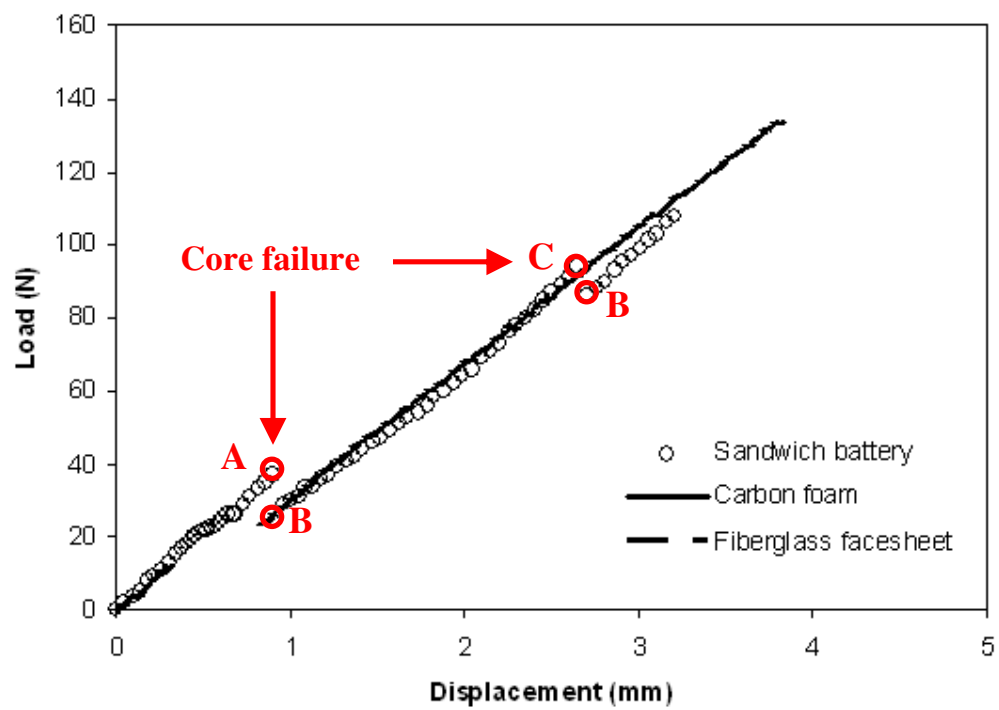




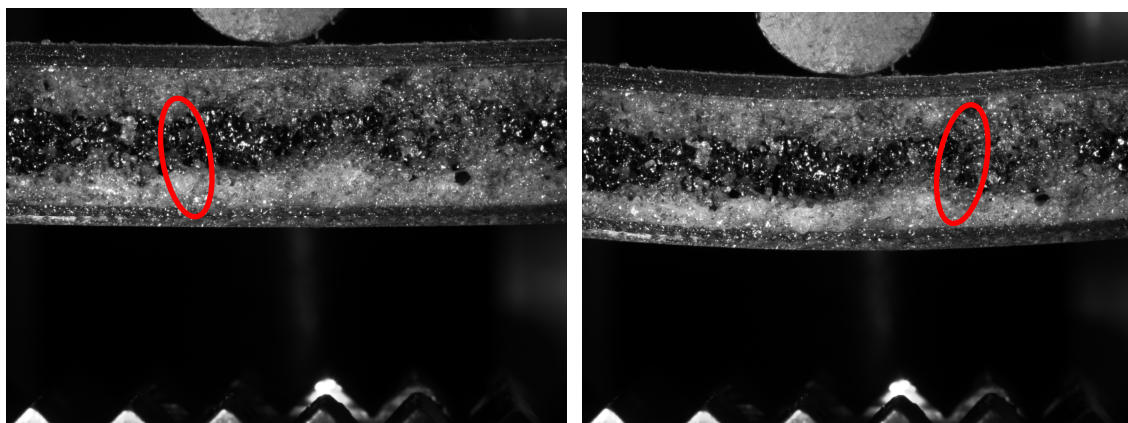
(c)

Figure 6.4 (a) Flexural response of the sandwich structural battery and contribution of core and facesheet in bending behavior, (b) the deformed images corresponding to points A (before core failure) and B (after core failure), (c) strain fields obtained from DIC of the images

The flexural behavior of the fiberglass facesheet sandwich structure has been depicted Figure 6.5 with the flexural behavior of the carbon foam core and two fiberglass facesheets without bond. The initial deformation of the sandwich battery is similar to that of carbon foam and after the initial core failure the global stiffness is more similar to that of the facesheet. The occurrence of the core failure causes a load drop and then, redistribution of the failed core contributes to the stiffness. The load drop due to core failure has been diagnosed in detail with the help of DIC of the images. The Figure 6.5(b) shows the images of the deformed sandwich specimen right after the core failure corresponding to AB and CD in Figure 6.5 (a). The failure initiation sites have been depicted. The DIC reveals this failure through the high tensile strains at the sites corresponding to core failure initiation.



(a)



(b)

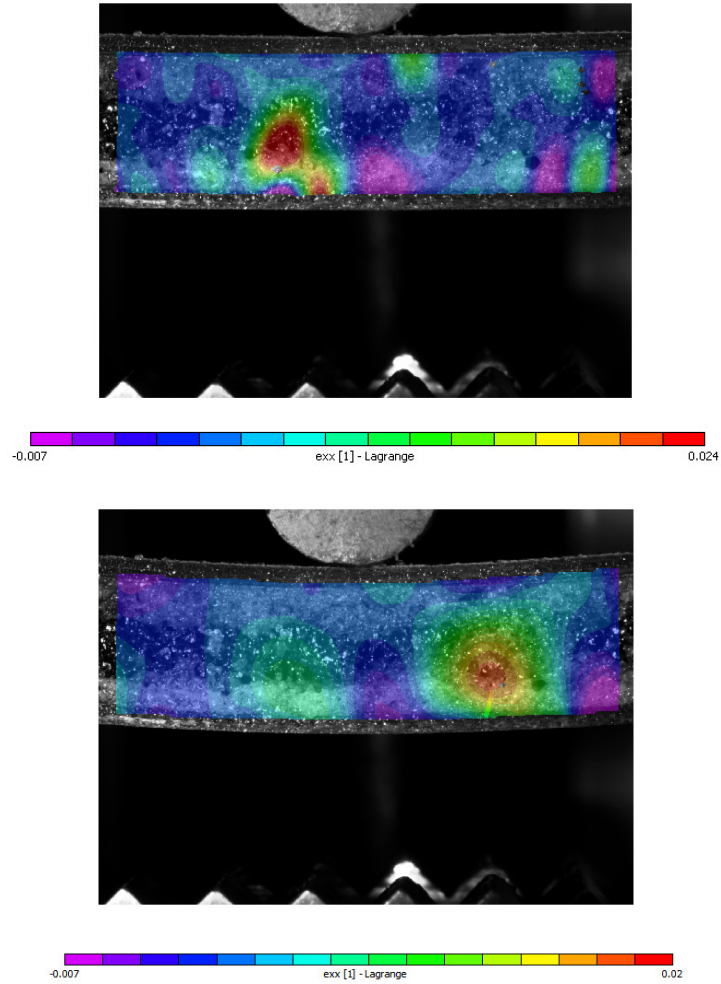


Figure 6.5 (a) Flexural response of the sandwich structural battery with fiberglass facesheet and contribution of carbon foam core and fiberglass facesheet in bending behavior, (b) the deformed images after core failure AB and CD, (c) strain fields obtained from DIC of the images

The interface strength of the structural battery has been characterized to understand the mechanical performance and study the curing effect. Figure 6.6 (a), (b) show the specimens typical battery specimens. The displacement-load response of the specimens with HTPB and epoxy based interface are depicted in Figure 6.7. The energy required for the delamination at the interface was determined to be 0.142 mJ/mm^2 . The curing of the epoxy was performed at 80°C for around 12 hours; however, the interface was pretty weak leading to delamination energy of 0.041 mJ/mm^2 . A curing of around 24 hours at a temperature of 110°C resulted in a stronger interface leading to the energy of 0.254 mJ/mm^2 .

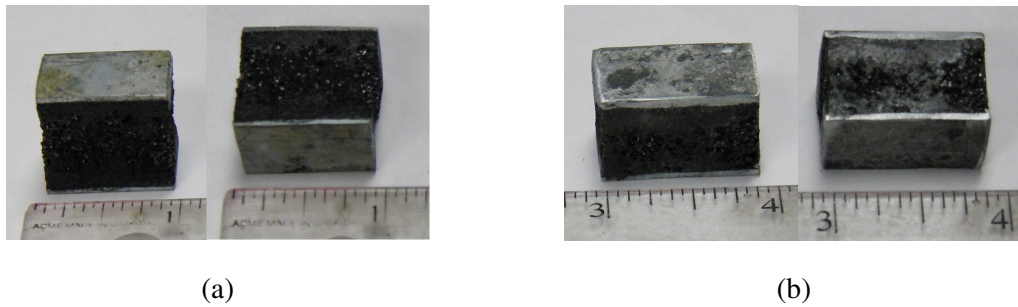


Figure 6.6 Battery specimens (a) HTPB polymer based interface, (b) epoxy based interface

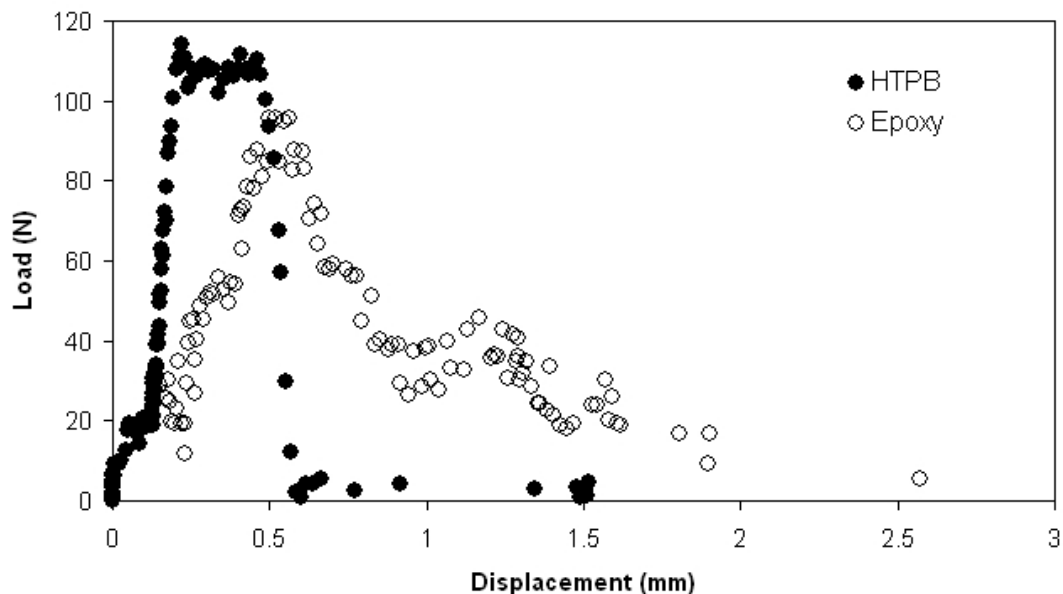


Figure 6.7 Response of battery specimens (Figure 6.6) with HTPB and epoxy based interface

6.3.2 Electrical Characterization

The potential between the carbon foam and the Zn facesheet was approximately 0.4 V, which is about 1/3rd of a normal alkaline battery in a similar volume. In this system as high as 0.9 – 1.0 V potential was achieved, which is twice that with the copper coated fiberglass.

It has been noted that the structural battery has a potential but any current was not flowing indicating the high resistance in the polymeric interface (i.e. almost no conductivity in the HTPB based interface intended to act as electrolyte). This was the barrier to gain any power (no current flow). To achieve the conductivity, carbon nano-fiber (CNF) of around 10 wt % was added to the polymer and salt mixer. The ingredients and the electrical properties of the batteries are listed in the Table 6.1 below obtained from typical specimens as shown in Figure 6.3. Apart from the HTPB based interface, an

epoxy-based (West System 105) interface has been used to fabricate the batteries due to the better adhesion properties of this polymer.

Battery Ingredients				Electrical Properties		
<i>Interfacial polymer</i>	<i>Facesheet</i>	<i>Salt (NH₄Cl + ZnCl₂)</i>	<i>CNF</i>	<i>Voltage (V)</i>	<i>Current (0.4mA/cm²)</i>	<i>Resistance (kΩ)</i>
HTPB	Zn	70%	0 %	0.15	0.004	240
HTPB	Zn	70 %	10 %	0.50	0.01332	512
Epoxy	Zn	70 %	10 %	0.11	0.0086	269
HTPB	Cu coated fiberglass	70%	10%	0.04	0.00014	105
Epoxy	Cu coated fiberglass	70%	10%	0.07	<0.0004	700
HTPB	Zn	70% + MnO ₂	10%	0.98	0.0004	450
Epoxy	Zn	70% + MnO ₂	10%	0.05	0.0004	260
HTPB	Cu coated fiberglass	70% + MnO ₂	10%	0.35	<0.0004	980
Epoxy	Cu coated fiberglass	70% + MnO ₂	10%	0.05	0.0012	260

Table 6.1 Ingredients and electrical properties of the structural batteries

6.4 Discussion of Results

Structural batteries have been fabricated using carbon foam (CF17) as core and copper coated fiberglass and Zn plates as facesheets. The results from prototype multifunctional sandwiches proves the potential of generating power in a sandwich structure. The materials have been selected using standard Zn-Carbon battery as template for the battery chemistry. Two types of polymers, HTPB and epoxy have been used to prepare the interfacial adhesive that also acts as electrolyte. The interfacial strength has been measured and has been tuned by increasing curing temperature of the interfacial material. However,

the power generated by the above mentioned battery is significantly low. The future work would include developing structural batteries from several other battery chemistries and increase the interfacial strength. However, as usual for in multifunctional structures, there will be a trade-off in the power performance and structural strength. A model will be developed identifying the parameters dictating the performance and the parameters will be optimally chosen for the required performance.

6.5 Summary

This chapter presents the effort toward developing structural batteries in sandwich configuration using a ceramic core material, carbon foam and the chemistry of Zn-carbon. The mechanical and electrical characterizations have been performed to identify the limitations of these material systems and to help lay path for future development toward a material system with enhanced multifunctional capabilities.

Chapter 7 Conclusions

This chapter will present the intellectual contributions and the anticipated benefits resulting from the advances reported as part of this dissertation.

7.1 Intellectual Contributions

The research work reported in this dissertation topic is expected to yield several contributions to the body of work in developing advanced sandwich composite structures with multifunctional capability as well as understanding the mechanics principles for energy absorption in the hierarchically structured composites. The dissertation is expected to be the first of its kind to make inroads into development of a sandwich composite structure with reinforcement towards achieving enhanced energy absorbance and damage resistance through the bioinspired core using the structural template of Palmetto wood. The three most important and potentially useful contributions are: (1) understanding mechanics for energy absorption, failure mechanisms, and role of porosity and reinforcement in damage evolution in hierarchically structured natural composite, Palmetto wood.; (2) translation of the mechanics principles by using the structural template of Palmetto wood into reinforced composite sandwich structure through reinforcement in the cellular foam core for enhanced mechanical behavior and understanding of the attributes of its components in the mechanical behavior of the reinforced sandwich composite; (3) development of multifunctional sandwich with limited capabilities and identification of the trade offs in mechanical characteristics.

7.1.1 Multi-scale Characterization and Modeling of a Hierarchically Structured Natural Composite: *Palmetto Wood*

As part of this effort, a naturally occurring composite, Palmetto wood has been experimentally characterized to investigate the mechanical behavior under quasi-static and dynamic load. The effect of macrofiber concentration in the porous cellulose matrix has been studied. The multiscale characterization technique employed here helps to elucidate the load transfer and failure mechanisms in Palmetto wood. The transfer of mechanical behavior across the length scales has been examined. The damage evolution in palmetto wood and the role of macrofiber and strain rate has been experimentally evaluated. Subsequently, a model has been proposed to account for the plastic strain due to pore collapse and associated evolution of damage.

7.1.2 Development, Characterization, and Modeling of a New Bioinspired Foam Core for Composite Sandwich Structures

Another significant contribution would be in using the template of Palmetto wood in developing sandwich structures with bioinspired core for enhanced mechanical behavior. Preliminary results show the improvement in the flexural response of the bioinspired sandwich materials.

Modeling of the behavior of bioinspired sandwich elucidated the role of macroscale reinforcement and the properties of constituent materials in the mechanical response of the sandwich structures. This will also help to develop the guidelines in choosing proper reinforcement to tune the mechanical behavior. It would be possible to develop a detailed map to depict the role of macroscale reinforcement and the transition of damage behavior of natural composite Palmetto wood, polymeric foam, bioinspired foam and ceramic

foam. It has been seen that ceramic foam (carbon foam) barely undergoes any plastic deformation and polymeric foam would undergo large plastic deformation. Using Palmetto wood as template and modeling bioinspired foam will help to develop the detailed picture of the role of reinforcement in damage behavior and stress-strain response.

7.1.3 Development of FEA Model for Bioinspired Foam Cores

A new FEA model was developed to simulate the mechanical behavior of the sandwich structures with and without reinforcement in the core. The simulation was conducted using with ABAQUS using elastic-plastic deformation with isotropic hardening for the face sheet, elastic-perfectly plastic foam behavior, and elastic deformation for the fiber. For damage initiation, a ductile and shear damage model was used based on equivalent plastic strain. To describe the elastic-plastic behavior of a composite sandwich structure with a bioinspired foam core, the mechanical behavior of the foam core was first modeled discretely using the fiber reinforcement at different locations relative to the neutral axis of the foam core. The resulting elastic-plastic deformation behavior was then used in a homogenized core in the composite sandwich structure to compare with experimental stress-strain flexure measurements in order to determine the appropriate material properties and fiber distribution for the discretely modeled bioinspired foam core.

In addition to the homogenized model, a complete discrete model of the composite sandwich structure with the bioinspired foam core was also developed in order to determine the localized deformation response of the bioinspired foam core to compare with the experimental DIC measurements and verify that we could translate the damage mechanisms to the new model. Thus, the combination of the homogenized and discrete

models allows for a multi-scale approach to designing composite sandwich structures with bioinspired foam cores.

7.1.4 Development of a Multifunctional Sandwich Composite Structure with Energy Storage Capability

As part of this effort, the feasibility of developing multifunctional structures with bioinspired cores for high mechanical energy absorption as well as energy storage has been investigated with the new multi-scale modeling and characterization approach. This was the first time that a multifunctional sandwich composite structure with energy storage capability has been demonstrated. The core of the sandwich structure consisted of a carbon foam, which represented one extreme of the design space using bioinspired foam cores. Thus, the characterization and modeling was able to verify only the extreme of the design space. However, it was sufficient to provide the foundation for continuing further exploration of the possibilities in the design space for optimizing energy storage capability and mechanical performance via the new multi-scale characterization and modeling approach. Another viable bioinspired core designs were proposed in Section 8.2.2 for further investigating the possibilities using embedded batteries. Using the multi-scale model, it is possible to identify several competing parameters (e.g., weight, mechanical performance, and electrical performance) in optimizing the parameters (e.g., matrix properties, fiber properties, fiber distribution, interfacial properties, embedded battery characteristics) for the two proposed bioinspired core designs.

7.2 Anticipated Benefits

The focus of this dissertation is on the design and fabrication of multifunctional sandwich structure with structural and electrical functionality. The bioinspired sandwich structures and structural batteries developed and modeled as part of this investigation would establish the methodology to develop high energy absorbing structural members with power functionality.

The results of this investigation can be utilized in developing sandwich structures high energy absorbing capability for several applications where structures are subject to impact load in several applications like marine structure.

The structural batteries developed as part of this effort will explore the potential of developing multifunctional material system with the optimal performance. The modeling part will help to select material, fabrication procedure and other related geometric parameters in developing sandwich materials with structure-power capabilities leading to increased system efficiency, waiving the requirement of batteries for small scale power resource.

Chapter 8 Future Work

In this chapter, the future directions of the present research that can be carried out toward further understanding of the mechanics of the reinforced foam core sandwich composite structures and develop energy absorbing multifunctional sandwich structures are identified and outlined. The scopes for further exploration are: (1) Detailed modeling of porous foam core to understand the failure mechanisms in the porous structure and effect of pore structure and reinforcement size on the mechanical behavior of the reinforced sandwich composites, (2) Incorporate bioinspired core in structural battery and integration of nano-scale reinforcement in the foam core for conductivity. The following sections will describe in detail the motivation and expected outcome for the further research.

8.1 Modeling of Porous Foam for Further Investigation of Failure Mechanisms

8.1.1 Motivation

The mechanical characterization of Palmetto wood revealed that higher volume fraction of macrofiber reinforcement increases the stiffness. A damage model was developed to decouple the effect of the flexural elastic strain and effect of plastic strain due to pore collapse in damage evolution. It has been seen that the reinforcement of macrofiber plays a significant role in the damage initiation strain and evolution of damage. However, in the experimental study, limited cases were investigated to obtain the damage behavior of the Palmetto wood. To utilize the mechanics principle of palmetto wood in developing bioinspired sandwich material and tailor their properties a detail understanding of the damage behavior is required.

Ajdari et al [95] developed a detailed finite element model to investigate the in-plane dynamic crushing of two dimensional honeycombs with both regular and irregular hexagonal arrangements with constant and graded density. The crushing behavior and energy absorption of honeycombs made of a linear elastic-perfectly plastic material with constant and functionally graded density has been studied. The simulations revealed three distinct crushing modes for honeycombs with a constant relative density: quasi-static, transition and dynamic as shown in Figure 8.2.

A detailed numerical analysis using full-fledged model with microstructural features like porous structure of the foam will help to understand the role of the reinforcement and porous matrix in the damage behavior of the composite sandwich structure in greater detail. Also it is not feasible to capture the effect of the size of pores, reinforcements in the properties. The detail model can capture the effect of the reinforcement size relative to pore size of the foam core, relative density of foam core. Therefore, the further detail model with microstructural features will fill in these gaps that can not be elucidated using uniform material model and will clearly identify the parameters that can be tailored to achieve required properties of the sandwich composite structure.

8.1.2 Approach

There are several literatures on the modeling of mechanical behavior foam core sandwich structures like plastic collapse of sandwich beam by Chen et al [96], interfacial fracture by Cancer and Bazan [97], modeling flexural behavior by Styles et al [98]. Motivated by the modeling approach mentioned above and especially, modeling foam to capture the crushing by Ajdari et al [95], finite element analysis can be performed for the

bioinspired foam core sandwich that has macroscale reinforcement in it as shown in Figure 8.1

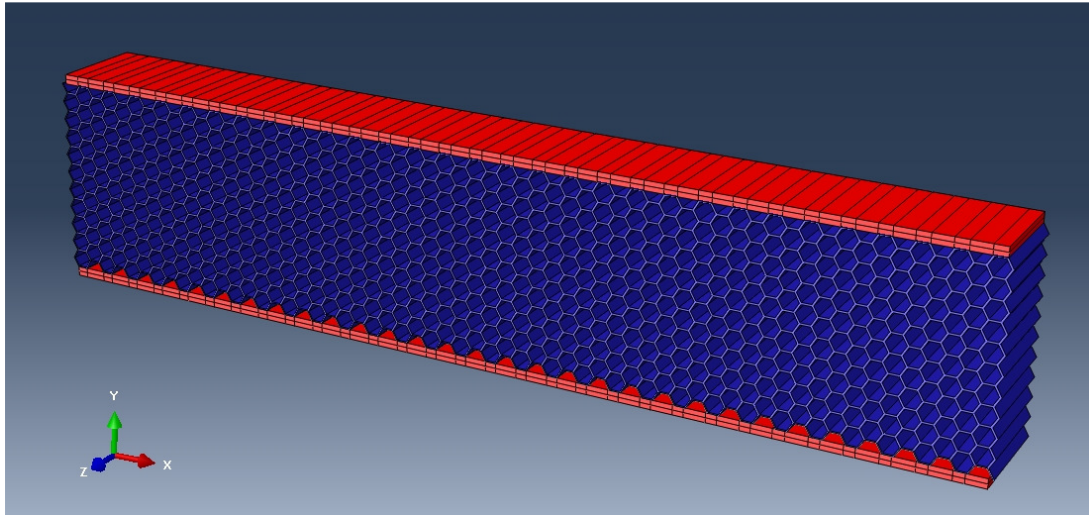


Figure 8.1 Detail modeling of the foam core for further investigation of failure mechanisms through foam cell response

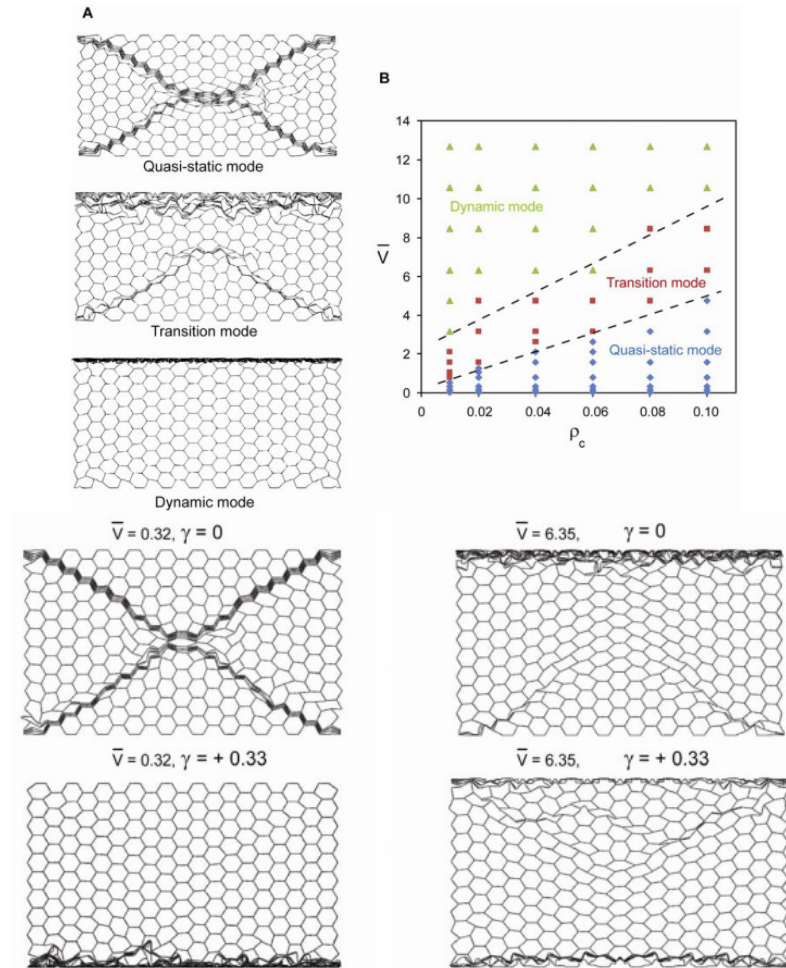


Figure 8.2 Deformation modes of a hexagonal regular honeycomb (a) three distinct deformation shapes and deformation map for a regular honeycomb subjected to dynamic crushing and (bottom) deformation shapes of regular cellular structures with constant and functionally graded relative density at 50% crushing at low and high crushing rates [95]

8.1.3 Expected Outcomes

The detailed FEM can study several geometrical and constituent property dependencies thereby exploring the design space for a foam core reinforced sandwich composite structure. The model can be used as a predictive tool to tune the mechanical behavior of the sandwich material with bioinspired foam core. The model can take in account the following parameters:

- 1) Amount and length scale of macroscale reinforcement

- 2) Processing parameters leading to different interfacial characteristics
- 3) Relative size scale of the porous foam core and reinforcement and effect of relative density of foam.

8.2 Incorporate the Bioinspired Core in Structural Battery and Integration of Conductive Nano-reinforcement in Foam

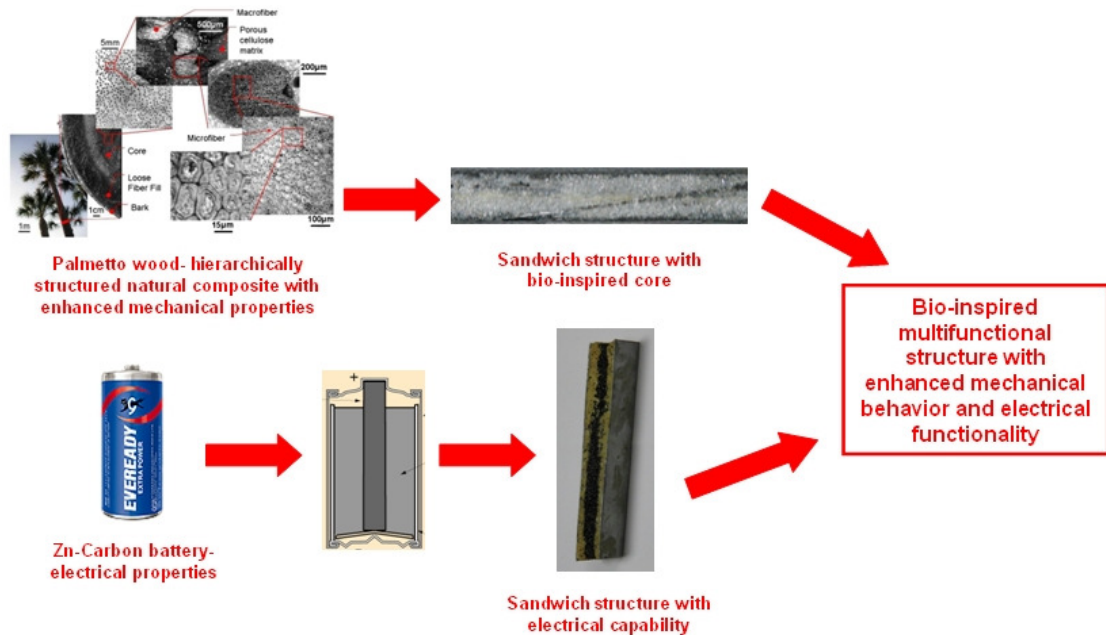
8.2.1 Motivation

The characterization of Palmetto wood revealed its failure mechanisms and damage mechanism under quasi-static and dynamic three-point bending and its energy absorbing capability. Palmetto wood, a naturally occurring porous material, exhibits enhanced mechanical behavior with the aid of macrofiber in its porous cellulose matrix. The experimental and numerical study on the flexural behavior of the sandwich composite structures with bioinspired polymeric foam core proved the enhancement in the flexural behavior, balanced energy absorbance and damage resistance.

Preliminary prototype structural batteries showed the capability of power generation, though very less, and structural strength at the extreme design space, using ceramic core. The carbon foam used in the prototype structural batteries being ceramic has very less mechanical energy absorbing capacity and barely deforms plastically leading to catastrophic failure of the foam core, and hence the sandwich composite structure. Hence, incorporating bioinspired polymeric foam with power functionality in the structural battery would enhance the mechanical performance.

8.2.2 Approach

The approach that may be adopted to incorporate the bioinspired foam core in developing structural battery with reinforcement in the foam core by a bottom-up processing technique as depicted in Figure 8.3. Once approach would be to embed battery in the bioinspired core of the sandwich composite structure, and another approach may be to integrate nanoenhancement to induce electrical conductivity in the core material that can perform as a terminal in battery chemistry. A prototype sandwich composite structure with embedded LiPoly battery in FM104 foam (Innovative Polymers) and a nanoenhanced core with reinforcement in the porous foam have been shown in Figure 8.3.



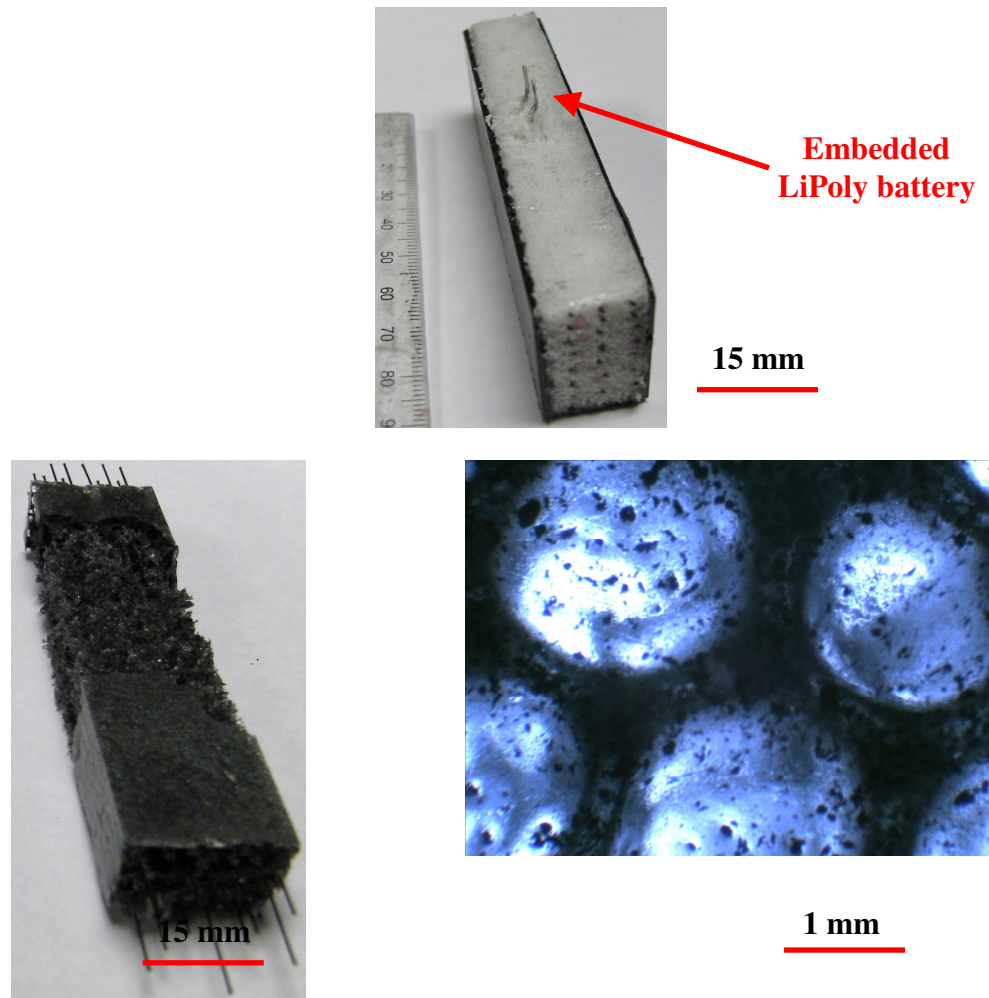


Figure 8.3 Approaches to incorporate bioinspired core in multifunctional sandwich

8.2.3 Expected Outcomes

The multifunctional sandwich composite with bioinspired core can be designed to achieve required enhanced structural behavior through tailoring the macroscale reinforcement of mechanical stronger material leading to increase in flexural stiffness compared to conventional sandwich composite structures. Nanoreinforcements (like Carbon Nano Tube, Exfoliated Graphite) have shown potential applications to induce electrical conductivity and potentially can be used to induce electrical conductivity in the foam core.

References

1. MesoScribe Technologies, Inc. (<http://www.mesoscribe.com/>)
2. Hexcel Composites, Hexwebtm honeycomb sandwich design technology
3. Corigliano A, Rizzi E, Papa E (2000) Experimental characterization and numerical simulations of a syntactic-foam/glass-fibre composite sandwich, *Composites Science and Technology*, 60(11): 2169-2180
4. Reyes G (2010) Mechanical Behavior of Thermoplastic FML-reinforced Sandwich Panels Using an Aluminum Foam Core: Experiments and Modeling, *Journal of Sandwich Structures and Materials*, 12: 81-96
5. Zhu F, Lu G (2007) A Review of Blast and Impact of Metallic and Sandwich Structures, *EJSE Special Issue: Loading on Structures*, 92-101
6. LeBlanc J, Shukla A (2011) Response of E-glass/vinyl ester composite panels to underwater explosive loading: Effects of laminate modifications, *International Journal of Impact Engineering* 38: 796-803
7. LeBlanc J, Shukla A (2011) Dynamic response of curved composite panels to underwater explosive loading: Experimental and computational comparisons, *Composite Structures*, doi:10.1016/j.compstruct.2011.04.017
8. Jackson M, Shukla A (2010) Performance of sandwich composites subjected to sequential impact and air blast loading, *Composites: Part B*, doi:10.1016/j.compositesb.2010.09.005
9. Hu H, Belouettar S, Ferry MP, Daya EM (2008) Review and assessment of various theories for modeling sandwich composites, *Composite Structures*, 84(3): 282-292
10. He QZ, Hu H, Belouettar S, Guinta G, Yu K, Liu Y, Biscani F, Carrera E, Ferry MP (2011) Multi-scale modelling of sandwich structures using hierarchical kinematics, *Composite Structures*, 93(9): 2375-2383
11. Takeda N, Minakuchi S, Okabe Y (2007) Smart Composite Sandwich Structures for Future Aerospace Application -Damage Detection and Suppression-: a Review, *Journal of Solid Mechanics and Materials Engineering*, 1: 3-17
12. Gibson RF (2010) A review of recent research on mechanics of multifunctional composite materials and structures, *Composite Structures*, 92: 2793-2810
13. Lee CS, Lim TS, Kwon JW and Lee DG (2003) Peel strength improvement of foam core sandwich beams by epoxy resin impregnation on the foam surface *Journal of Adhesion Science and Technology*, 17(5): 687-701
14. Vinson JR (2005) Sandwich structure: past, present, and future, *Sandwich Structures 7: Advancing with Sandwich Structures and Materials*, 3-12
15. Wadley HNG, Fleck NA and Evans AG (2003) Fabrication and structural performance of periodic cellular metal sandwich structures *Composites Science and Technology*, 63(16): 2331-2343
16. Grohn M, Voss D, Hintz C, Sahm PR In: J. Barnhart, M.F. Ashby and N. Fleck, Editors, *Cellular Metals and Metal Foaming Technology*, MIT-Verlag (2001), pp. 197-202.
17. INCO Ltd, Canada, Incofoam Data Product Sheet, www.inco.com, 1998.
18. Frame C, www.porvair.com, 2000.
19. Sypeck DJ, Parrish PA, Wadley HNG (1998) Novel Hollow Powder Porous Structures, *Materials Research Society Symposium Proceedings*, 521: 205-210

20. Chen F, D. He. In: J. Banhart, M.F. Ashby and N.A. Fleck, Editors, *Metal Foams and Porous Metal Structures*, MIT-Verlag Bremen (2001), pp. 163–166.11
21. Deshpande VS, Fleck NA (2001) Collapse of truss core sandwich beams in 3-point bending, *International Journal of Solids and Structures*, 38(36-37): 6275-6305
22. Wang J, Evans AG, Dharmasena K and Wadley HNG (2003) On the performance of truss panels with Kagomé cores, *International Journal of Solids and Structures*, 40(25) 6981-6988
23. Herrmann A, Zahlen P, Zuardy I (2005) *Sandwich Structures Technology in Commercial Aviation Present Applications and Future Trends*, *Sandwich Structures 7: Advancing with Sandwich Structures and Materials, Part-I*, 13-26
24. Haibin Ning H, Janowski GM, Vaidya UK, Husman G (2007) Thermoplastic sandwich structure design and manufacturing for the body panel of mass transit vehicle, *Composite Structures*, 80(1): 82-91
25. Gdoutos EE, Daniel IM (2008) Failure modes of composite sandwich beams, *Theoretical and Applied Mechanics*, 35(1-3): 105–118
26. Daniel IM, Abot JL (2000) Fabrication testing and analysis of composite sandwich beams, *Composite Science and Technology*, 60: 2455-2463
27. Hadi BK, Matthews FL (2000) Development of Benson-Mayers theory on the wrinkling of anisotropic sandwich panels, *Composite Structures*, 49: 425-434
28. Soden PD (1996) Indentation of composite sandwich beams, *Journal of Strain Analysis.*, 31: 353-360.
29. Triantafillou TC, Gibson LJ (1987) Failure mode maps for foam core sandwich beams, *Material Science and Engineering*, 95: 37-53.
30. Xiong J, Ma L, Wu LZ, Liu JY, Vaziri A (2011) Mechanical behavior and failure of composite pyramidal truss core sandwich columns, *Composites Part B – Engineering*, 42(4): 938-945
31. Triantafillou TC, Gibson LJ (1989) Debonding in foam-core sandwich panels, *Materials and Structures*, 22: 64-69
32. Thouless MD, Jensen HM (1992) Elastic Fracture Mechanics of the Peel-Test Geometry, *Journal of Adhesion*, 38: 185-197
33. Cantwell WJ, Scudamore R, Ratcliffe J, Davies P (1999) Interfacial fracture in sandwich laminates, *Composites Science and Technology*, 59(14): 2079-2085
34. Sun SY, Chen HR (2011) The interfacial fracture behavior of foam core composite sandwich structures by a viscoelastic cohesive model, *Science China-Physics Mechanics and Astronomy*, 54(8): 1481-1487
35. Xu LR, Rosakis AJ (2002) Impact failure characteristics in sandwich structures Part I: Basic failure mode selection, *International Journal of Solids and Structures* 39: 4215–4235
36. Semenski D, Rosakis AJ (1999) Dynamic crack initiation and growth in light-core sandwich composite materials. In: *Proceedings of the 17th Danubia-Adria Symposium on Experimental Mechanics in Solid Mechanics*, Prague, 297–300.
37. Wang B, Wu LZ, Ma L, Feng JC (2011) Low-velocity impact characteristics and residual tensile strength of carbon fiber composite lattice core sandwich structures, *Composites: Part B*, 42: 891-897

38. Chakrabarti A, Shu LH (2010) Biologically inspired design, *Artificial Intelligence for Engineering Design, Analysis and Manufacturing*, 24: 453–454
39. Shu LH, Ueda K, Chiu I, Cheong H (2011) Biologically inspired design, *CIRP Annals - Manufacturing Technology*, 60(2): 673-693
40. Oka K, Aoyagi S, Arai Y, Isono Y, Hashiguchi G, Fujita H (2002) Fabrication of a Micro Needle for a Trace Blood Test, *Sensors and Actuators A: Physical*, 97-98: 478–485
41. Pogula S, Patwardhan S, Perry C, Gillespie J, Yarlagadda S, Kiick K (2007) Continuous Silica Coatings on Glass Fibers Via Bioinspired Approaches, *Langmuir*, 23(12): 6677–6683
42. Koh YH, Sun JJ, Kim HE (2007) Freeze Casting of Porous Ni–YSZ Cermets, *Materials Letters*, 61(6): 1283–1287
43. Jones KD, Bradshaw CJ, Papadopoulos J, Platzer MF (2005) Bioinspired design of flapping-wing micro air vehicles, *The Aeronautical Journal*
44. Madangopal R, Khan ZA, Agrawal SK (2005) Biologically inspired design of small flapping wing air vehicles using four-bar mechanisms and quasi-steady aerodynamics, *Journal of Mechanical Design*, 27: 809-816
45. Mueller D, Bruck HA, Gupta SK (2010) Measurement of thrust and lift forces associated with drag of compliant flapping wing for micro air vehicles using a new test stand design, *Experimental Mechanics*, 50(6):725–735
46. Bejgerowski W, Ananthanarayanan A, Mueller D, Gupta SK (2009) Integrated product and process design for a flapping wing drive-mechanism, *ASME Journal of Mechanical Design*, 131: 061006
47. Meyers MA, Chen PY, Lin AUM, Seki Y (2008) Biological materials: Structure and mechanical properties, *Progress in Materials Science*, 53(1): 1-206
48. Zhou BL (2000) Bioinspired study of structural materials, *Materials Science and Engineering: C*, 11(1): 13-18
49. Li SH, Fu SY, Zhou BL (1994) Reformed bamboo and reformed bamboo/Al composite: Part I. Manufactural technique, structure and static properties, *Journal of Material Science*, 29: 5990–5996
50. Craciunescu O, Moldovan L (2011) Designing Bioinspired Composite Materials for Medical Applications, *Nanocomposites and Polymers with Analytical Methods*, 309-334
51. P. Ball (2001) Life's lessons in design, *Nature*, 409: 413–416
52. Bruck HA, Evans JJ, Peterson ML (2002) The role of mechanics in biological and biologically inspired materials, *Experimental Mechanics*, 42(4): 361-371
53. Vural M, Ravichandran G (2003) Microstructural aspects and modeling of failure in naturally occurring porous composites, *Mechanics of Materials*, 35(3-6): 523-536
54. Vural M, Ravichandran G (2004) Failure mode transition and energy dissipation in naturally occurring composites, *Composites Part B: Engineering*, 35(6-8): 639-646
55. Vural M, Ravichandran G (2003) Dynamic response and energy dissipation characteristics of balsa wood: experiment and analysis, *International Journal of Solids and Structures*, 40(9): 2147-2170

56. Thomas JP, Qidwai MA, Matic P, Everett RK (2001) Composite materials with multifunctional structure-power capabilities, American Society for Composites (ASC) 16th Technical Conference Proceedings
57. Evans AG, Hutchinson JW, Ashby MF (1998) Multifunctionality of cellular metal systems, *Progress in Material Science*, 43: 171–221
58. Bauhofer W, Kovacs JZ (2009) A review and analysis of electrical percolation in carbon nanotube polymer composites, *Composite Science Technology*, 69(10): 1486–98
59. Queheillalt DT, Carbajal G, Peterson GP, Wadley HNG (2008) A multifunctional heat pipe sandwich panel structure, *International Journal of Heat and Mass Transfer*, 51(1-2): 312-326
60. Vaidya AS, Vaidya UK, Uddin N (2008) Impact response of three-dimensional multifunctional sandwich composite, *Materials Science and Engineering: A*, 472(1-2): 52-58
61. Wadley HNG (2006) Multifunctional periodic cellular metals, *Philosophical Transaction of Royal Society A* 3641838: 31–68
62. Roper CS (2011) Multiobjective optimization for design of multifunctional sandwich panel heat pipes with micro-architected truss cores, *International Journal of Heat and Fluid Flow*, 32(1): 239-248
63. Keller T, Vassilopoulos AP, Manshadi BD (2010) Thermomechanical Behavior of Multifunctional GFRP Sandwich Structures with Encapsulated Photovoltaic Cells, *Journal of Composites for Construction*, 14(4): 470
64. Adams DO, Yarger C, Webb N, Hunter A, Oborn K, Saether E, Wilson JW, Badavi FF (2008) Multi-functional sandwich composite concepts for spacecraft applications, *SAMPE Journal*, 44(2): 38–49
65. Rion J, Leterrier Y, Manson JAE, Blairon JM (2009) Ultra-light asymmetric photovoltaic sandwich structures, *Composites Part A: Applied Science and Manufacturing*, 40(8): 1167-1173
66. Qian H, Diao H, Shirshova N, Greenhalgh ES, Steinke JG, Shaffer MS, Bismarck A (2013) Activation of structural carbon fibres for potential applications in multifunctional structural supercapacitors., *J Colloid Interface Science*, 395: 241-248
67. Shirshova N, Qian H, Shaffer MSP, Steinke JHG, Greenhalgh ES, Curtis PT, Kucernak A, Bismarck A (2013) Structural composite supercapacitors, *Composites A*, 46: 96-107
68. Gershon AL, Bruck HA, Xu S, Sutton MA, Tiwari V (2010) Multiscale mechanical and structural characterizations of Palmetto wood for bioinspired hierarchically structured polymer composites. *Materials Science and Engineering C*, 30: 235–244
69. Halder S, Gheewala N, Grande-Allen J, Sutton MA, and Bruck HA (2010) Multi-scale Mechanical Characterization of Palmetto Wood for Biologically-inspired Polymer Composites, DOI: 10.1007/s11340-010-9422-7
70. Halder S, Bruck H A (2013) Characterization of Dynamic Damage Mechanisms in Palmetto Wood as Biological Inspiration for Impact Resistant Polymer Composites, *Mechanics of Materials*, 57: 97-108

71. Pan B, Qian K, Xie H, Asundi A (2009) Two-dimensional digital image correlation for in-plane displacement and strain measurement: a review, *Measurement Science and Technology*, 20(062001)
72. Hild F and Roux S (2006) Digital Image Correlation: from Displacement measurement to Identification of Elastic Properties – a Review, *Strain*, 42(2): 69 – 80
73. Berfield TA, Patel JK, Shimmin RG, Braun PV, Lambros J, Sottos NR (2007) Micro- and nanoscale deformation measurement of surface and internal Planes via digital image correlation. *Experimental Mechanics* 47: 51–62
74. Davea S, Songa X, Hofmann F, Dragnevskia K, Korsunsky AM (2009) Digital image correlation and finite element analysis of inter- and intra-granular deformation. *Procedia Engineering* 1: 197-200
75. Ya'akovovitz A, Krylov S, Hanein Y (2010) Nanoscale displacement measurement of electrostatically actuated micro-devices using optical microscopy and digital image correlation, *Sensors and Actuators A: Physical*, 162(1): 1-7
76. Lord, JD, Roebuck B, Morrell R, Lube T (2010) 25 Year perspective Aspects of strain and strength measurement in miniaturised testing for engineering metals and ceramics. *Materials Science and Technology* 26(2): 127-148
77. Zhang D, Arola DD (2004) Applications of digital image correlation to biological tissues. *Journal of Biomedical Optics* 9(4): 691–699
78. Krehbiel JD, Lambros J, Viator JA, Sottos NR (2010) Digital Image Correlation for Improved Detection of Basal Cell Carcinoma, *Experimental Mechanics* 50(6): 813-824
79. Gonzalez J, Knauss WG (1998) Strain inhomogeneity and discontinuous crack growth in particulate composite. *Journal of Mechanics and Physics of Solids* 35(09): 1981-1985
80. Rjafiallah S, Guessasma S (2011) Three-phase model and digital image correlation to assess the interphase effect on the elasticity of carbohydrate polymer-based composites reinforced with glass silica beads, *Carbohydrate Polymers* 83(1): 246-256
81. Choi S, Shah SP (1997) Measurement of deformations on concrete subjected to compression using image correlation. *Experimental Mechanics* 37(3): 307-313
82. Wang Y, Cuitiño AM (2002) Full-field measurements of heterogeneous deformation patterns on polymeric foams using digital image correlation. *International Journal of Solids and Structures*, 39(13-14): 3777-3796
83. Tong W (1997) Detection of plastic deformation patterns in a binary aluminum alloy. *Experimental Mechanics* 37(4): 452-459
84. Bastawros AF, Bart-Smith H, Evans AG (2000) Experimental analysis of deformation mechanisms in a closed-cell aluminum alloy foam. *Journal of the Mechanics and Physics of Solids*, 48(2): 301-322
85. Zhang, J, Cai YX, Ye WJ, Yu TX (2011) On the use of the digital image correlation method for heterogeneous deformation measurement of porous solids, *Optics and Lasers in Engineering* 49(2): 200-209
86. Heinz SR, Wiggins JS (2010) Uniaxial compression analysis of glassy polymer networks using digital image correlation, *Polymer Testing*, 29(8): 925-932

87. Pan B, Wu DF, Wang ZY, Xia Y (2011) High-temperature digital image correlation method for full-field deformation measurement at 1200 degrees C, *Measurement Science and Technology* 22(1): 015701, DOI: 10.1088/0957-0233/22/1/015701
88. Bing P, Hui-min X, Tao H, Asundi A (2009) Measurement of coefficient of thermal expansion of films using digital image correlation method, *Polymer Testing*, 28(1): 75-83
89. Kartal ME, Mulvihill DM, Nowell D, Hills DA (2010) Determination of the Frictional Properties of Titanium and Nickel Alloys Using the Digital Image Correlation Method, *Experimental Mechanics*, DOI: 10.1007/s11340-010-9366-y
90. B. Shen B, Paulino GH (2010) Direct Extraction of Cohesive Fracture Properties from Digital Image Correlation: A Hybrid Inverse Technique, *Experimental Mechanics*, DOI: 10.1007/s11340-010-9342-6
91. Catalanotti G, Camanho PP, Xavier J, Dávila CG, Marques AT (2010) Measurement of resistance curves in the longitudinal failure of composites using digital image correlation, *Composites Science and Technology* 70(13): 1986-1993
92. Hild F, Roux S, Guerrero N, Marante ME, Florez-Lopez J (2011) Calibration of constitutive models of steel beams subject to local buckling by using digital image correlation, *European Journal of Mechanics A-Solids* 30(1): 1-10
93. C.A. Featherston, J. Mortimer, M.J. Eaton, Richard L. Burguete, Rhiannon Johns (2010) The Dynamic Buckling of Stiffened Panels –A Study Using High Speed Digital Image Correlation. *Applied Mechanics and Materials*, 24-25, 331
94. Koerber H, Xavier J, Camanho JJ (2010) High strain rate characterization of unidirectional carbon-epoxy IM7-8552 in transverse compression and in-plane shear using digital image correlation. *Mechanics of Materials* 42(11): 1004-1019
95. Ajdari A, Hashemi HN, Vaziri A (2003) Dynamic crushing and energy absorption of regular, irregular and functionally graded cellular structures, *International Journal of Solids and Structures*, 48(3-4): 506-516
96. Chen C, Harte AM, Fleck NA (2001) The plastic collapse of sandwich beams with a metallic foam core, *International Journal of Mechanical Sciences*, 43(6): 1483-1506
97. Caner FC, Bažan ZP (2009) Size effect on strength of laminate-foam sandwich plates: Finite element analysis with interface fracture, *Composites Part B: Engineering*, 40(5): 337-348
98. Styles M, Compston P, Kalyanasundaram S (2008) Finite element modeling of core thickness effects in aluminum foam/composite sandwich structures under flexural loading, *Composite Structures*, 86(1-3): 227-232
99. Valenza A, Fiore V, Calabrese L (2010) Three-Point Flexural Behaviour of GFRP Sandwich Composites: A Failure Map, *Advanced Composite Materials*, 19: 79 – 90
100. Hooputra H, Gese H, Dell H, Werner H (2004) A Comprehensive Failure Model for Crashworthiness Simulation of Aluminium Extrusions, *International Journal of Crashworthiness*, 9(5): 449–464
101. ABAQUS Theory Manual, Simulia